NASA CR134877
MDC G6029

VALVE CONTAMINATION AVOIDANCE DEVICES

by

D. L. Endicott

McDonnell Douglas Astronautics Company

Prepared for

NATIONAL AERONAUTICS AND SPACE ADMINISTRATION

NASA Lewis Research Center
Contract NAS3-17812
J. Notardonato, Project Manager

1. Report No.	2. Government Accession No.	3. Recipient's Catalog No.
CR 134877		

4. Title and Subtitle	5. Report Date
VALVE CONTAMINATION AVOIDANCE DEVICE	November 1975
	6. Performing Organization Code

7. Author(s)	8. Performing Organization Report No.
	MDC G6029
	10. Work Unit No.

9. Performing Organization Name and Address	11. Contract or Grant No
McDonnell Douglas Astronautics Company 5301 Bolsa Ave. Huntington Beach, CA 92647	NAS3-17812
	13. Type of Report and Period Covered
12. Sponsoring Agency Name and Address	Final - May 1974-July 1975
National Aeronautics and Space Administration Lewis Research Center Cleveland, OH 44135	14. Sponsoring Agency Code

15. Supplementary Notes

16. Abstract

The gain in component reliability for long term reusable space vehicles was investigated in a two-part program. Mechanical redesign methods were used to minimize contamination damage of conventional fluid components and a unique type of contamination separator device was developed. The redesign techniques were incorporated into an existing 50.8 MM (2 in) poppet valve and tested for damage tolerance in a full size open loop flow system with gaseous and liquid nitrogen. Cyclic and steady flow conditions were tested with particles of 125 to 420 μM aluminum oxide dispersed in the test fluids. Non-flow cycle life tests (100,000 cycles) were made with two valve configurations in gaseous hydrogen. The redesigned valve had an acceptable cycle life and improved tolerance to contamination damage when the primary sealing surfaces were coated with thin coatings of hard plastic (Teflon S and Kynar).

Analytical studies and flow testing was completed on four different versions of the in-line venturi type of the separator. Overall separation efficiencies in the 55-90% range was measured when these non-optimum configurations were tested in GN_2 and LH_2 flow systems with contamination particles of aluminum oxide, aluminum and stainless steel. The effects of velocity (momentum) changes on separation efficiency was measured in a gaseous flow system. High separation efficiencies were measured over the velocity range of 15-90 M/S tested.

17. Key Words (Suggested by Author(s))	18 Distribution Statement
Particulate Contamination, Spacecraft Propulsion Fluid System Components, Poppet Valves, Particulate Separation, Filtration, Contamination Damage Tolerance, Flow Tests, Cyclic Valve Tests, Dynamic Separation, Prefilter	Attached

19. Security Classif. (of this report)	20. Security Classif. (of this page)	21. No. of Pages	22. Price*
None	None	121	

*For sale by the National Technical Information Service, Springfield, Virginia 22151

NASA-C-168 (Rev 6-71)

CONTENTS

FIGURES

TABLES

Section 1

SUMMARY

A program to develop the design criteria for propellant feed system hardware for long-term reusable vehicles has been completed. Since the reusable space vehicle propellant systems are expected to be exposed to greater quantities of potentially harmful contaminants, the need for contamination damage control of feed system components has been identified as an important technology area for the Space Shuttle/Space Tug type of vehicles. This program has dealt with two important aspects of contamination damage tolerances of feed system components:

A. The improvement in the contamination damage tolerance of the basic feed system components, such as shutoff valves, to higher levels and larger sizes of particulate contamination in liquid and gaseous fluid systems.

B. The evaluation of particulate separation devices (prefilters) which can reduce the level of contamination in liquid and gaseous fluid systems.

The specific work covered on this program was accomplished in three work tasks.

1.1 EVALUATION OF A DYNAMIC PARTICLE SEPARATION DEVICE

The basic 180-deg venturi type of separator test on this program was conceived on Contract NAS8-14375. This separator was configured into a number of different versions and tested in both liquid (LN_2) and gaseous (GN_2) flow systems. The configurations analyzed and tested included four different venturi configurations and three different particulate trapping arrangements. These devices were tested in an open-loop operation mode, with 50.8 mm (2-in) line size components, using aluminum oxide (Al_2O_3), metallic aluminum, and stainless steel particles in the 75 to 420 micron size range.

The best separator configurations tested were found to be capable of removing 80 to 95 percent of the particulate contamination under the conditions tested. The non-optimum configuratiions tested had measured separation efficiencies of 50 percent or less under some test conditions. The configurations tested on this program were selected to provide a set of baseline data for four different separator configurations. The present work did not include the modification or optimization of any one design for use in a real propellant system. Further work will be required to convert the baseline design into discrete separator designs for system applications. It was found that both the venturi directors and the particulate trapping arrangements behave differently in the ambient gaseous tests and in the cryogenic liquid tests, and no single design configuration was identified for universal service. The

design principles incorporated into the separator configurations appear capable of lowering the amount of contamination in a typical fluid system by a significant amount when the separator configuration is optimized for the particular type of system selected. The low pressure loss, nonplugging features of this separator design were demonstrated in full flow testing, and further work on this concept appears to be justified.

The key problem areas remaining include:

A. Determination of the effects of venturi inlet cone angle on the particle flow path.

B. Establishment of the overall separator efficiency change with changes in the area of the particulate trap inlet to the flow bypass area.

C. Determination of the effects of particle size and shape on the acceleration characteristics of the particles in the venturi director.

The resolution of these key problem areas will materially assist in the translation of this design concept into a working prefilter for propellant fluid systems. The present separator design can be used at the present state of development as a system prefilter, and some benefits would occur in the fluid cleanup process. Since the present design configuration is capable of removing 50 percent or more of the system contamination, its use as a prefilter should minimize potential filter problems on most space vehicle propulsion systems. With further work in improving the separator efficiency, a further improvement in the prefilter/filter combination should occur. Depending on the specific system requirements, the separator may be able to accomplish the fluid cleanup operation without a secondary filter.

1.2 VALVE CONTAMINATION TOLERANCE TESTING

One method of improving the contamination damage tolerance of a fluid shutoff valve is accomplished by providing a seat sealing surface which is hard enough to maintain the correct mechanical properties for a specified number of operational cycles while being soft enough to permit complete particle embedment into the sealing surface when contaminant particles are present. This method of approach was evaluated on this program and a series of 10 verification tests were run under simulated full-flow conditions. The seat sealing surfaces tested consisted of three types of hard, thin plastic coatings operating in a plastic-on-plastic mode and a plastic-on-bare-metal mode. The materials tested consisted of multiple layers of Teflon S, Xylon 1010, and a single thick layer of Kynar 202. The embedability characteristics of these materials were determined using Al_2O_3 particles in the 125 to 250 micron and 250 to 420 micron size range.

The tests were conducted using a modified 50.8 mm (2 in) line size pneumatically actuated valve and with gaseous hydrogen (GH_2) as a test media.

The results obtained indicated:

A. The high-build Teflon S material has acceptable embedability characteristics within the limitations imposed by the coating thickness; however, coating thicknesses of over 0.050 mm (0.002 in) could not be obtained with the coating techniques used.

B. The Xylon 1010 material could be coated with a greater thickness than was obtained with the Teflon S material; however, the thicker coatings of Xylon had unacceptable mechanical properties. The embedability characteristics of this Xylon material was satisfactory.

C. The Kynar 202 material was coated to thicknesses of 0.25 mm (0.010 in) and still retained acceptable mechanical properties. The Kynar material operated satisfactorily under the ambient temperature condition used for these tests; however, the performance of this material under cryogenic temperatures has not been established.

1.3 VALVE CYCLE LIFE TESTS

The utilization of plastic coatings with good particulate embedability characteristics is limited by the effects of the mechanical properties of the coatings on the cycle life of the component. Hence, the two best coating combinations identified in the valve contamination tolerance testing were subjected to a cycle life test series of 100,000 cycles. These two tests were conducted in a pressurized nonflow condition using GH_2 at ambient temperatures. The coating combinations tested were:

A. Kynar 207/202 on uncoated Inconel 718.

B. Teflon S on Teflon S - three coats each with chemical preclean.

Both coating combinations performed satisfactorily for the 100,000 cycles of operation. The Kynar coating was tested with an average seat stress of 1.3×10^7 N/m^2 (1900 psi). The harder Teflon S was tested at 1.7×10^7 N/m^2 (2500 psi). The internal leakage rate for both combinations remained well under the 1 SCCM limit (at 6.89×10^5 N/m^2 [100 psig] with GHe) throughout the test duration. The leakage rates remained relatively constant throughout the test except for a minor leak encountered on the Kynar film (6000 N) due to film separation from the substrate metal during the last few cycles of the Kynar test. The Kynar 202 film was applied over a Kynar 207 primer coating. The tests completed indicate that the Kynar 207 primer is not the optimum primer material for propulsive feed system components and either Kynar 204 or 205 should be investigated for future utilization.

Section 2

INTRODUCTION

2.1 OBJECTIVE

The objective of this program was to develop the technology required to improve the contamination damage avoidance characteristics of fluid system components. The steps needed to develop contamination damage control criteria are shown in Figure 2-1. This figure shows the overall technology steps and the specific steps completed on the original program and on the present program. The original effort was conducted on Contract NAS3-14375 and was reported previously (Reference 1). The present effort has been conducted on Contract NAS3-17812. Two basic approaches to contamination damage control are shown in Figure 2-1. Both approaches were studied on this program and a number of key steps were completed.

The first method investigated covered the evaluation of a particulate separation device which was capable of removing potentially harmful contaminant particles from flowing fluids with a minimum of flow pressure losses. The design criteria for the contamination separator (prefilter) were demonstrated for four versions of the 1T43824 dynamic separator (50.8 mm - 2 in), 180 deg, venturi, nonregenerative, constant velocity type developed on Contract NAS3-14375. The second method investigated covered the evaluation of the inherent resistance to contamination damage of a modified poppet type shutoff valve. The valve modifications included the addition of specific thin plastic coatings on the seat sealing surfaces of the poppet and seat and minor mechanical redesign of the valve. The design criteria for the contamination damage tolerance method were developed and demonstrated with two existing 1T32095 valves (50.8 mm - 2 in) pneumatically actuated, 90-deg flow offset, poppet type, developed on Contract NAS3-12029 (reported in Reference 2), and partially tested on Contract NAS3-14375.

This effort included:

A. The determination of the operating characteristics of a venturi type of dynamic particulate separator (prefilter) under full-scale operating conditions with both liquid and gaseous test fluids.

B. Evaluation of the contamination damage resistance of a 50.8 mm (2-in) poppet valve using thin coated plastic seat coating materials under full-flow test conditions, with controlled contamination, in a GH_2 test fluid.

C. The determination of the cycle life characteristics of the 50.8 mm (2 in) poppet valve with thin plastic seat coating materials while operating in a GH_2 environment.

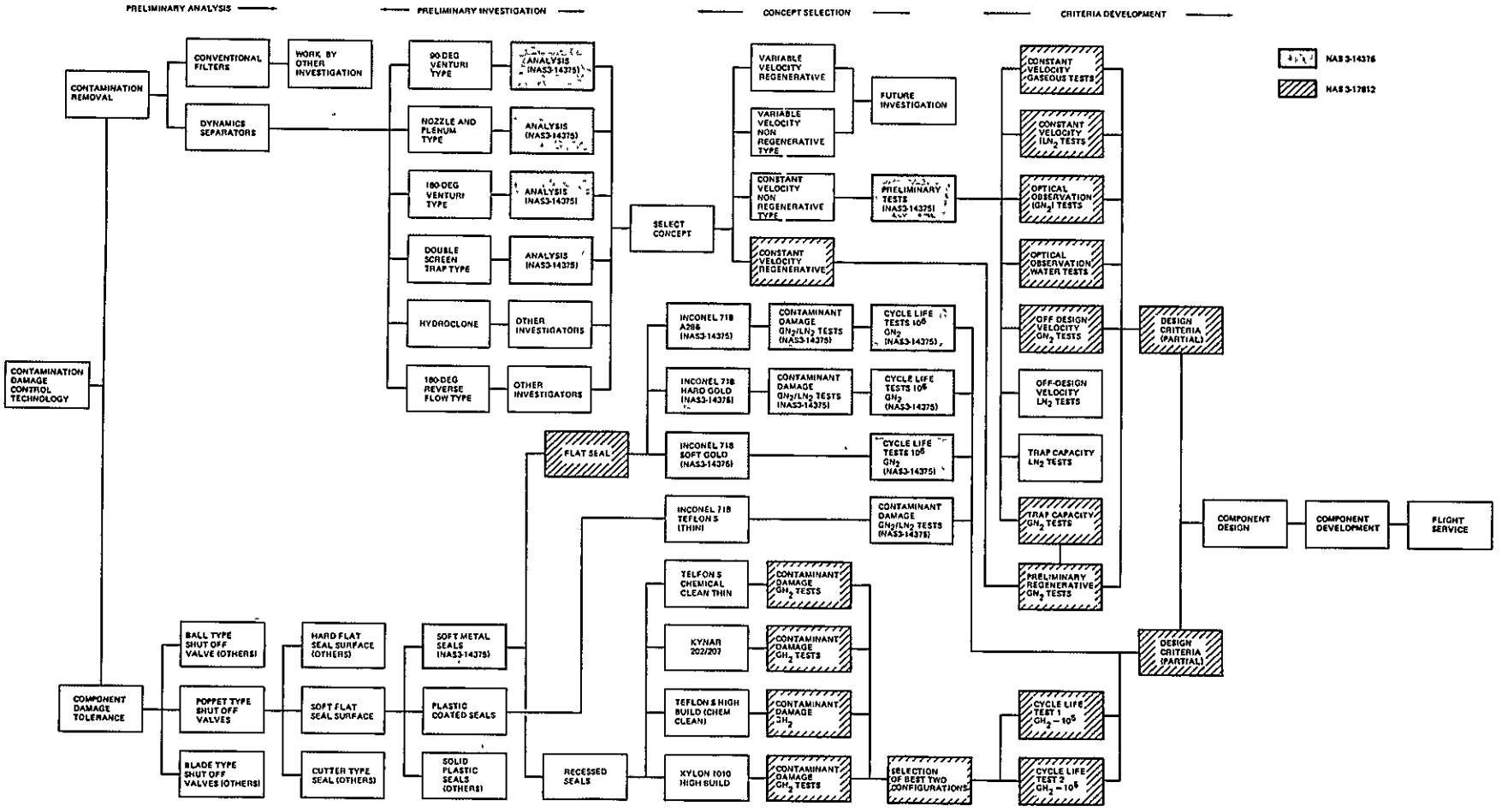

Figure 2-1. Leakage Control of Components to Particulate Contamination

The approach that was used to achieve these objectives during the 15-month period was to:

A. Conduct optical observation tests of a transparent, two-dimensional model of the separator in a water flow loop to determine the trajectory of particles flowing through the separator model.

B. Conduct an analysis of the screen blockage effects of the contaminant trapping device on the overall efficiency of the contamination separator. This analysis included investigating the change in fluid flow characteristics across the separator.

C. Conduct a design study of potential separator trap configurations. The trap design effort included consideration of flow oscillation, back flow, zero gravity, and separator orientation.

D. Fabrication of a redesigned separator configuration. The parts fabricated were sufficient to provide two complete 50.8 mm (2 in) test assemblies and four different test configurations. These configurations were based on the results obtained on the optical evaluation test, the screen blockage analysis, and the trap design study.

E. Conduct constant-velocity, steady-state flow tests with four different separator configurations; four different sizes and three different types of particulate contamination. These tests were conducted in both liquid and gaseous nitrogen flow media.

F. Conduct off-design velocity tests. These tests measured the performance of two separator configurations at five different flow velocities. These tests were conducted using Al_2O_3 particulate powder in two size ranges and were conducted with GN_2 as the test media.

G. Conduct trap capacity tests. These tests measured the capacity of two separator trap configurations to determine the quantity of particulate which could be stored in the trap and to determine the change in separation efficiency as the trap storage approached the maximum storage limit. These tests were conducted using two sizes of Al_2O_3 particulate contamination powder and with various quantities of powder injected on each run. The test media was GN_2.

H. Conduct a test to measure the contamination damage tolerance of a modified version of the 1T32095-507 valve during cyclic operating condition in a GH_2 flow environment. The valve modifications included the addition of contamination relief grooves in the poppet seat assembly and covered the use of five different plastic coating material combinations on the poppet seat. The plastic coatings tested consisted of two basic types. One was a polyimide type with an entrained Teflon release agent. The other was a polyvinylidene fluoride (PVF_2) material.

I. Conduct a test series to determine the cycle life characteristics of the two best material coating combinations identified in the valve contamination tolerance test effort. This was accomplished by transferring the 1T32095-507 valve from the gaseous flow loop to an existing cycle life test fixture and then conducting two-cycle life tests of 100,000 cycles each in a pressurized environment. The two materials tested were Teflon S on Teflon S and Kynar 207/202 on Inconel 718. Both materials were tested for 100,000 cycles of operation.

This approach was implemented by the three-task program summarized below.

2.2 TASK I - EVALUATION OF THE DYNAMIC PARTICLE SEPARATION DEVICE

Performance characteristics and efficiency of the dynamic particle separation device were determined by experimental and analytical investigations. These included:

A. Optical Tests - A series of 12 tests was conducted to determine the trajectory of contaminant particles entrained in a moving fluid stream through a clear, two-dimensional model of the basic dynamic separator. These tests were conducted using a high-intensity strobe light and photographic recording systems.

B. Screen Blockage Analysis - An analysis was made to evaluate the effects of various degrees of screen blockage on the pressure drop through the separator, the changes in velocity profile, and the changes in overall separation efficiency. The results from this analysis was used to assess the design of the director venturi and screen trapping arrangement and to provide the basis for further design optimization.

C. Separator Trap Design - Using the results of the analytical study described in Task IB, a new trap design was made. This design was made with consideration of the factors of: (1) flow oscillations, (2) back flow, (3) zero gravity, and (4) separator orientation. The efficiency of the new trap design was determined by flow testing.

D. Fabrication of Redesigned Units - One completely new separator assembly was fabricated for Task I testing. A second assembly was fabricated to the Task IC design configuration using the existing separator hardware (from Contract NAS3-14375). Two additional venturi sections were fabricated so that four different venturi configurations were evaluated.

E. Steady-State (Design Velocity) Flow Tests - A series of 96 steady-state flow separator tests were conducted using three different types of contaminant materials. Half of these tests were run with LN_2 and half with gaseous nitrogen.

The test powders used consisted of particles of Al_2O_3, aluminum, and stainless steel (CRES) in the following four size ranges: 63 to 106 microns, 106 to 180 microns, 180 to 250 microns, and 250 to 400 microns. The aluminum particles and some of the CRES used for these tests were graded spherical type particles. The inlet flow velocity was 30 m/s (100 ft/sec) for the GN_2 tests and was selected to produce a venturi throat velocity of 30 m/s (100 ft/sec) for the LN_2 tests when possible.

F. Off-Design Velocity - A series of tests was conducted under 32 off-design steady-state velocity conditions. These tests were conducted using the same GN_2 flow loop that was used for the steady-state flow tests.

The off-design velocity tests were conducted at 15, 22.5, 30, 45, and 90 m/s inlet flow velocity. The test powder was two different sizes of Al_2O_3 powders used in the constant-velocity test. Two different venturi designs were tested at off-design velocity conditions.

G. Design Criteria for Variable Velocity Separator Model - The design criteria for a variable velocity separator were studied using the test information determined for the particulate separator.

H. Trap Capacity Tests - A series of tests was made to determine the trapping capacity of two nonregenerative separator designs. The venturi design which produced the highest separation efficiency in the steady flow tests were used for the trap capacity tests. These tests were conducted using GN_2 as a test fluid. The quantity of particulate was increased in equal increments for each of two particle sizes. The test powders were screened Al_2O_3 particles.

I. Regenerative Separator Evaluation - The basic unit used for the trap capacity tests was modified to incorporate a simple regeneration system into the trapping screens. The type of regenerative system was determined using the results of the trap capacity tests. This regenerative unit was tested to evaluate the change in trapping capacity that occurs with the addition of the regenerative system. The tests consisted of a short series of runs in LN_2 and then a complete series of tests in GN_2.

J. Separator Performance Map - The information obtained on all of the Task I test efforts was used to evaluate the performance map generated on Contract NAS3-14375. The revision of the performance map was studied in an attempt to establish a set of generalized guidelines which could be used to provide the design criteria for a venturi type particulate separator.

2.3 TASK II - VALVE CONTAMINATION TOLERANCE TESTING

The existing 50.8 mm (2 in) poppet type valve was used to evaluate contamination damage tolerance under GH_2 flow conditions.

A. Valve Modification - The existing 1T32095-505 valve was modified to a 1T32095-507 configuration. The modified valve was then refurbished to bring the valve back to a condition suitable for testing. The existing spare parts for the -505 valve and the complete -503 valve (both available from Contract NAS3-14375) were used to maintain the working condition of the -507 configuration.

The -507 valve configuration incorporated thin plastic coatings on the poppet sealing surface, on the seat sealing surface, or on both surfaces. The coating combination consisted of one coat to six coats total on the seal interface. The coatings tested included a Teflon S coating, Xylon 1010 coatings, and Kynar 207/202 coatings. A chemical precoating treatment was used with the Teflon S material.

B. Contaminant Tolerance Testing - The modified valve was used in a series of 10 tests to evaluate the contamination damage tolerance of five coating combinations. These tests were conducted using gaseous hydrogen (GH_2) as a test medium. Each test consisted of an intermittent type of cyclic run wherein the valve was cycled open and closed five times while the valve inlet was pressurized at the normal design value of 6.89×10^5 N/m^2 (100 psig). The test powders injected into the valve were Al_2O_3 of two different size ranges. The quantity of contaminants injected was similar to those used on Contract NAS3-14375. These size ranges were 125 to 250 microns for the fine powder and 250 to 420 microns for the coarse powder. A filter assembly with a rating of 18 microns absolute was installed downstream of the test valve such that the amount of test powder which passed through the test valve could be measured. The internal leakage rate of the valve was measured before and after each test run. The changes in internal leakage rates and the observed deterioration of the sealing surfaces were used to evaluate the contamination damage tolerance of each seat surface combination.

C. The test valve was refurbished to the extent required to provide valid test data before each test run of the Task II effort. The seat sealing surfaces were replaced or refinished as necessary.

2.4 TASK III - VALVE CYCLE LIFE TEST

The existing 50.8 mm (2 in) poppet type valve was used to evaluate the cycle life of selected seat sealing materials as determined by changes in internal leakage rates.

A. The 1T32095-507 valve was refurbished using the Kynar 207/202 on Inconel 718 sealing material combination. The valve was restored to the condition necessary to produce valid test data on a 100,000-cycle life test series.

B. The internal leakage rate of the test valve was measured at ambient temperature conditions prior to the start of the cycle life testing and at the completion of the cycle test.

C. The test valve was installed in the MDAC cycle life evaluation test fixture and a cycle life test conducted. Pressurized GH_2 was applied to both the inlet and outlet of the valve in such a manner that no propellant flow occurred through the valve during the cycle test sequence. This test was continued until the valve has accumulated a total of 100,000 operating cycles. The internal leakage rate was measured at intervals during the cycle life test (with GHe at 6.89×10^5 N/m^2) such that not more than 10,000 cycles were accumulated between leakage measurements and at least one measurement was made during each test day. The valve was pressurized internally to 6.89×10^5 N/m^2 with GH_2 at ambient temperature during cycle testing.

D. After completion of the first cycle life test, the 1T32095-507 valve was refurbished to the extent required for a second cycle life test using the Teflon S on Teflon S seat-sealing material. The refurbished valve was then used for a second 100,000-cycle life test which was conducted in the same manner as the first cycle life test.

Section 3

TECHNICAL DISCUSSION

3.1 TASK I – EVALUATION OF THE DYNAMIC PARTICLE SEPARATOR DEVICE

This task consisted of conducting a series of experimental investigations and analytical studies to evaluate the performance potential of the 180-deg venturi type (straight-through flow) dynamic separator concept (1T43824). This basic configuration is shown in Figure 3-1. The initial analytical studies and preliminary test results for this device were completed on Contract NAS3-14375 and reported in Reference 1. To continue the evaluation of this device, a 10-part experimental investigation was carried out to (1) study the positioning capabilities of the venturi section, the entrapment capabilities of the contaminant trapping arrangement, and the off-design velocity characteristics of the basic separator design, and (2) to conduct a preliminary investigation of a potential regenerative (self-cleaning) version of this design concept. The results of these tests will assist in providing the design criteria specified in Figure 3-2.

This figure shows the steps needed to provide qualitative design criteria for future separator designs. Items A through F, H, and I were investigated on this contract. By using the information generated on the previous con-

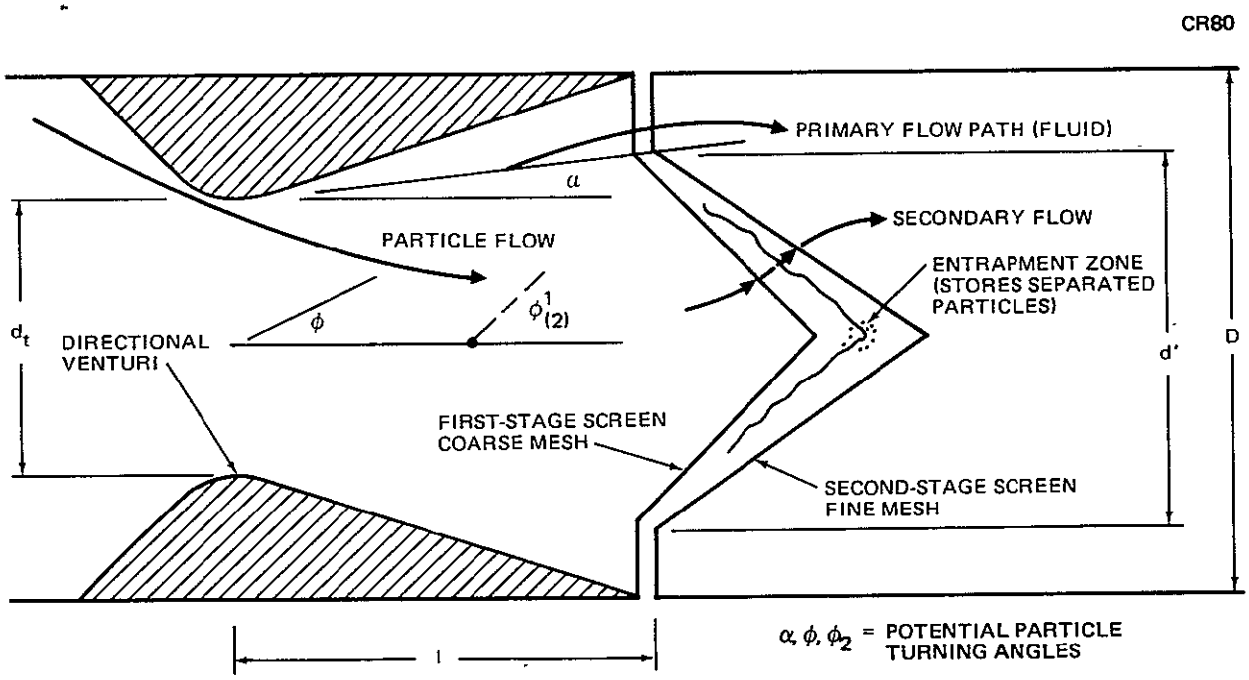

Figure 3-1. Basic Dynamic Separator Design

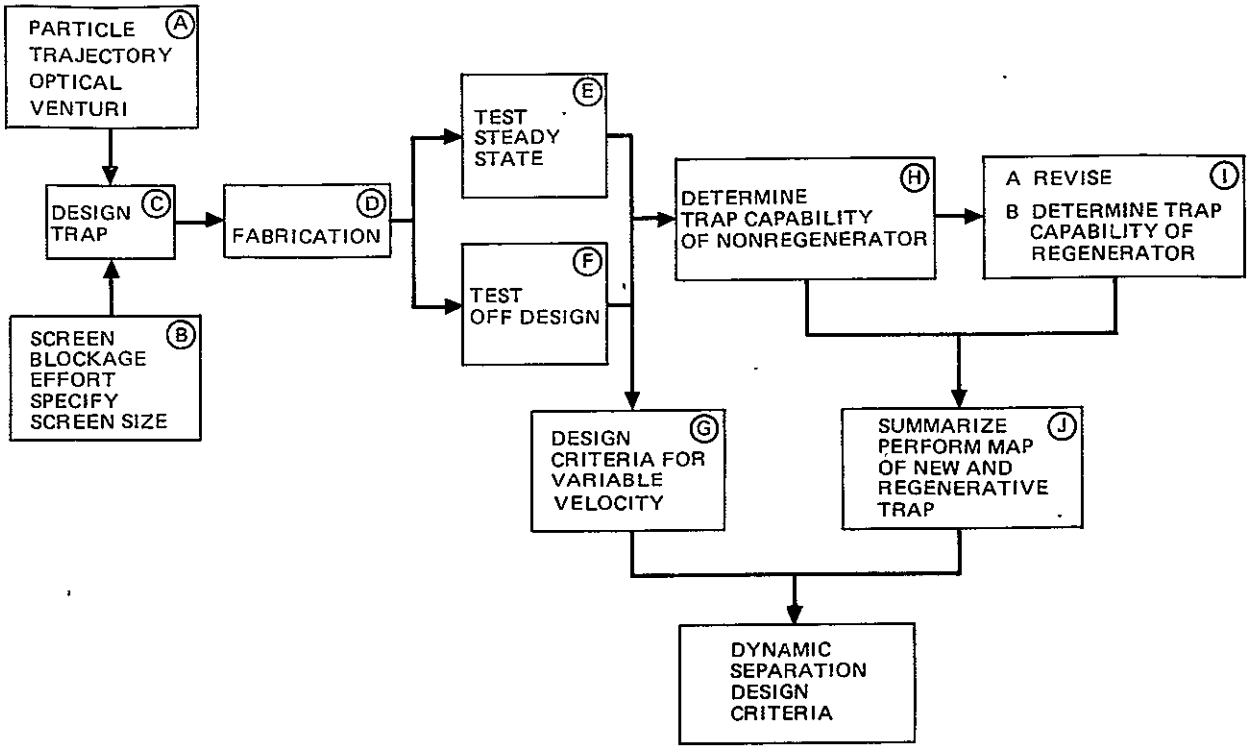

Figure 3-2. Dynamic Particle Separator Technology Development

tract and on this program, it was possible to demonstrate overall particulate separation and storage efficiencies of over 90 percent under some conditions of flow with both ambient gaseous and cryogenic liquid flow. While a number of different configurations were tested, no optimum design was identified for both liquid and gaseous service. The differences in density of the flowing fluids and the contaminant particles varied to the extent that different design characteristics are applicable for each system. The basic separator configuration appears to be capable of operating with high overall efficiencies in either type of system; however, the separator must be configured somewhat differently for gaseous or cryogenic liquid systems. Several key problem areas were identified during the program, and further work on these problems will be needed before a workable separator can be configured for field service. These problem areas included:

A. Optimization of the venturi inlet cone angle.

B. Optimization of the trap inlet area to the flow bypass area.

C. Determination of the effects of particle size and shape on the acceleration characteristics of the particles in the venturi section.

The original intent of this program was to develop the test data needed to verify or correct the generalized performance map generated on the preceding contract (Figure 3-3). The test data obtained to date indicate that some difficulty will be experienced in trying to correlate all of the system variables on a single performance map. The major deficiencies identified to date were:

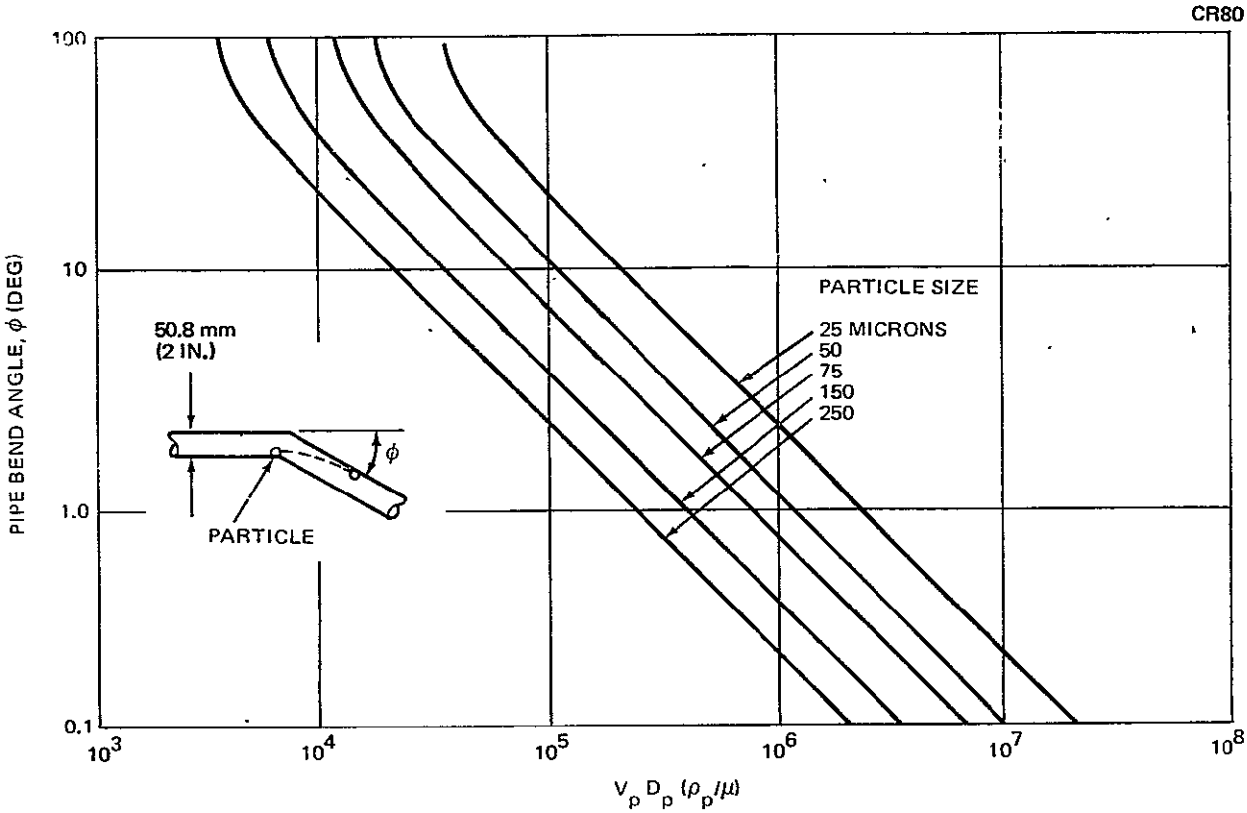

Figure 3-3. Minimum Pipe Bend Angle Required for Particle Impact on Pipe Wall — Separator Performance Map

A. Lack of particle trajectory/acceleration data.

B. Lack of a factor which can account for the difference in density (particle to fluid) in the Reynolds number term on the original performance map.

Both of these factors are sufficiently different from the basic assumption used in the original analysis to have a profound effect on the final design criteria. Both of these factors can be evaluated with analytical techniques; however, these analytical studies will be somewhat complicated and were not included within the scope of the work completed on this program.

A considerable amount of design information was developed and verified on this program. Each portion of this overall investigation was covered in subtasks which are presented separated in the following sections.

3.1.1 Optical Tests

The test setup for the water flow/optical tests is shown in Figures 3-4 and 3-5. The water tank used has a capacity of 3.4 m^3 (900 gallons) and was capable of operating at pressures up to 8.26×10^6 N/m^2 (1200 psig). The water tank was pressurized with GN_2 from storage bottles. The water flowrate was controlled by a hand valve located at the separator inlet. A two-dimensional plastic flow model (shown in Figure 3-6) was used for the optical tests. The key flow passage dimensions are shown in Figure 3-6. The contamination particles were prepared before each test and placed in

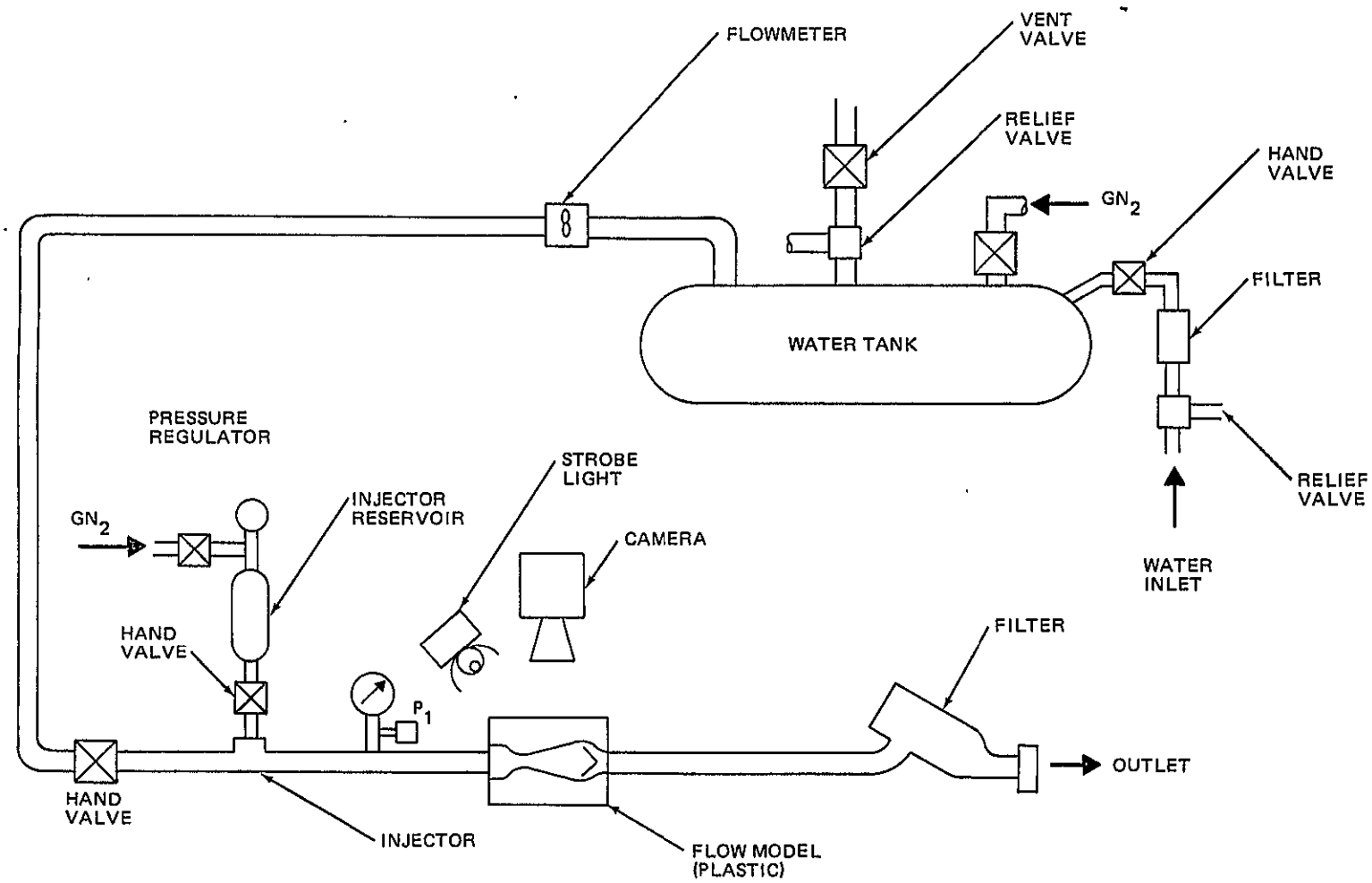

Figure 3-4. Water Flow Test Setup

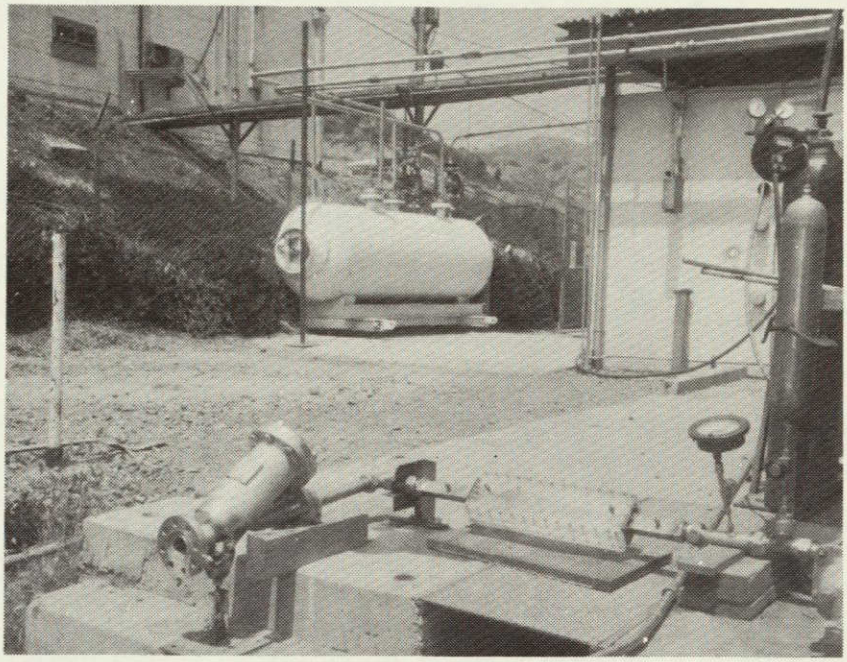

Figure 3-5. Test Setup for Water Flow Tests

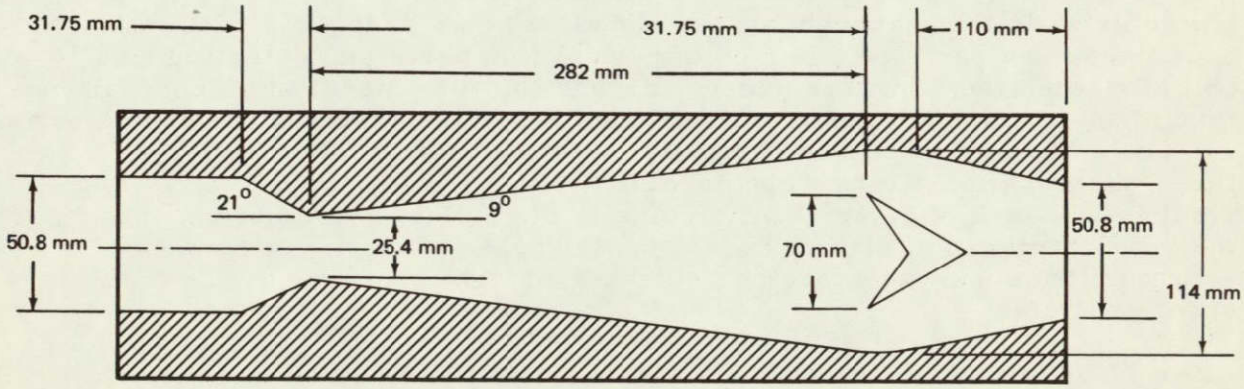

Figure 3-6. Flow Passage Configuration for Plastic 2D Model

the contaminant injection system. A test was conducted by establishing the water flow through the test model with the flow control valve and then injecting the particulate and particulate carrier fluid into the flow system. Visual observation of the particle trajectories was made during the test run. Preliminary testing had been completed with this setup and two-dimensional flow models prior to the start of this program.

Two problem areas were known to exist at the start of this test series. These were:

A. Particle Injection Rate

B. Optical Detection Methods

The particle injection rate problem resulted from the inability of the existing liquid injection system to inject particles into a flowing liquid system at a slow steady rate without the introduction of gas bubbles into the flow stream. The original injection system would inject all of the particulate material at one time (and hence flood the flow passage) or would not inject any of the particles. This difficulty was due to the settling of the particles into the bottom of the injector reservoir and in the orifice plugging characteristics of the wet particulate. After evaluating four types of injection systems and a number of different orifice sizes, the system shown in Figure 3-7 was developed. With the new system the particles are permitted to settle in the bottom of the particulate reservoir before a test run is started and then "flushed" up into the particulate reservoir. This "premixed" particulate/carrier fluid is then injected into the flow stream at a rate controlled by the setting of the injection control valve and the amount of pressure used on the carrier fluid supply tank. This injection system has resulted in increasing the injection time from a fraction of a second to injection periods of over 5-second duration with a relatively uniform injection rate. The utilization of this type of injection system provided a substantial improvement in the ability of the test system to produce test conditions which were similar to real operating conditions.

The second problem encountered related to the recording of the particle trajectories in the transparent test model. A Sony videotape system had been used previously on a series of optical flow tests and detection was obtained when the particles passed through the flow model in a dense "cloud" type of injection. The test runs made with the videotape and the new injection system would not produce a detectable trace of individual particles when these individual particles were passing through the test model (at a slow rate). This lack of detectability is due to the relatively slow scan rate on the video camera (30 pictures a second) and the similarity of the video scanning trace and the expected "streaks" of light produced by the high-speed particles.

After 30 preliminary test runs were made with the video tape recorder and Al_2O_3 particles, a change was made to the metallic aluminum particles. The "shiny" aluminum particles could be detected by eye, without difficulty, as they passed through the test model. The use of strobe lights or other auxiliary lighting systems was not required for visual particle detection. With this improvement in the equipment it was possible to complete the optical test series using a high-speed (1/400) Polaroid still camera (with high-intensity strobe lighting) for recording the trajectory of the contaminant particles. In addition to the normal camera coverage, two runs were made with a high-speed movie camera. The final optical recording methods were adequate for this type of testing and acceptable photographs of the flow process were obtained.

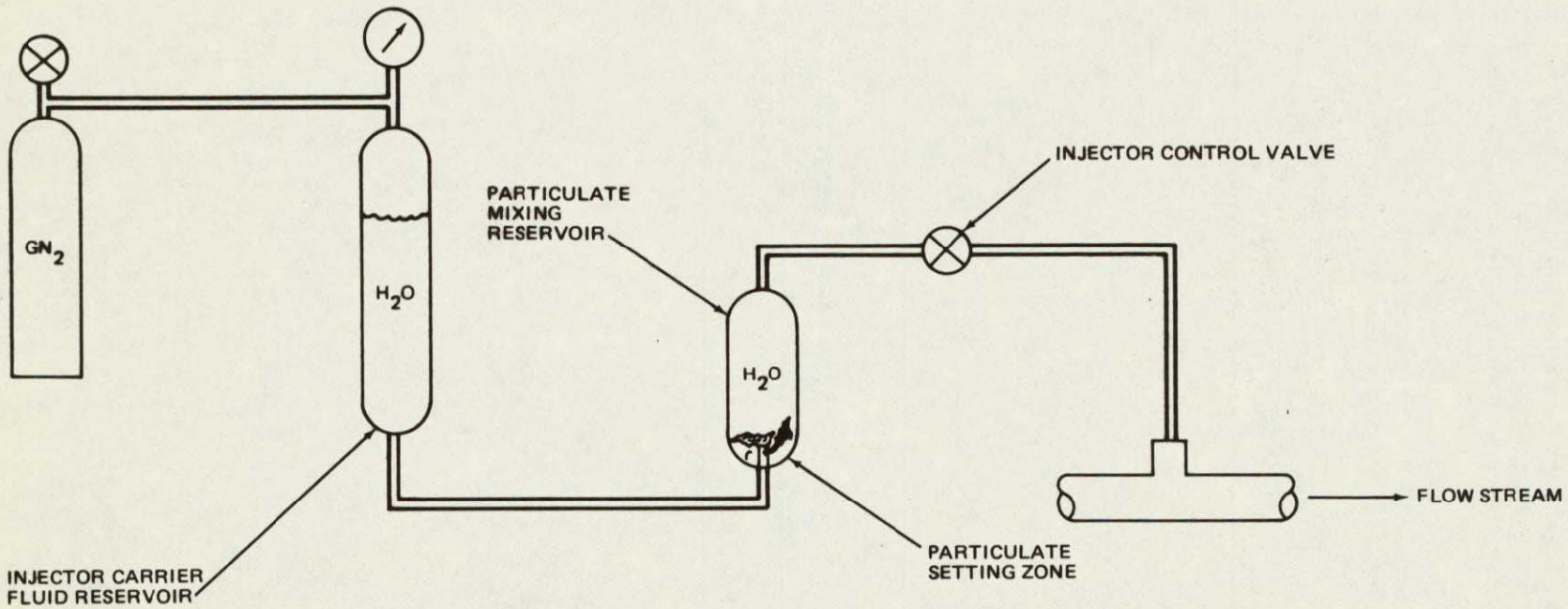

Figure 3-7. Particulate Injector for Liquid System

The 12 scheduled optical flow tests were completed using the revised test setup. The test powders originally scheduled for the optical flow tests are shown in Table 3-1. While tests were run with most of these materials, only the shiny aluminum metal particles were detectable. The test matrix for these tests is shown in Table 3-2. A view of a typical test run photo is shown in Figure 3-8. This photo shows a relatively uniform distribution of particles across the expansion cone area of the venturi. Flow separation and reverse

Table 3-1

POWDER NUMBER

Size (micron)	Aluminum Oxide	Aluminum Metal*	Stainless Steel
63-106	A1	B1	C1
106-180	A2	B2	C2
125-150	--	--	CX_2*
180-250	A3	B3	C3
250-425	A4	B4	C4

*Spherical particles

Table 3-2

OPTICAL FLOW TESTS - 2D

Run No.	Test Powder	Inlet Pressure (N/m^2)	(psig)
1	A4	6.89×10^4	10
2	A4	13.78×10^4	20
3	C2	6.89×10^4	10
4	C_2	13.78×10^4	20
5	B1	6.89×10^4	10
6	B_1	13.78×10^4	20
7	B_2	6.89×10^4	10
8	B_2	13.78×10^4	20
9	B_3	6.89×10^4	10
10	B_3	13.78×10^4	20
11	B_4	13.78×10^4	20
12	B_4	20.67×10^4	30

Figure 3-8. Optical Test Photograph-Aluminum Particles – 63 to 180μ (11 m/s)

flow along the exit cone wall can be seen in the upper portion of the photograph. In the high-speed movies, this flow separation is more pronounced and the reverse flow was shown to occur over a relatively large area in the screen trap area. The flow pattern in the movie runs is shown in Figure 3-9. The most significant result of the optical tests was related to the dimensions of the converging cone section (inlet) of the venturi. The original 2D flow model had a half angle of 21 deg on the convergence cone inlet. This is the same angle used on the 1T43824-1 separator tested on Contract NAS3-14375. The optical flow tests revealed that this angle is too large and in operation the particles entering on one side of the flow duct are deflected completely across the duct and around the trap assembly on the opposite side. This flow path arrangement is shown in Figure 3-10a. This undesirable crossflow was corrected by decreasing the inlet cone half angle to 11 ± 1 deg and adding a 12 mm (1/2 in.) transition section to the venturi throat. This arrangement is shown in Figure 3-10b. Since the effective turning angle of the particles is improved by keeping the particles in the center of the flow stream to a point as close to the trap assembly as possible, this inlet cone directing effort can be used very effectively to increase the overall separation efficiency of the separator under known flow conditions. It appears that half angles of 10 to 12 deg on the inlet cone will be optimum for conditions of low velocity (low momentum) and this optimum angle will increase as the flow momentum increases. Based on the optical flow test results the inlet cone angle was changed on the new separator configurations evaluated on this program.

Except for the results obtained on the directivity of the inlet cone angle, the two-dimensional tests did not produce as much information as expected. The following comments apply to the 2D optical tests.

A. The nonsimilarity of two-dimensional models with the corresponding three-dimensional configuration limits the effectiveness of 2D testing under certain conditions. The test method used would be more effective, when the conditions are correct for a high separation efficiency, i.e., heavy particles at high velocities in a low-density fluid. Under conditions of low particle density, low velocity and a dense test fluid, the validity of the testing is diminished for most purposes. Hence, further optical testing should be considered primarily for testing with a gaseous flow media.

B. The optical recording method used was adequate for recording the particle movements and is recommended for future optical testing. The key photographic data were:

Still Camera

Shuttle Speed	1/400 sec
Strobe Light Speed	1/2000 sec
Film Speed	ASA 75

Movie Camera

Shuttle Speed	1/8000 sec
Lighting	2-1000 Watts at 0.45m (18 in)
Film Speed	ASA 160

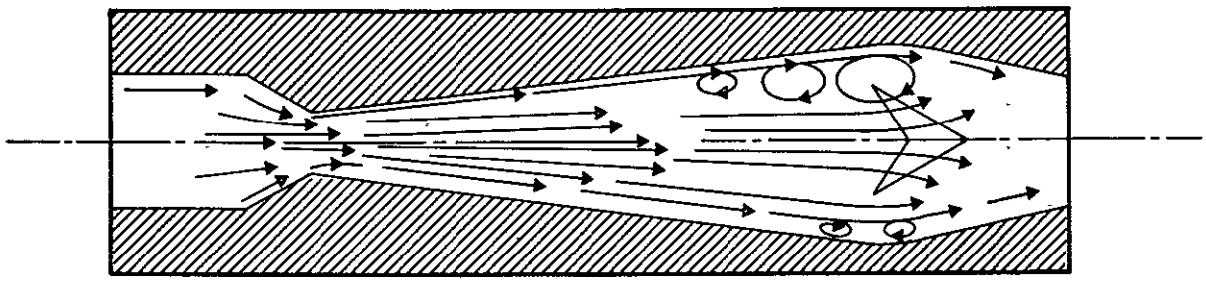

Figure 3-9. Fluid Flow Pattern – 2D Model

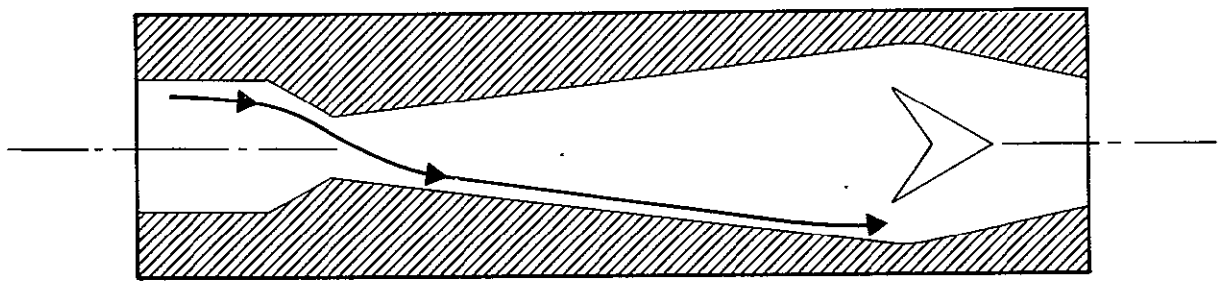

a. PARTICLE FLOW PATH WITH 21-DEG ENTRY CONE

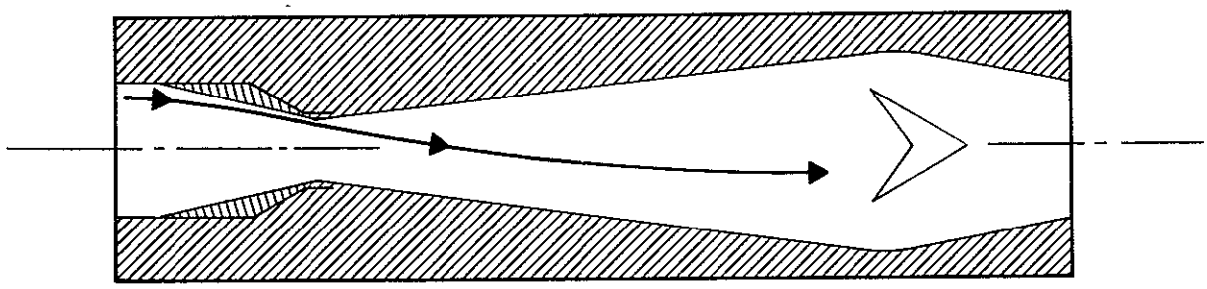

b. PARTICLE FLOW PATH WITH 11-DEG ENTRY CONE

Figure 3-10. Particle Flow Paths

C. The flow conditions tested on this test series were such that little or no difference in particle trajectory was detected for the different particle types and flow velocities tested. The present results are, therefore, qualitative and not quantitative. This difficulty is due mainly to the flow separation characteristics of the exit cone of the 2D model. The exit cone dimensions require that the length of the exit cone on the 2D model be nearly twice as long physically as the actual exit cone on an equivalent full 3D separator, and hence separation occurs in this extra section of the flow duct. The results of the optical tests are such that other areas of optical evaluation are indicated. Since the length of the "light streaks" of the particle images obtained with the high-speed still camera is a function of particle velocity (acceleration) of the particles as they pass through the inlet section of the venturi cone, this method may be used to measure particle acceleration under actual flow conditions. If the camera was set up to view the duct ahead of the venturi and the venturi throat section, the difference in length of particle images would represent the ΔV of the particles. These characteristics were not investigated on the optical tests completed because the flow area of greatest interest was in the expansion cone area immediately ahead of the trap screen section. Optical test measurements in the inlet area could produce predictions of the velocity characteristics of particles of different shapes, densities, and in different test fluids. This information on particle acceleration is not presently available and the development of this information would improve the accuracy of the analytical program. The velocity term in the Reynolds number used on the basic separator performance map relates to the particle velocity and not the flow stream velocity and hence a direct measurement of particle velocity would be very valuable. The analytical study covered in Section 3.1.2 is based entirely on the fluid flow characteristics and while this portion of the study is very important, it can only be applied to estimating overall separator efficiency with some degree of inaccuracy. The optical method of determining the acceleration characteristics of contamination particles should be given further consideration.

3.1.2 Screen Blockage Analysis

A screen blockage analysis was completed for compressible and incompressible flow conditions. This analysis was accomplished by setting up a basic computer program for the constant-velocity nonregenerative separator model. The details of this program are presented in Appendix A.

The basic program is designed to relate the interactions of a number of different separator variables to determine the characteristics of the fluid flow through different separator configurations. This arrangement permits inputting different values of pressure, density, viscosity, screen type, sizes, etc., and then calculating the effect of these changes on the system flow characteristics. All of the work completed to date has been directed at calculating the changes in system pressure loss (ΔP) with changes in physical

configuration. Four potential separator configurations were used as baseline configurations:

1T43824-501	35 mm (1.38 in) venturi throat	9 deg exit cone	12.7 cm (5 in) length
1T43824-503	43 mm (1.71 in) venturi throat	7 deg exit cone	12.7 cm (5 in) length
1T43824-505	19 mm (0.75 in) venturi throat	9 deg exit cone	17.8 cm (7 in) length
1T43824-507	29 mm (1.15 in) venturi throat	7 deg exit cone	17.8 cm (7 in) length

The baseline screen arrangement consisted of four conical screens nested together with a difference of 2.5-deg half angle between each of the separate screens. The screens selected were square mesh screens of 60, 80, 150, and 250 mesh. The pressure losses across the complete separator assembly were then calculated as a function of venturi throat velocity and with no screen blockage and up to 99.9 percent blockage. The results of the GN_2 calculation LN velocity effects are shown in Figure 3-11 and the LN_2 results in Figure 3-12. The effects of screen blockage were found to be relatively small in all cases although the absolute pressure and, therefore, pressure losses are noticeably higher for the LN_2 than for the GN_2 case. Part of this difference is due to the incompressible nature of the LN_2 and part of it is required to prevent cavitation in the venturi throat with the cryogenic liquid. This problem of fluid cavitation with cryogenic liquids will limit the range of design conditions which are feasible with this fluid. Since the separator performance is based on particle velocity (of the entrained contaminant particles) and since the particle velocity is assumed to be close to the fluid velocity in the liquid system, it appears that the most accurate predictions can be made using inlet velocity for calculations of gaseous flow conditions and venturi throat velocity for liquid flow conditions. This arrangement should be used for all further work until the actual particle velocity is measured (by optical tests) or calculated by a separate analytical study.

The baseline separator model used for the screen blockage analysis is configured such that the bypass area around the screen trap assembly was made equal to the cross-sectional areas of the inlet duct. This arrangement will produce a velocity in the bypass area equal to the inlet velocity if one or more of the screens is completely blocked. This bypass area can be reduced (the screen diameter increased) in all cases where complete screen blockage is unlikely, since part of the fluid can go directly through the screens as secondary flow. Since the overall separator efficiency will increase as the screen diameter increases, it is desirable to use the largest screen diameter practical (small bypass area). The effects of changes in screen diameter were calculated for both the 35 mm (1.38 in) venturi and the 29 mm (1.15 in) venturi configurations. These data are shown on Figures 3-13 and 3-14. In both cases, the bypass area can be reduced significantly if the expected blockage is less than 0.9 (90 percent). Between 90 percent and 99.9 percent blockage, the separator ΔP increases rather rapidly; however, it appears that the bypass/inlet area ratio could be dropped to about 0.75 without undue pressure losses in a system flowing gaseous media. These data indicate that a secondary bleed rate of about 10 percent of the main fluid stream can be used on a regenerative separator without altering the sensitivity of the separator to change in screen blockage. The changes in

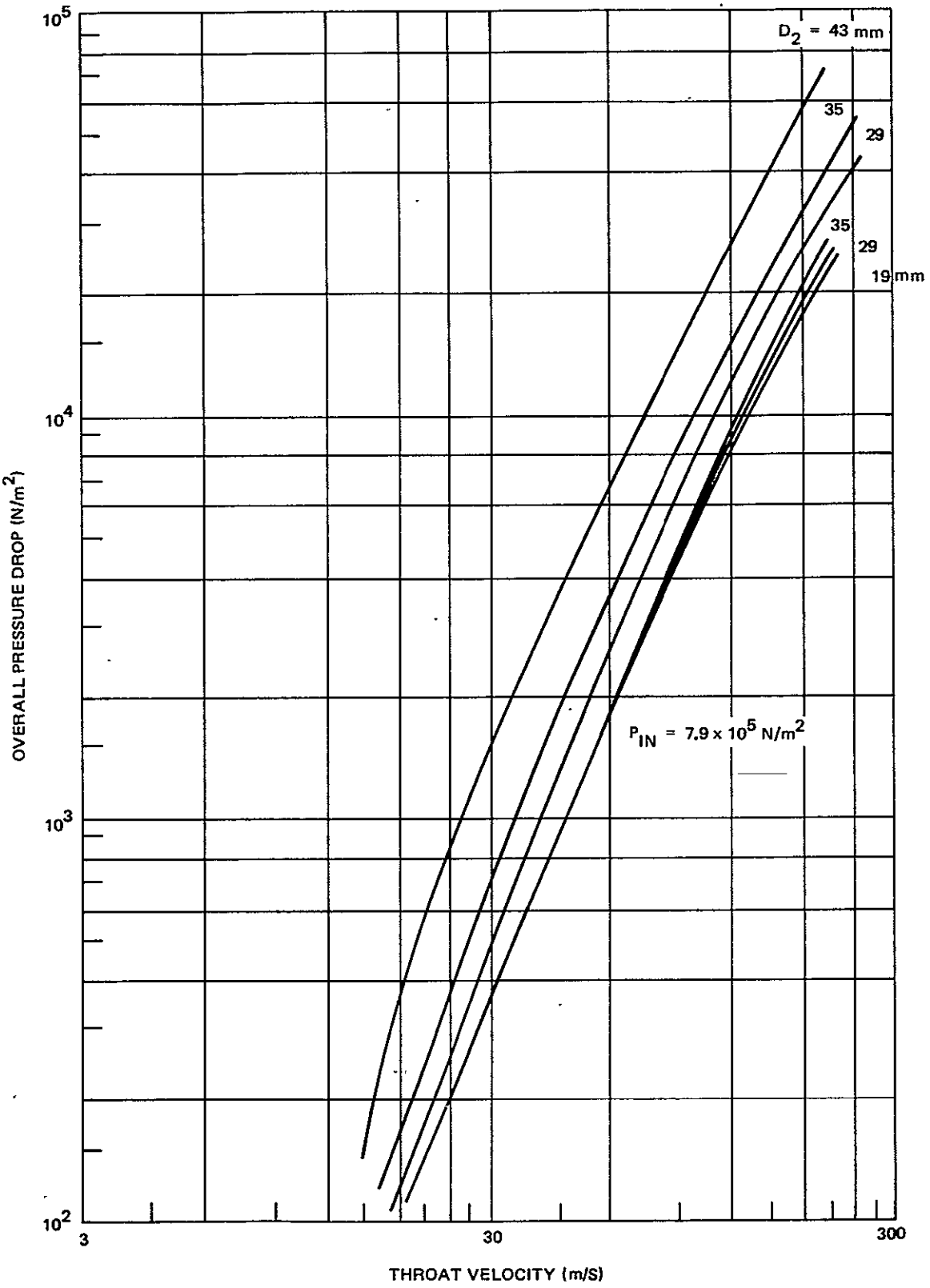

Figure 3-11. Separator Pressure Drop with GN_2 Flow

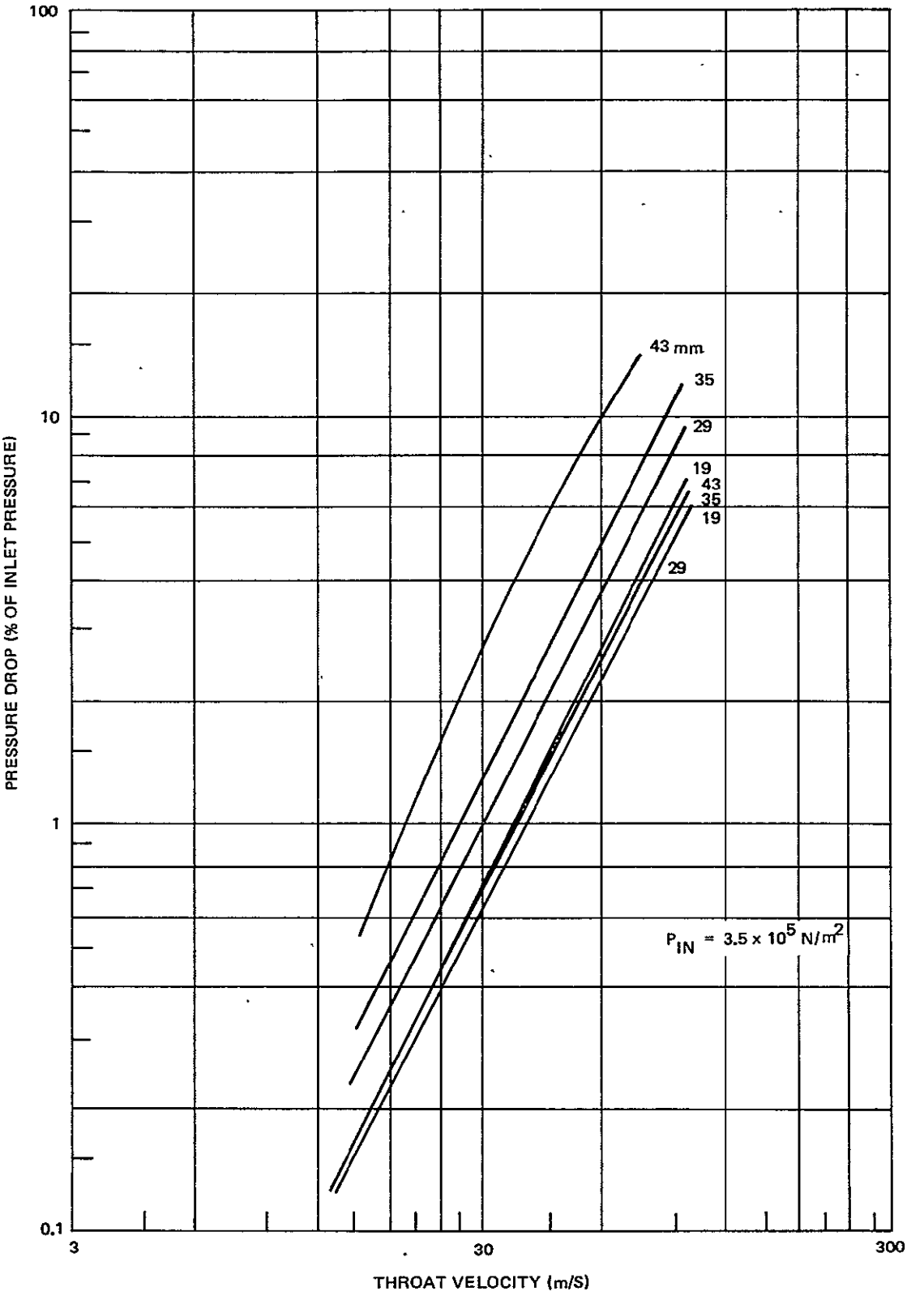

Figure 3-12. Separator Pressure Drop with LN_2 Flow

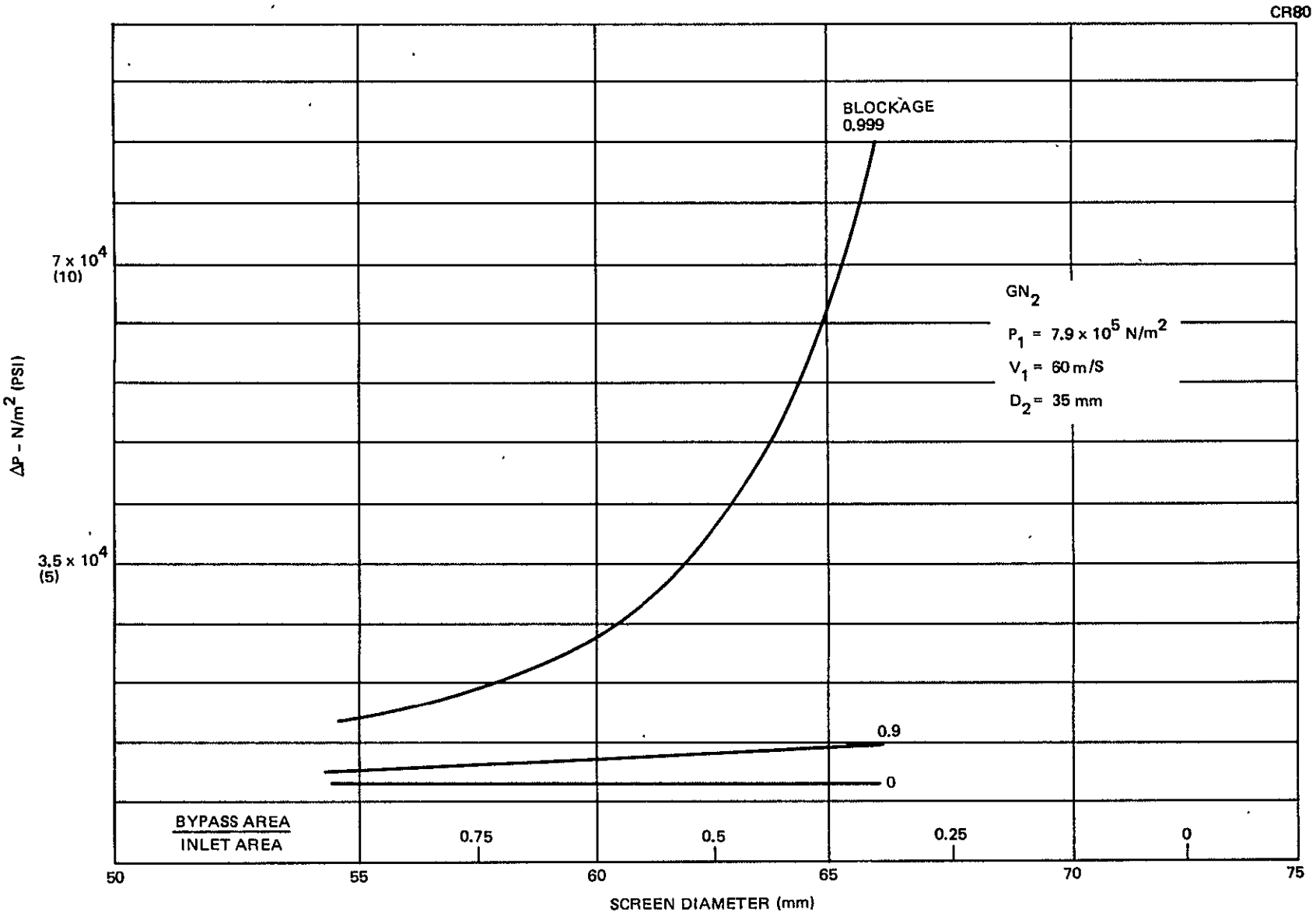

Figure 3-13. Effects of Changing Bypass Area with 35-mm Venturi (GN_2)

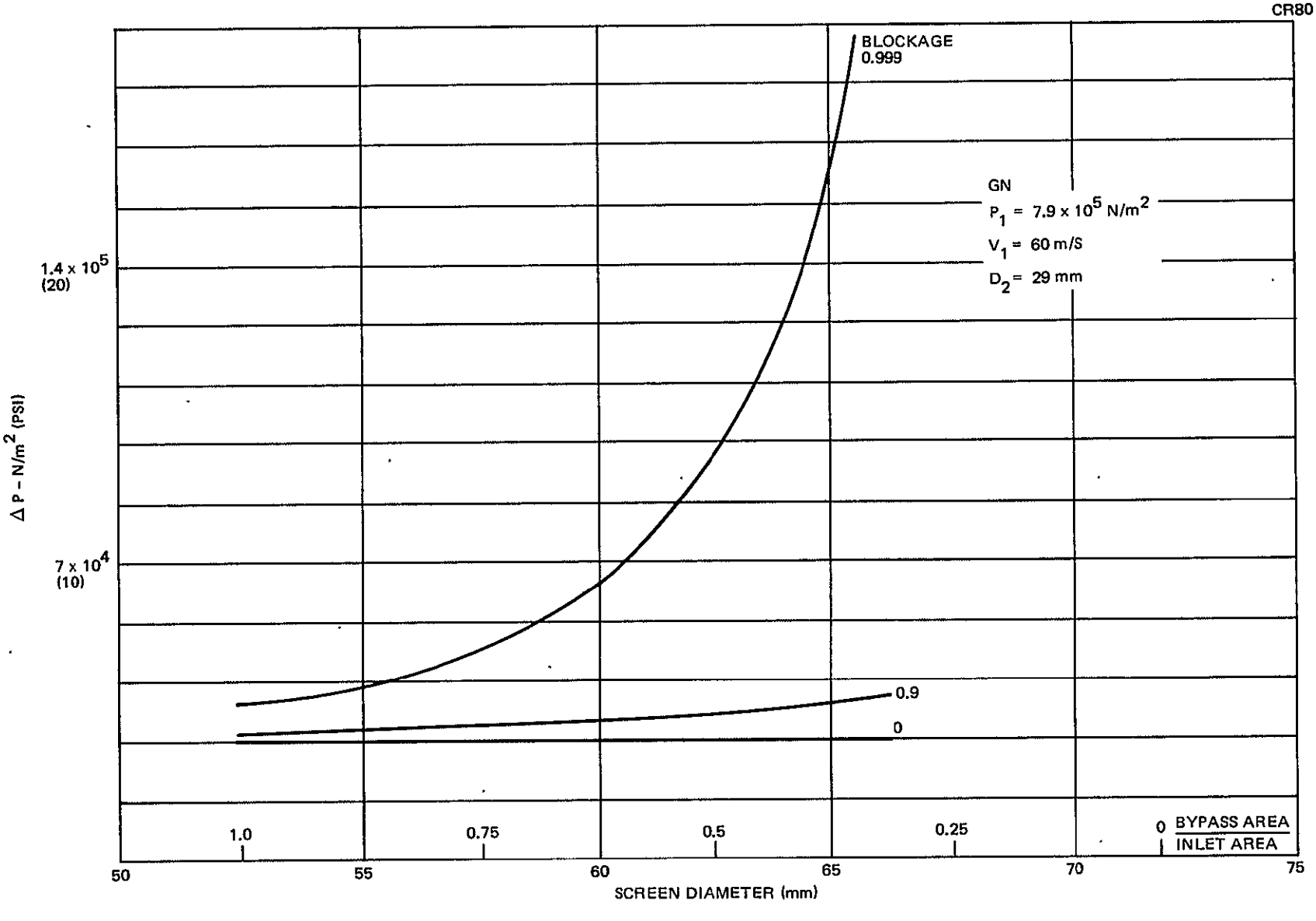

Figure 3-14. Effects of Changing Bypass Area with 29-mm Venturi (GN_2)

separator ΔP with blockages between the 90 percent and 99.9 percent value should be investigated to determine the minimum practical size for a secondary bleed on a regenerative separator model.

3.1.3 Screen Trap Design

A screen trap design study was completed. The new screen assembly (1T453 19) consisted of two to four conical screens "stacked" together as required. This screen assembly configuration was evaluated in the screen blockage analysis and its potential performance appeared to be acceptable. A number of design considerations were evaluated in selecting the 1T453 19 screen configuration. These included the following:

A. This screen design is interchangeable with the original screen assembly and can be used on the existing screen adapter plate.

B. The effects of flow oscillation will be minimized with the four screen trap assembly. Flow oscillations produce corresponding changes in particle velocity as some function of the particle acceleration characteristics and, therefore, the operating point on the performance map will change with flow oscillations. The extent of the changes in separator efficiency is a relatively complex interaction between a number of design parameters. The flow oscillations will not affect particles which are trapped in the screen trap assembly unless a complete flow reversal occurs. Without flow reversals the momentum of the secondary fluid flow (the flow which goes through the screens and not around them) should retain the particles in the screen opening.

B. The particles will not be completely retained in the new trap assembly under conditions of reverse flow. The new trap screens will exhibit the same reverse flow characteristics (for cleaning) as a conventional filter. Under conditions of reverse flow at a very high velocity (not a normal condition), the conical screens can collapse and suffer permanent physical damage. Low or moderate reverse flows will not damage the screens and can be used to partially clean the entrapped material from the screens. It should be noted that with the present separator design it is not likely that a reverse flow cleaning operation would ever be required in normal operating service; however, such an operation may be useful in the component testing portion of this program.

D. The effects of zero-g conditions on the operating characteristics of the separator is insignificant under fluid flow conditions (the separator will work somewhat better at 0-g than at 1-g) and the entrapment characteristics of the trap assembly under nonflow 0-g conditions will be improved with the addition of more screens in the trap assembly (with smaller variation between adjacent screens). Without a secondary disturbing force (such as shock, vibration, etc.), the present four-screen trap should be capable of retaining a high percentage of the entrapped particles under nonflow conditions. For operations where significant secondary forces are likely to occur and where some loss of entrapped particles cannot be permitted it will be necessary to use a regenerative type of separator with a separate particle storage provision.

E. The orientation of the separator under 1-g test conditions will not produce a noticeable effect during flow operations; however, some changes in entrapment efficiency measurements will occur under nonflow post-test conditions. Under worst-case flow conditions, it has been estimated that a 1-g side force will displace the moving particles less than 0.76 mm (0.030 in) in the proposed test model. This amount of displacement will have an insignificant effect on separation efficiency. After the completion of the fluid flow cycle there will be a tendency for the particles to fall out of the traps due to the 1-g force. If the separator is tested in the vertical position with the flow going up, the particulate fallout will be the maximum while with the flow going downward, there should be a zero fallout. By testing in the horizontal direction, a compromise was reached between the two vertical conditions and testing in the horizontal direction was accomplished on the GN_2 systems.

3.1.4 Separator Design and Fabrication

The final design of the new separator configurations was based on the results of the optical flow tests, the screen blockage analysis, and the screen trap design study. The details of the four test configurations are shown in Table 3-3 and Figure 3-15.

Figure 3-15 shows the location of the key parameters schematically. The -501 configuration is the same configuration as the -1 version tested on the original program except that the four-element screen traps are used in the new -501 configuration.

The separator parts fabricated include:

A. One 1T45363-501 Housing

B. Three 1T45361 Venturi Section

C. One 1T45362 Screen Assembly

D. One 1T45360 Adapter

Table 3-3

SEPARATOR DESIGN CONFIGURATIONS

Number	Venturi (mm)	Inlet Angle (deg)	Exit Angle (deg)	Overall Length (cm)	Screen Type
1T43824-501	35	21	9	21	60/80/150/250
1T43824-503	43	12	7		60/80/150/250
1T43824-505	19	12	9	27	60/80/150/250
1T43824-507	29	12	7		60/80/150/250

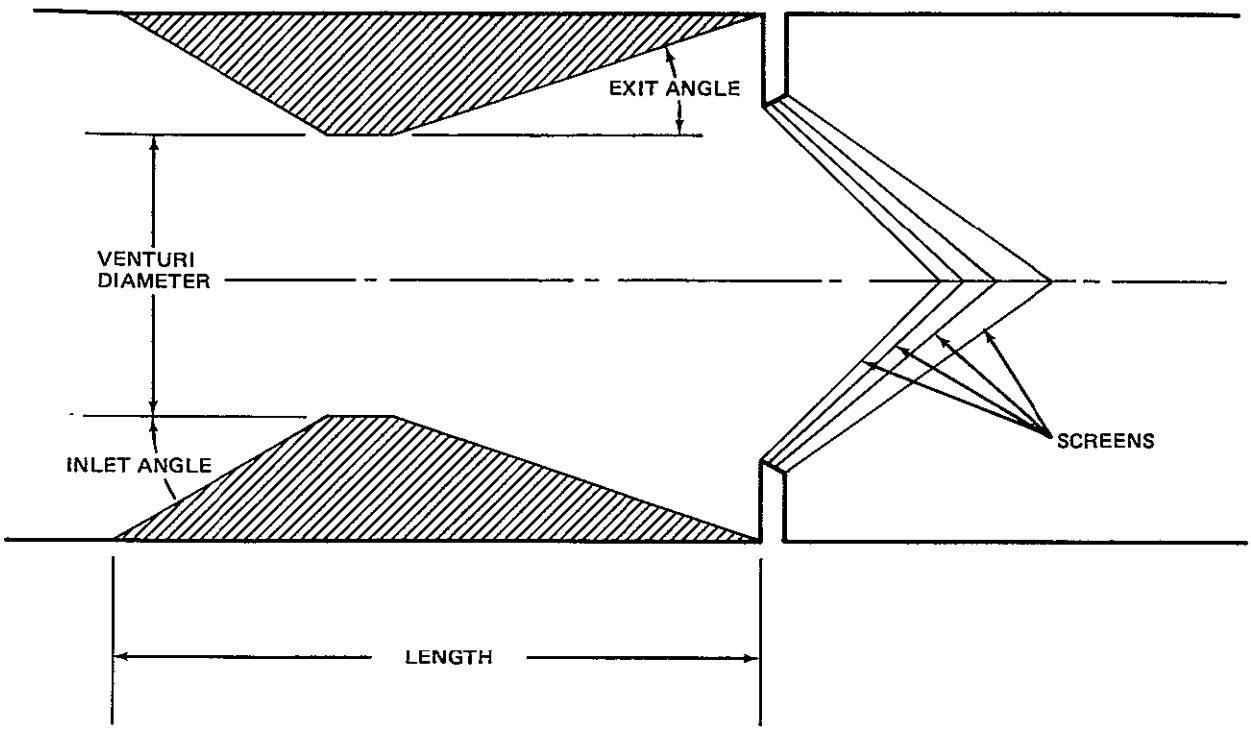

Figure 3-15. Particulate Separator Variables

With these parts the total number of pieces was sufficient to assemble two complete separator assemblies in four possible configurations such that one separator assembly was available for LN_2 testing at the same time that one assembly was available for GN_2 testing.

The design concepts used on the original 1T43824-1 were retained in the new configuration. These features included the interchangeability of venturi sections in a line-mounted housing and a demountable trap screen adapter assembly. These features were incorporated to minimize the testing time required to evaluate a number of different separator configurations. These features would not normally be incorporated in a final separator design and improved separator performance should be obtained when the test fixture compromises are eliminated.

The four designs selected were configurated to evaluate a broad range of venturi area ratios (0.375 to 0.855) while holding the other critical parameters nearly constant. It should be noted that the testing completed later in the program determined that higher separation performance should be obtained if the inlet cone angle is optimized for each venturi area ratio and not held constant.

The difficulty with the constant inlet angle is that for small venturi throat diameters a 12-deg inlet angle produces a severe overdirection of the particles (particularly in gaseous service) and the particle crossover phenomenon noted on the 2D optical tests can occur on the normal 3D unit. On future designs this particle crossover problem can be minimized by selecting the inlet cone angle such that the apex of the cone angle is located

at or near the plane of the screen trap inlet. While this arrangement will lengthen the overall separator unit in some cases, it will minimize the crossover problem and better performance should result. A complete separator assembly is shown (disassembled) in Figure 3-16.

3.1.5 Design Velocity Flow Tests

The design velocity flow tests were conducted at the A12 test facility on both gaseous (GN_2) and cryogenic liquid (LN_2) test pads. While these tests were completed on a concurrent time basis, they will be discussed separately.

3.1.5.1 Liquid Flow Tests (LN_2)

The LN_2 testing system consisted of a high-pressure test tank (HPTT), set vertically, with a bottom outlet which feeds a vertically mounted particulate separator as shown in Figures 3-17 and 3-18. The checkout runs of this system were made using the existing 1T43824-1 separator modified to incorporate the four-screen trap assembly. This new configuration (1T43824-501) uses the 35-mm venturi throat and the 21-deg inlet cone angle. This combination was expected to give a comparison between the high angle inlet cone of the original design and the newer designs using a lower inlet cone angle. The particulate injection system used on the early tests was a completely submerged LN_2 model derived from the water flow optical tests.

The preliminary test runs were conducted using an equal mix of A_1 and A_3 test powders (discussed in Appendix B). This mixture was selected so that the maximum amount of information could be obtained on each test run and hence the number of test runs could be minimized. With the use of the four-screen trap design the different sizes of test particles were stopped by different screens in the screen assembly and no one screen was overloaded with particulate; therefore, the results of the two powder tests runs should have been the same as a single powder test. The test matrix for the LN_2 design velocity tests is shown in Table 3-4.

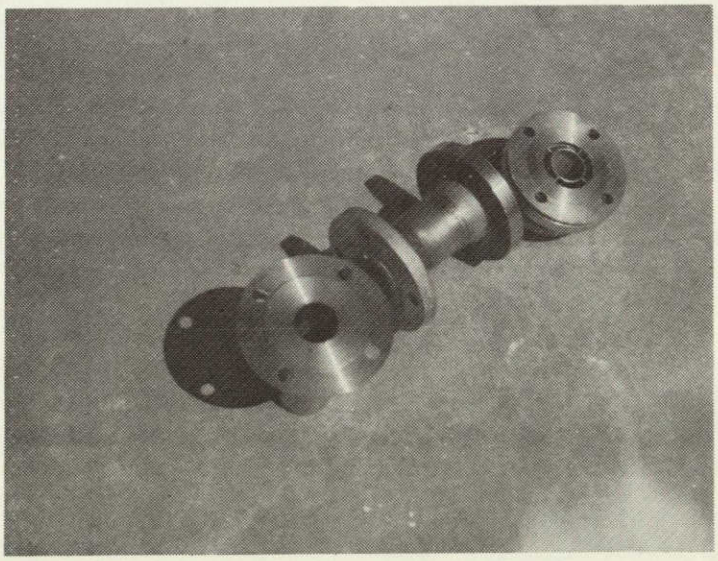

Figure 3-16. Disassembled Separator

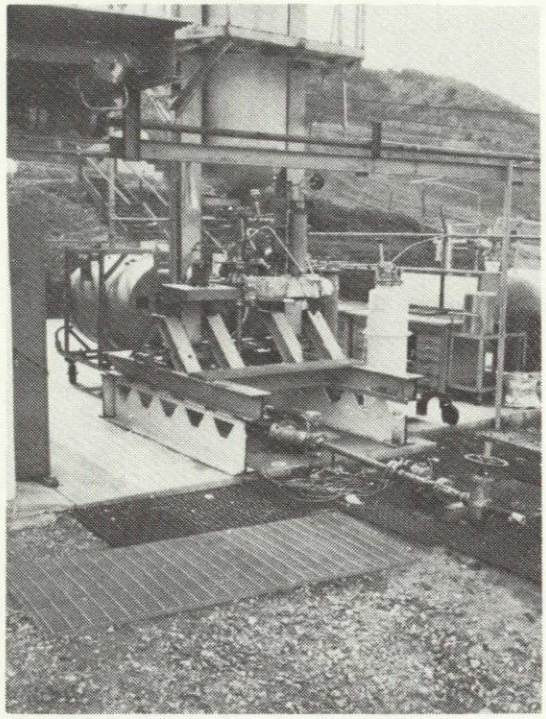

Figure 3-17. LN_2 Test System for Separator Evaluation Testing

On the first checkout run the injector failed to inject in the flow time available. This condition was corrected by increasing the orifice size in the injector assembly. On the next run the injector valve failed to open due to icing of the valve poppet. On the next run the injector iced up and no injection occurred although the injector valve operated properly. On this test run it was discovered that the fine-mesh screen in the separator trap (No. 4) had opened a seam and would not have been capable of retaining the test particulate if it had been injected. This seam failure appeared to be due to ice forming on the separator screen assembly. Two more runs were made with no separator screens installed and with the downstream filter monitored for ice formation. On both tests the downstream filter iced excessively. The entire LN_2 system and feedline were then dried in preparation for formal testing. The first formal test was completed successfully using 1.5 grams each of A_2 and A_4 test powder. The overall separator efficiency was measured at 69 percent. It should be noted that the absolute value of separator efficiency will be influenced by a number of variables, such as: (1) test method, (2) quantity of particulate injection, (3) degree of screen icing, and (4) throat cavitation. The early test runs made on the LN_2 flow stand indicated a very low separator efficiency, a wide discrepancy in finding the correct particle sizes in the correct screen traps, and in the failure to recover the total amount of particulate injected. These discrepancies were found to be due to the following two basic system problems:

A. The LN_2 flowing into the separator had a significant residual "swirl" and hence a vortex existed at the separator inlet.

B. The particulate placed in the injector was back flowing into various cavities in the injector system and after these cavities accumulated enough particulate, an uncontrolled surplus of particulate was injected into the test loop.

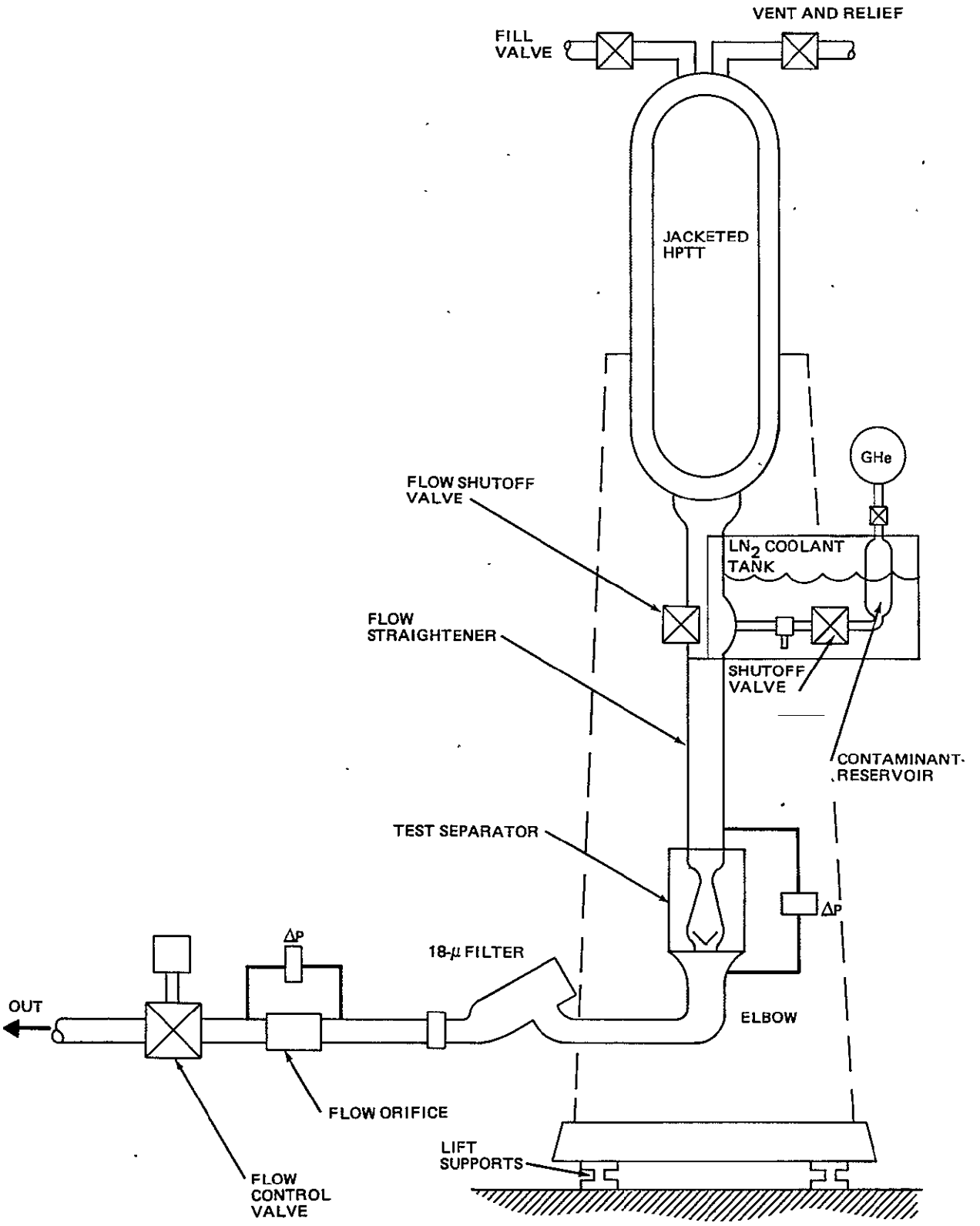

Figure 3-18. LN_2 Flow Test Setup

Table 3-4

SEPARATOR FLOW TESTS - LN_2

Run No.	Configuration	Test Powder	Run No.	Configuration	Test Powder
L 1	1T43824-505	A1	L25	1T43824-501	A1
L 2		A2	L26		A2
L 3		A3	L27		A3
L 4		A4	L28		A4
L 5		B1	L29		B1
L 6		B2	L30		B2
L 7		B3	L31		B3
L 8		B4	L32		B4
L 9		C1	L33		C1
L10		C2	L34		C2
L11		C3	L35		C3
L12		C4	L36		C4
L13	1T43824-507	A1	L37	1T43824-503	A1
L14		A2	L38		A2
L15		A3	L39		A3
L16		A4	L40		A4
L17		B1	L41		B1
L18		B2	L42		B2
L19		B3	L43		B3
L20		B4	L44		B4
L21		C1	L45		C1
L22		C2	L46		C2
L23		C3	L47		C3
L24		C4	L48		C4

The LN_2 "swirl" was corrected by placing a flow straightener in the flow passage between the test tank isolation valve and the separator inlet. The flow straightener was a simple cross type of guide vane which was approximately 20 cm (8 in) long. On the next test run a large quantity of epoxy was found in the separator screens and in the downstream filter. An examination of the straightener revealed that the "swirl" had been severe enough to bend over the leading edges of the straightener vanes and destroy the epoxy joints. A second straightener section was made from CRES with the overlapping joints brazed together. This assembly was used successfully for all additional flow tests without difficulty.

The injector design problem was found to be more difficult to correct. The injectors used on both the LN_2 and GN_2 flow test stands use the same fluid for an injector carrier fluid and for a test fluid. While this arrangement results in the least amount of flow disturbances to the test fluid, it has some practical problems in system design. The original LN_2 injector system is shown in Figure 3-19a. With this injector system some of the particulate would fall out of the carrier fluid in the injector control valve housing and injector valve leakage resulted. With this condition it is difficult to get a controlled injection of particulate.

When the injector reservoir was pressurized before the flow conditions were established in the flow line, a portion of the particulate injector fluid (and contamination) leaked into the flow at a low velocity and under these conditions the separator could not remove the particulate. When the reservoir was not pressurized until after the flow loop was pressurized, a back flow occurred through the injector system and little or no particulate was injected in the normal injector time. These problems were improved by using the revised injector system shown in Figure 3-19b. This arrangement eliminated the problem of control valve leakage; however, the particulate must still pass through the check valve during the injection operation and leakage of the check valve could result. Since the revised system was less sensitive to leakage of the check valve, this revised arrangement was installed on the LN_2 test system.

The revised LN_2 system was then used for a series of design velocity (constant velocity) separator evaluation tests. These tests were conducted using 0.5 gram of size 2 powder and 0.5 gram of size 3 powder for each test run. The small number 1 powder was deleted from these tests after it was found that some of this small powder could pass completely through the separator screen assembly under dynamic flow conditions and hence yielded misleading results. The larger No. 4 powder was eliminated after it was determined that this powder size could bounce out of the first screen in the screen trap assembly and this loss of powder from the No. 1 screen could also produce misleading results. The intermediate powders, No. 2 and No. 3, could be stopped by the two intermediate screens in the separator trap assembly and this condition minimizes the loss of test powder during the test runs and during the post-test weighing operation. A total of eight test runs were completed using the revised LN_2 test system. The data from these runs are shown on Table 3-5.

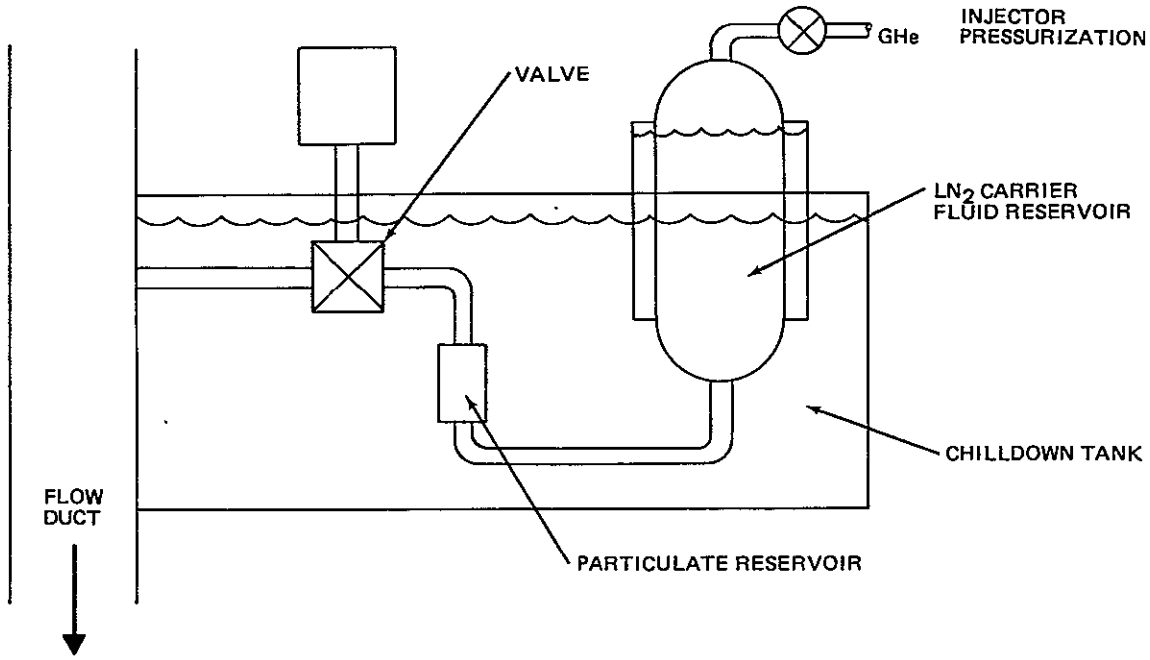

a. ORIGINAL LN_2 INJECTION SYSTEM

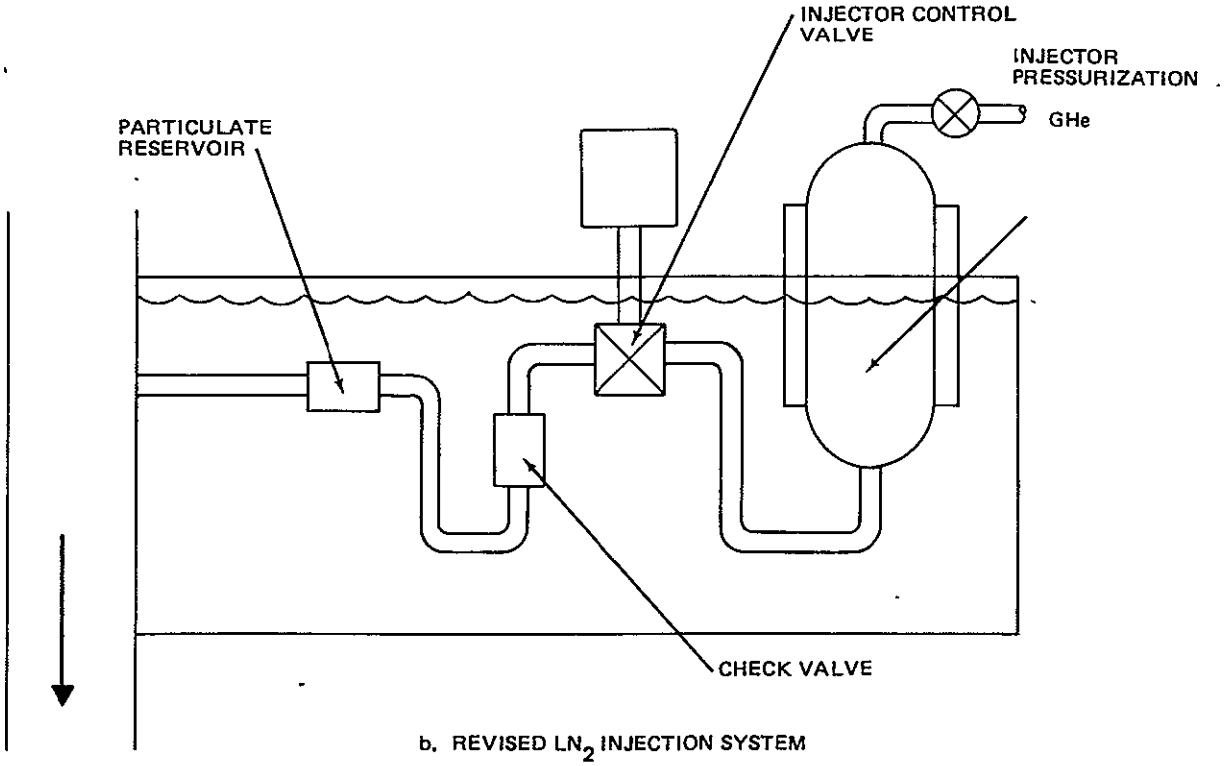

b. REVISED LN_2 INJECTION SYSTEM

Figure 3-19. LN_2 Injection Systems

Table 3-5

SEPARATOR EFFICIENCY FOR CONSTANT-VELOCITY TESTS IN LN_2 WITH SMALL TRAP SCREENS

Test Powder 0.5 Gram Each	Separator Configuration (1T43824) -501 (35mm)	-503 (43)	-505 (19)	-507 (29)
A2/A3	65	90	74	
B2/B3	63	64	60	
C2/C3	84	72		

The wide spread in the efficiency measurements obtained on the LN_2 testing indicated that the separator was not working correctly. One of the possible reasons was that premature plugging of the screens in the separator trap assembly was occurring. The trap capacity tests conducted on the GN_2 system had indicated trap capacities of 2 grams (2000 mg) or more without undue blockage of the screens. Since the separators tested in LN_2 showed low efficiencies with that quantity of test powders, a study was made to determine a worst-case condition for screen plugging. This study assumed an average particle size for each grade of powder, that all particles had the volume of a sphere and that each individual particle plugged one individual hole in the screen mesh. The final results of this study are shown in Table 3-6.

Table 3-6

MINIMUM PARTICLE WEIGHT FOR COMPLETE SCREEN PLUGGING

Powder (μm)	Weight (mg) Al_2O_3	Aluminum	CRES
1. 250	1.4	1	3
2. 150	3.8	2.8	8.1
3. 80	8.1	6	17.4
4. 60	16.5	12.3	35.7

At this stage, it was decided to investigate screen cones with increased surface area (hence increased trapping capacity) and to revise the test schedule to permit the evaluation of the new screens. The revised test schedule is shown in Table 3-7.

The revised trap arrangement consisted of a two-screen configuration. The first screen was an intermediate mesh screen (1T45319-501) from the original short design. The second screen was a new design which was twice as long as the original screen (1T45319-509) and which utilized a pleated construction. This new screen configuration is shown in Figure 3-20.

Two versions of the new design were fabricated. The first version (1T45319-507) was made from 250 x 250 square mesh screen. A second version (1T45319-509) was made of 50 x 250 Dutch weave screen material. Both of these new designs had the same filtration rating but did not have the same flow resistance. To evaluate these differences in flow resistance, a test run was made with each configuration under the conditions shown for L13. The results of these tests are shown in Table 3-8. Since the square mesh screen performed slightly better than the Dutch weave version, the square mesh was selected for further testing.

The data shown on the separator performance tables are all in a consistent format. The weight of test powder recovered from each screen in the trap assembly is listed separately by number. Since either two or four screens were usually used, the weights for No. 1 and 2 or No. 1, 2, 3, and 4 are shown. The amount of particulate recovered from the downstream filter is shown under the filter heading. The overall efficiency is determined by dividing the combined weight recovered in the trap screens by the total weight of powder recovered in the trap screens and the downstream filter. The losses incurred in the recovery and weighing process were usually less than 10 percent, and hence the combined weight in the trap assembly and the filter was usually over 90 percent of the total injected.

The remaining tests in the LN_2 test series were completed using the pleated screens (4.5×10^{-2} m^2, or 70 in^2, area). The results from this test series are shown in Table 3-8 and Figure 3-21. A comparison between the data obtained with the small trap screens (shown on Table 3-5) and the large pleated screens shows some interesting features. With the 35 mm venturi configuration, a somewhat higher efficiency was obtained with the pleated screens; however, this improvement was not very large. With the large 43 mm venturi, the absolute efficiency values measured were about the same for both screen sizes; however, the response to particle density was theoretically correct for the large screen and completely random for the small screen version. Based on the slight efficiency improvement and the more predictable response to particle density, it appears that the larger screen area is somewhat better than were the original small screens. However, it appears that other factors, particularly the variations in inlet cone angle and the cryogenic boiloff effects of the present test method, play a significant role in the LN_2 flow tests. Optimization of the inlet cone angle should minimize the overdirecting problem and thus permit a more comprehensive evaluation of the capacity of the screen traps in the cryogenic liquid system. Both optimization of the inlet cone angle and verification of the trap capacity are needed before a realistic separator design can be configured for service on an operational vehicle.

These data indicate that the 19 mm venturi encountered overdirection of particles and hence somewhat erratic operation. The first test made with the very small venturi produced results which indicate that the separator venturi throat was the smallest orifice in the flow loop and was acting as a cavitating venturi throttle. To correct this situation, a number of outlet (plug) orifices were designed to produce the desired flowrate in the flow system. The second outlet orifice tested produced the desired 0.53 m^3 per minute flowrate. This flowrate gives the desired throat velocity of approximately 30 m/s; however, since the area ratio for this venturi is so high (A_1/A_T = 7), the inlet velocity in the flow duct was low. This low inlet velocity could produce flow discontinuities for the fluid and the particles, and this condition would magnify the overdirecting characteristics of this venturi. While these difficulties can be minimized by modifying the inlet cone approach area, this method of approach was not covered on this contract.

Table 3-7

SEPARATOR FLOW TESTS - LN_2

Run No.	Configuration	Test Powder	Run No.	Configuration	Test Powder
L1	1T43824-501	A2	L13	1T43824-505*	A2/A3
L2		A3	L14		B2/B3
L3		B2	L15		CX2
L4		B3	L16	1T43824-507*	A2/A3
L5		C2	L17		B2/B3
L6		C3	L18		CX2
L7	1T43824-503	A2	L19	1T43824-501*	A2/A3
L8		A3	L20		B2/B3
L9		B2	L21		CX2
L10		B3	L22	1T43824-503*	A2/A3
L11		C2	L23		B2/B3
L12		C3	L24		CX2

NOTE: These tests were run with two powders injected per test. These are A2/A3, B2/B3, and C2/C3.

* Pleated Screen Trap Assembly
Test L13 was run with both a square weave and a Dutch Twill weave. Tests L14-24 were run with the screen design found best on test L13

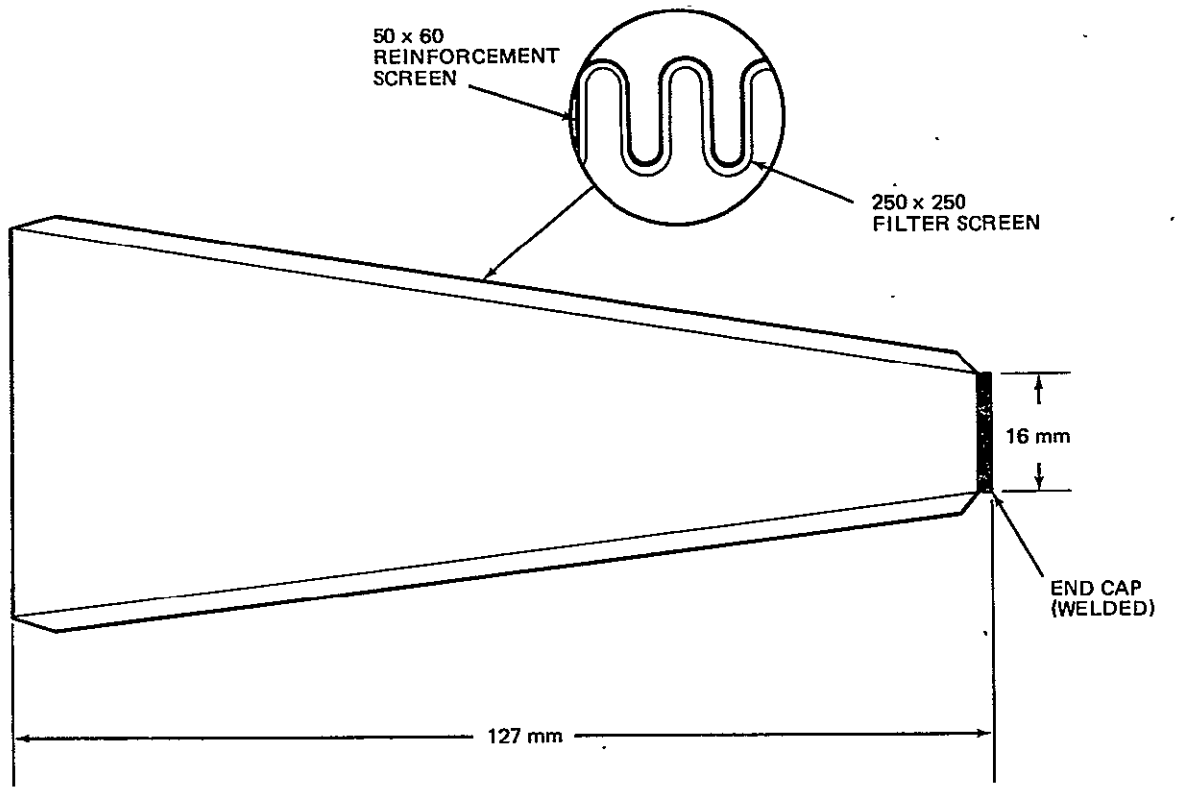

Figure 3-20. Design of Pleated 4.5 x 10^{-2} m^2 (70 in^2) Screen

The performance of the three larger venturis was more representative of the performance expected with this separator design and the trap screen with a 4.5 x 10^{-2} m^2 (70 in^2) flow area appears to be sufficient for the quantity of test power used for these tests. As anticipated, the heavier CX_2 stainless steel particles require less direction from the venturi when compared to the lighter Al_2O_3 and aluminum particles. It should be noted that the tests with the smaller venturis were made with a longer preinjection LN_2 flow to minimize the cryogenic boiloff problem with this test system; however, the data obtained may still reflect some degree of flow disturbances from the fluid boiloff and higher efficiencies may be possible under other flow conditions. The extent of the cryogenic boiloff on the separator efficiency could be evaluated by repeating this test series using water as a flow medium; however, time and funding limitations did not permit such testing on this program. The design velocity testing completed indicated that particle separation can be achieved efficiently in a cryogenic flow with the separator design principles being evaluated.

3.1.5.2 Gaseous Flow Tests (GN_2)

The test setup of the GN_2 flow tests was installed on the Unit 1, Pad 1 test area at the A12 facility. This setup is similar to and shared a number of components with the test setup used on the previous contract and on the Task II effort on this program. The test setup is shown schematically in Figure 3-22 and the actual installation is shown in Figure 3-23. The test system is an open-loop – blowdown type of system which can test full-size

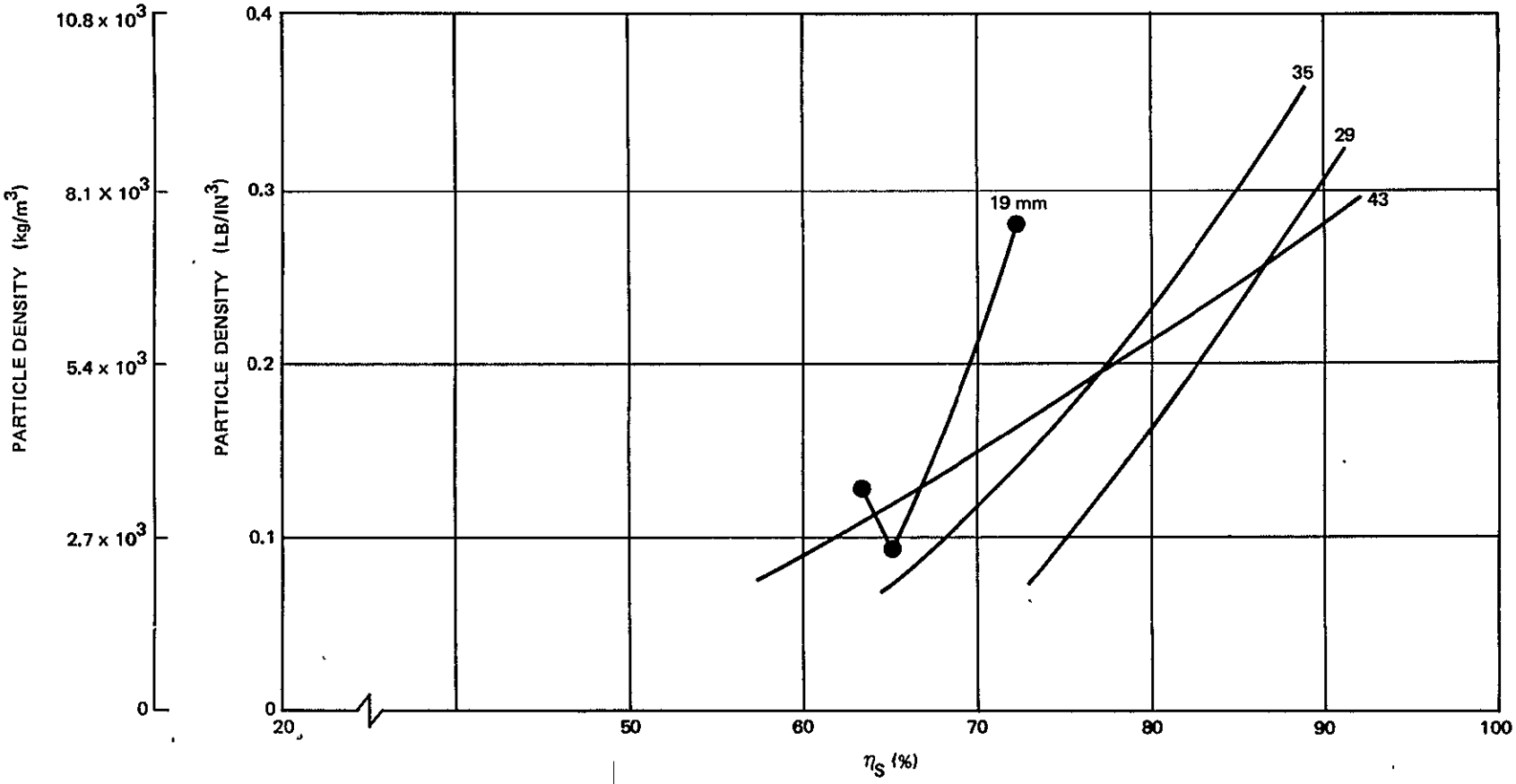

Figure 3-21. LN_2 with Pleated Screen

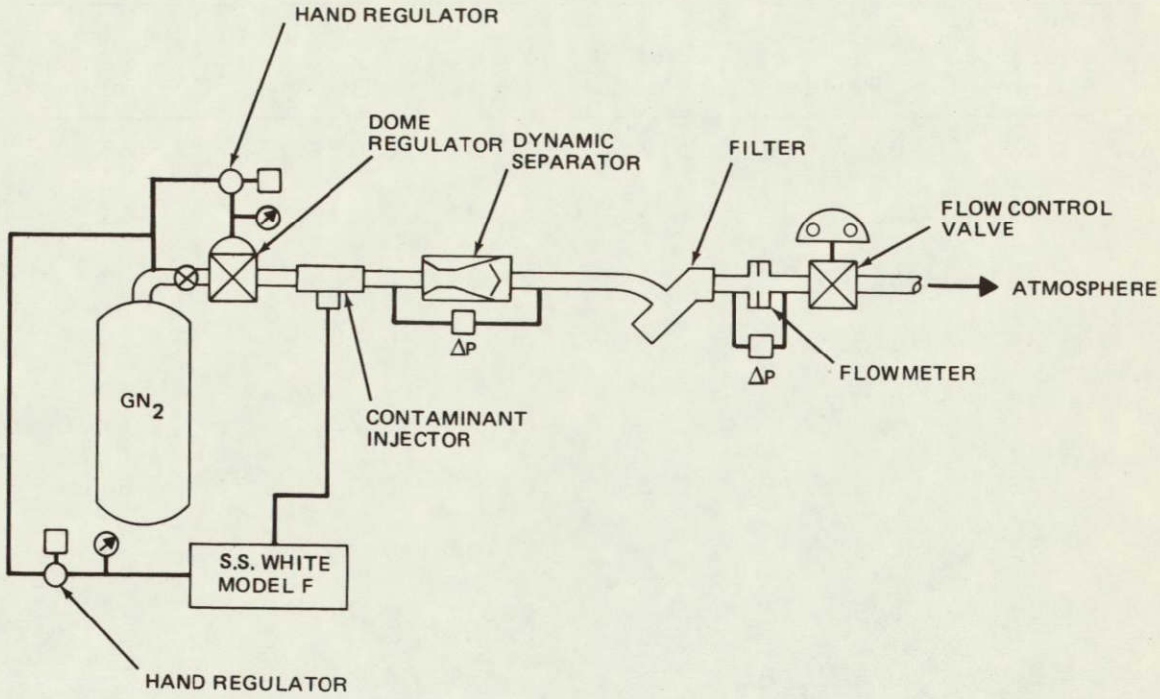

Figure 3-22. GN_2 Flow Test Setup

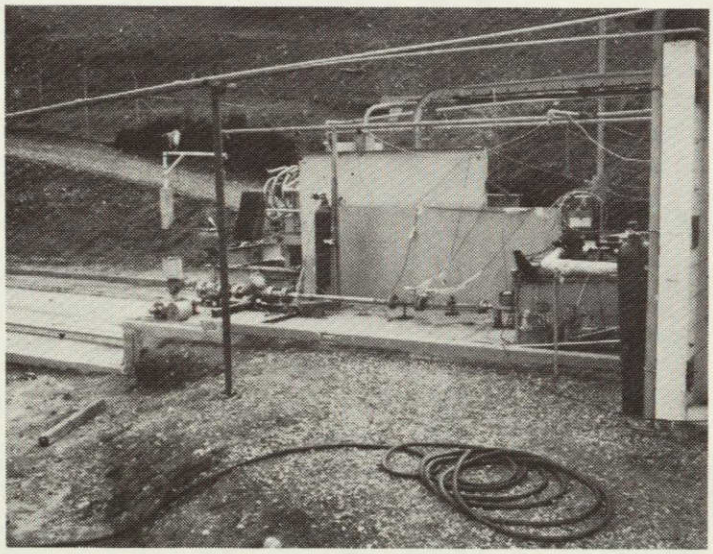

Figure 3-23. GN_2 Test Setup

Table 3-8

SEPARATOR PERFORMANCE IN LN_2 WITH LARGE PLEATED SCREEN

Run No.	Venturi Diameter (mm)	Powder	Weight No. 1	Weight No. 2	Filter	η Efficiency (%)
L13A	43	0.5 A_2/A_3	0.274	0.238	0.257	66
L13B	43	0.5 A_2/A_3	0.335	0.222	0.319	63
L14	43	0.5 B_2/B_3	0.384	0.194	0.386	60
L15	43	1 CX_2	0.016	0.876	0.094	90
L16	35	0.5 A_2/A_3		0.580	0.234	71
L17	35	0.5 B_2/B_3	0.230	0.376	0.316	66
L18	35	1 CX_2		0.792	0.163	83
L19	29	0.5 A_2/A_3		0.617	0.191	76
L20	29	0.5 B_2/B_3		0.655	0.212	75
L21	29	1 CX_2		0.831	0.110	88
L22	19	0.5 A_2/A_3		0.590	0.352	63
L23	19	0.5 B_2/B_3		0.565	0.300	65
L24	19	1 CX_2		0.714	0.271	72

components at representative flowrates. The original test setup utilized a flow control valve in the main flow section to control the mass flowrate through the test specimen. A series of flow calibration runs were completed as the first step of the design velocity runs and the flow control valve was adjusted to the flowrate which gave a 30-m/s inlet velocity into the test separator. After this original setting was made the flow control valve was left in this baseline position for all steady flow design velocity tests. While this arrangement resulted in a slight variation in the inlet velocities obtained with the different venturi throat combinations, this variation was smaller than the variation obtained by trying to reset the flow control valve for each different configuration. (Note: It was determined later during the off-design velocity tests that the separator is very insensitive to small changes in inlet velocity and either type of testing would have been equally valid.)

The primary difference in the GN_2 test setup used on these tests and on the previous work was in the gas storage system. The former GN_2 high-pressure storage system was not available for this program so a new two-reservoir system was installed for these tests.

The checkout and calibration runs of the GN_2 system were conducted concurrently with the LN_2 testing. Since the GN_2 system required less time to prepare for a test run (no chilldown time and post-test warmup time), this system was used to evaluate potential improvements in the test method. Test runs were made using the 1T43824-505 separator (19-mm venturi). Tests were conducted with two different inlet flow conditions with three different injector locations. The injector configuration selected was a GN_2 version of the LN_2 system and not the S. S. White unit used previously. This change was made to provide better control of the amount of particulate injected on each test run. A short test series was run to determine the amount of particulate which could be injected without overloading the trap screens in the separator. Values of between 50 and 82 percent efficiency were measured on this preliminary trap capacity test. The high efficiency being obtained with about 1 gram of particles being injected and the lower values obtained with 4 grams or more of injectant. A value of 2 to 3 grams of total injectant powder, composed of equal amounts of two powder sizes appeared to be the optimum combination for the determination of comparative separator performance.

The gaseous flow test system encountered the same difficulties as those experienced on the liquid system. These difficulties were improved substantially by incorporating both a flow straightener and the revised injector system. The design velocity tests were then completed using a dual powder test procedure. With this method, two different sizes of test powders were injected on each test run. The two powders injected (on each test) were in different size categories and were sufficiently different in size to be stopped on different separator screens. The tests were run using sizes 1 and 3 together and sizes 2 and 4 together. The data obtained on the GN_2 design velocity is shown in Table 3-9. These test data reveal that under the dynamic conditions of operation of the separator a significant portion of the particles pass through the screen meshes which have openings that are smaller in diameter than are the particles. This failure to trap the injected particles in the correct screen mesh was probably due to a combination of three factors:

A. The screen material expands under dynamic loading conditions and the openings become larger.

B. Some of the particles fracture on impact under these velocities.

C. Some of the particles were long and thin and would wedge their way through the screens at high velocity but would not pass through a corresponding screen on the particle grading machine. This is particularly true of the CRES powder (C1 to C4).

Table 3-9

SEPARATOR EFFICIENCY FOR CONSTANT-VELOCITY TESTS IN GN_2

Test Powder (0.5 Gram Each)	Separator Configuration (1T43824)			
	-501	-503	-505	-507
A1/A3	93	93	89	88
A2/A4	84	90	62	85
B1/B3	87	90	54	77
B2/B4	87	91	58	72
C1/C3	83	89	82	75
C2/C4	80	88	83	75

These effects are reflected in the measured separator efficiencies but they are not significant on an absolute basis if the range of screen sizes in the separator trap is changed to account for these size effects. The separator efficiency values (of over 90 percent) measured on these tests were very encouraging and these data are of value in selecting a final separator configuration.

The data shown in Table 3-9 are also presented in Figure 3-24 in a slightly different form. This curve shows the overall separator efficiency as a function of the venturi area ratio. It will be noted that the largest venturi throat (43-mm diameter -503) gives a consistently high separator performance while the very small venturi throat (19 mm -505) gives a wide spread in measured efficiency. This characteristic indicates that the very small venturi section is overdirecting the particles under the test conditions and depending on the density (and mass) of the contamination particles, these overdirected particles may or may not be directed into the correct flow path. This characteristic was detected earlier on the optical flow test and this information led to the reduction of the inlet cone angle from 21 to 12 deg in the newer separation configuration. Since the particle crossover potential (overdirecting) improves as the venturi throat diameter increases and the venturi inlet cone angle decreases, it should be possible to optimize a given separator design to fit a given set of flow conditions. To evaluate the effects of particle crossover further, two extra test runs were made with the venturi sections removed from the separators. In this case, the 50.8-mm inlet duct connected directly to the 76-mm separator housing and the difference in diameters of these two sections provides the only particle direction in the test.

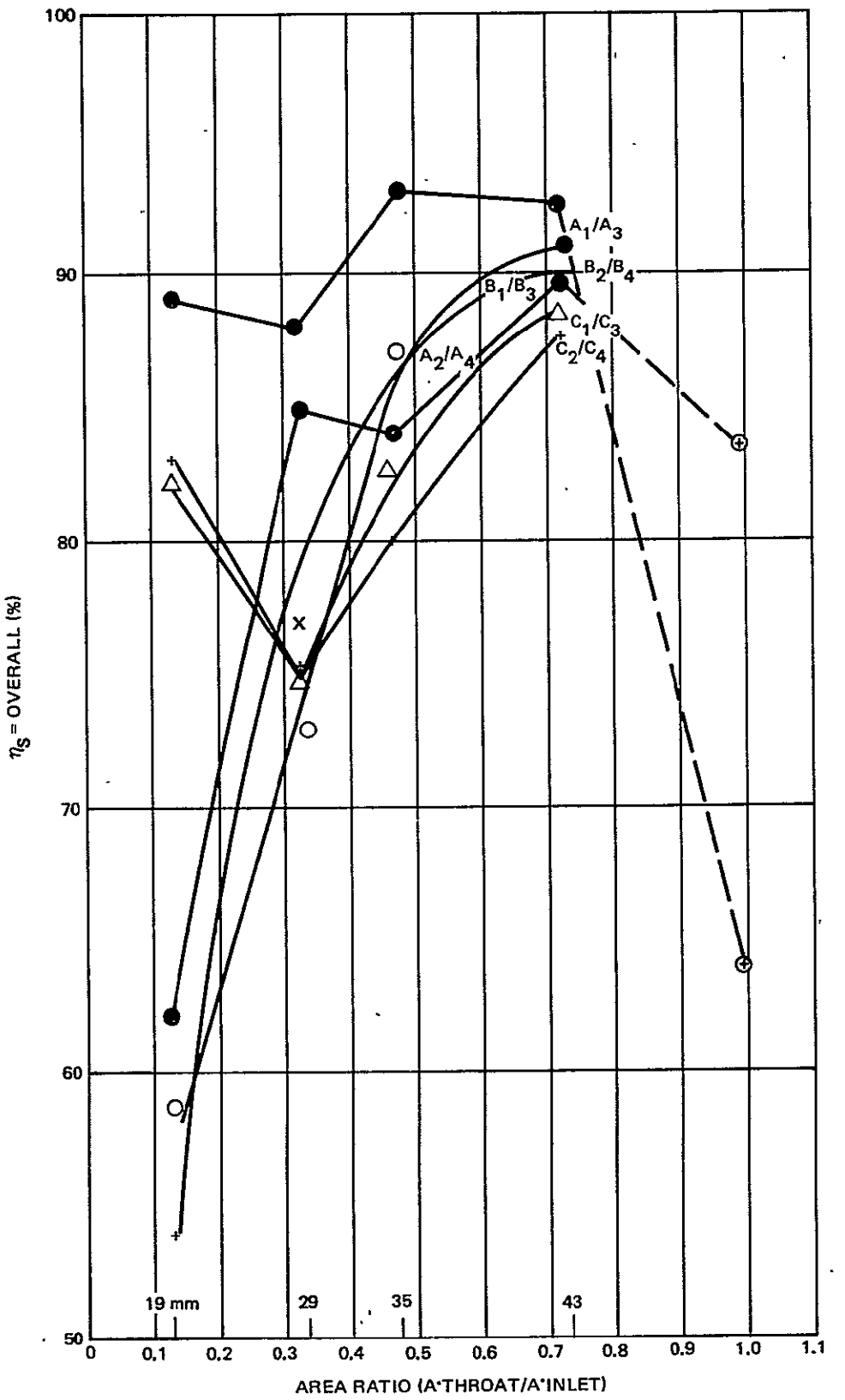

Figure 3-24. Separator Characteristics in GN_2 at 30 m/s

These two tests were made using the lighter A2 powder and the heavier A3 powder. These test points are plotted on Figure 3-24 at the area ratio = 1.0 position and the dotted lines added to connect the points to the curve which correspond to the closest test conditions. Under these conditions, it is seen that the underdirected (Ar-1.0) condition is reasonably efficient for the lightweight powder; however, the performance drops significantly for the heavier (No. 3) powder and is almost as low as the values obtained with the overdirected (-505) configuration. It is also interesting to note the comparative performance of the -501 (At = 0.43) and the -507 (At = 0.33). In this case, the -507 has a 12-deg inlet cone angle while the -501 has a 21-deg inlet cone angle.

However, the larger throat diameter of the -501 configuration appears to overcome the inlet angle drawback in most cases. It further appears that the overdirection can be so severe that the particles bounce off of the opposite side and back into the flow stream and hence bring the separator back to the higher efficiency levels obtained when no overdirection occurs. This condition appears to have occurred on three of the test runs made with the very small -505 configuration and two of the test runs with the -507 version.

It appears from the data obtained on the GN_2 tests that if the density difference is great enough between the flowing media and the contamination particles, the directing requirement is minimized and the original particle flow trajectory correction is sufficient to direct the particles into the separator trap area. Hence, the venturi throat area ratios can be made fairly close to the ratio of one to one without difficulty. With the particle densities tested in GN_2, it appears that an area ratio of 0.7 to 0.9 can be used effectively under these conditions. Since these high area ratios also produce the least flow losses, a very efficient separation system can be designed. It would be expected that as the difference in density between the contamination and flow stream decreases, this characteristic will also decrease and the separator will become more sensitive to the particle turning angle.

There was enough time available to conduct additional separator tests in the GN_2 flow system (concurrent with the LN_2 runs). To utilize this time efficiently, a complete test series was made with the large pleated screens. The data from these tests are shown in Table 3-10. These data indicate that the trap design (screen area) is not a limitation on the GN_2 flow at the contaminant level of 1 gram powder per test and under these conditions the separator performance is controlled by the venturi director design, flow loop parameters, etc.

3.1.6 Off-Design Velocity Tests

Two off-design velocity tests were made in the GN_2 system using the -503 and -507 configurations. These tests were made using 1 gram of contaminant powder per run and tested with both the A2 and A3 powders for each velocity. The flow velocity was controlled by installing a fixed restrictor orifice at the exit to the flow loop and then opening the normal flow control valve to a wide

Table 3-10

SEPARATOR PERFORMANCE IN GN_2 WITH PLEATED SCREEN TRAP

Run No.	Venturi Diameter (mm)	Powder	Weight No. 1	Weight No. 2	Filter	$\eta_{Efficiency}$ (%)
GP1	43	0.5 A_2/A_3	0.163	0.693	0.145	86
GP2	43	0.5 B_2/B_3	0.141	0.654	0.079	91
GP3	43	1 CX_2	0.005	0.679	0.190	78
GP4	35	0.5 A_2/A_3	0.121	0.639	0.205	79
GP5	35	0.5 B_2/B_3	0.227	0.555	0.235	78
GP6	35	1 CX_2	0.002	0.673	0.236	74
GP7	19	0.5 A_2/A_3	0.080	0.741	0.132	86
GP8	19	0.5 B_2/B_3	0.152	0.486	0.303	68
GP9	19	1 CX_2	0.002	0.665	0.275	71
GP10	29	0.5 A_2/A_3	0.147	0.685	0.183	83
GP11	29	0.5 B_2/B_3	0.150	0.390	0.303	64
GP12	29	1 CX_2	0.001	0.683	0.227	75

open position. The fixed restriction orifices were made from standard tube fittings and were modified to provide the theoretically correct orifice area for the desired flow velocity. While the actual flow velocity obtained with these orifices may vary slightly from the theoretical flow velocity, the repeatability of corresponding test points is excellent and good test data was obtained.

The results of the off-design velocity tests are shown in Table 3-11 and in Figure 3-25. It should be noted that the separator with the large-diameter venturi (43 mm -503) shows a high overall efficiency over the complete 15 to 90 m/s flow velocity range while the small venturi throat model (29 mm -507) shows greater sensitivity to off-design velocity changes. The corresponding throat velocity ranges for these tests were 20 to 125 m/s in the -503 and 50 to 275 m/s for the -507 model. The off-design sensitivity of the more severe area change of the -507 separator is reasonable. However, the peak efficiency at the design velocity conditions should have been considerably better than was achieved on these tests. This relatively low efficiency at design velocity conditions with the -507 separator appears to be the result of the particle crossover phenomenon discussed previously and this condition should improve with further changes in the inlet cone angle of this unit.

Table 3-11

OFF-DESIGN VELOCITY TESTS

Flow Velocity (m/s)	-503 (43 mm)		-507 (29 mm)	
	A2	A3	A2	A3
15	91	88	85	83
22.5	93	88	89	85
30	92	92	88	80
45	92	87	92	84
90	91	88	82	80

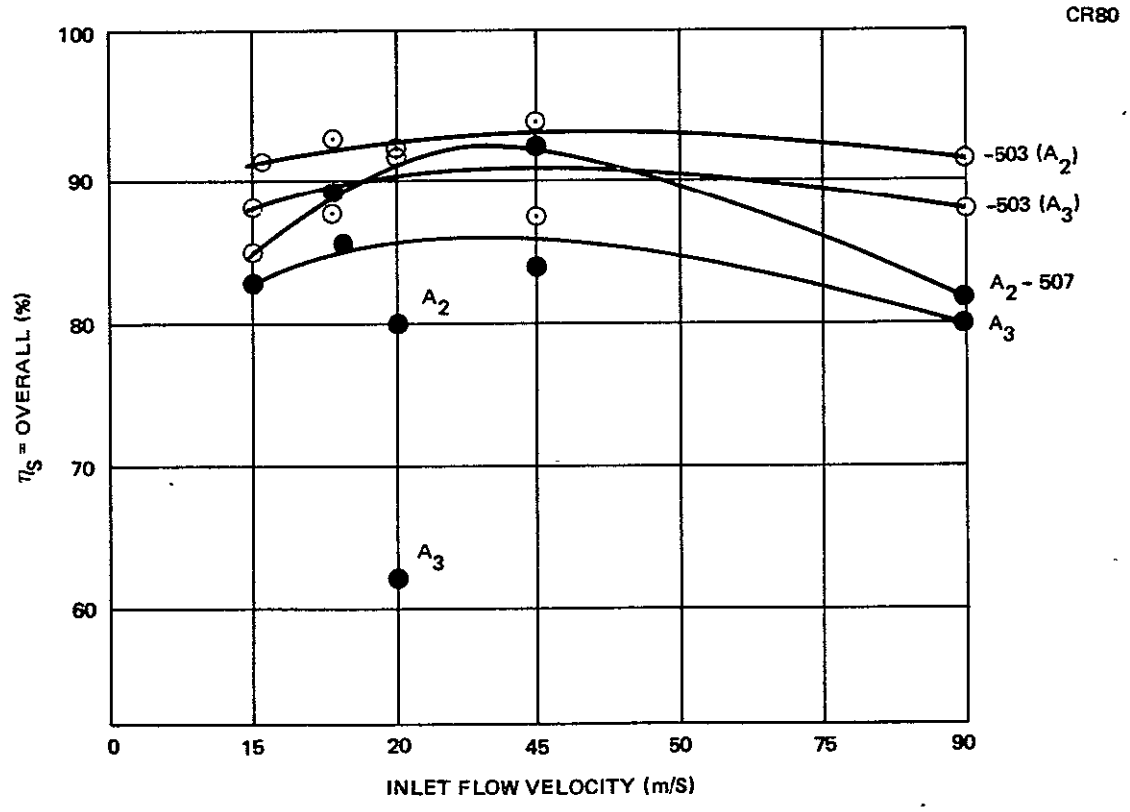

Figure 3-25. Separator Performance at Various Velocities Injector Directed Downstream

3.1.7 Trap Capacity Tests

The total amount of particulate which can be stored in the screen trap assembly is one of the key design parameters for the particulate separator. Also, the rate of efficiency dropoff with increases in the quantity of stored particulate is important to separator design. These two factors were investigated on the GN_2 test system using both the small 4.5×10^{-3} m^2 size of screens and the larger 4.5×10^{-2} m^2 size of pleated screen. The design velocity flow tests in both gaseous and liquid systems indicated that a completely different limitation to storage capacity exists between the two systems. The high momentum of the liquid system will keep almost all of the particulate pressed against the screen material and little or no fallout of these trapped particles occurs while the fluid is flowing. Under these conditions the capacity of the simple fixed trap is a function of the number of openings in the most critical screen wire. The criticality of these screens is determined by the type, size, and grading of the particulate being tested. With the liquid system the capacity of the trap assembly is a function of the surface area (and number of openings) of the screens used in the trap assembly. The characteristics in the gaseous system are somewhat different than those of the liquid system. The low momentum of the gases is insufficient to lock the particles on the surface of the screen cones. Therefore, the particles can fall out and settle in the enclosed volume between adjacent screens. Since a greater number of particles can be stored in the enclosed volume before a significant flow restriction is encountered, the trap capacity is considerably greater in the gaseous operating mode than in the liquid operating mode.

The separator efficiency is more difficult to predict in the volume filling mode (gaseous flow) so the trap capacity tests were conducted in the GN_2 flow loop. These tests were accomplished by injecting total quantities of from 0.5 to 6 grams of 50/50 mix of A2 and A3 test powders per test run. The injection was made in a single operation (in the same time period) on each test and therefore the particulate flowrate was considerably greater on the runs made with the larger total quantity of particulate. This characteristic was a function of the type of injection system used and does not represent an ideal condition. Ideally, the injection rate should be held constant during the test runs and the length of injection time changed to control the total quantity of material injected. However, the operation of such a system is difficult and the design of such a system was not undertaken on this program.

The results of the trap capacity tests are shown on Figure 3-26. These tests were made with the 1T43824-503 configuration (43-mm venturi) which was the best combination tested in the GN_2 design velocity tests. The range of quantities tested cover a moderate to severe condition for a 50.8-mm line size separator. The 6 grams of test powder represents a value of something greater than 1.6×10^8 particles per injection.

While the quantities of particulate selected for these tests represent a convenient figure for test purposes, it is unlikely that these quantities of contaminants would be encountered in a closed propellant system on a future space vehicle. Hence the small screen design would appear to be adequate for normal use in a gaseous system and may or may not be acceptable in a liquid flow system.

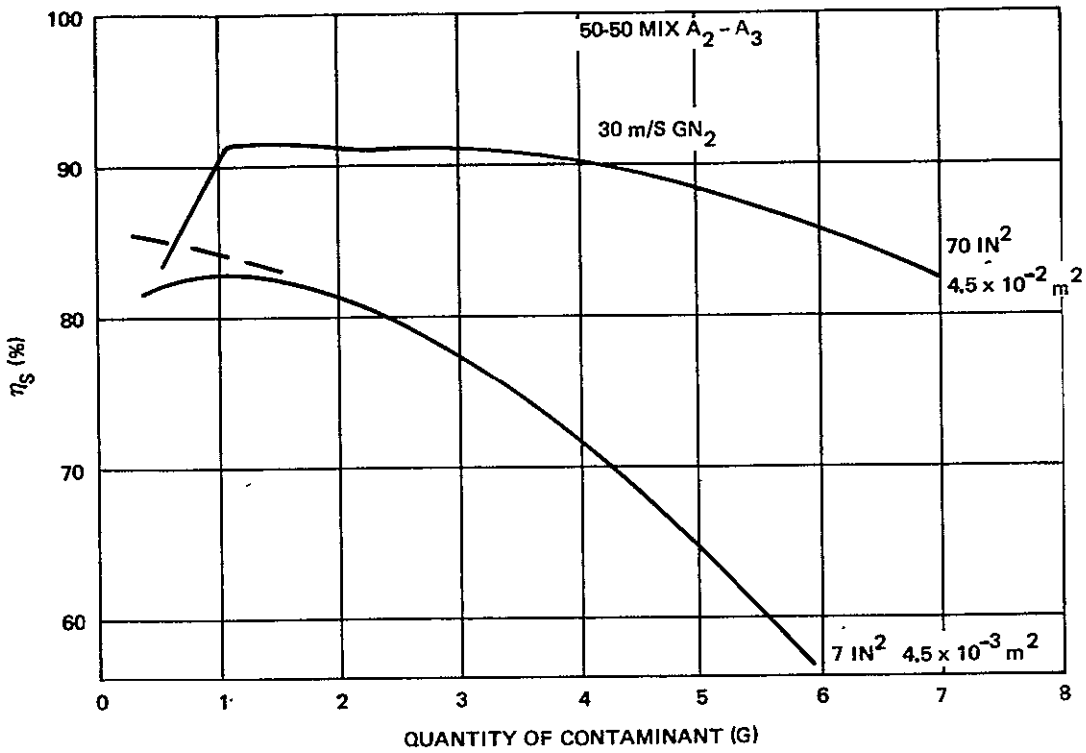

Figure 3-26. Trap Capacity Nonregenerative (Side Injection)

In any case it appears that a pleated screen wire assembly of 3.2×10^{-2} to 4.5×10^{-2} m^2 area should be acceptable in a normal liquid system in a 50.8-mm line size. The area of the screens should be scaled in the direct proportion to the line size for future systems.

3.1.8 Regenerative Separator Evaluation

A regenerative separator is a device which has self-cleaning capabilities. One method of accomplishing regeneration on the 1T43824 type of dynamic separator can be obtained by providing a particulate removal passage from the contaminant storage area of the trap screen assembly to an overboard particulate storage area. The secondary overboard storage area can be mounted remotely from the in-line separator, can be of unlimited size, can incorporate easy cleaning provision, and can be connected in such a way that the regenerative carrier propellant can be returned to the main flow duct after the particulate has been removed in the secondary particulate storage area.

A simple version of a regenerative separator is shown in Figure 3-27a. The success of this system depends upon the ability of a regenerative design to maintain a secondary fluid flow across the trap assembly (to prevent a stagnation pressure buildup at the trap inlet) while still providing a usable regenerative flow stream to the external particulate collection device. Peak operating efficiency of the regenerative system will be obtained when the fluid flow bypassed through the regenerative system is the lowest amount that can be bypassed with no pressure buildup on the main trap assembly.

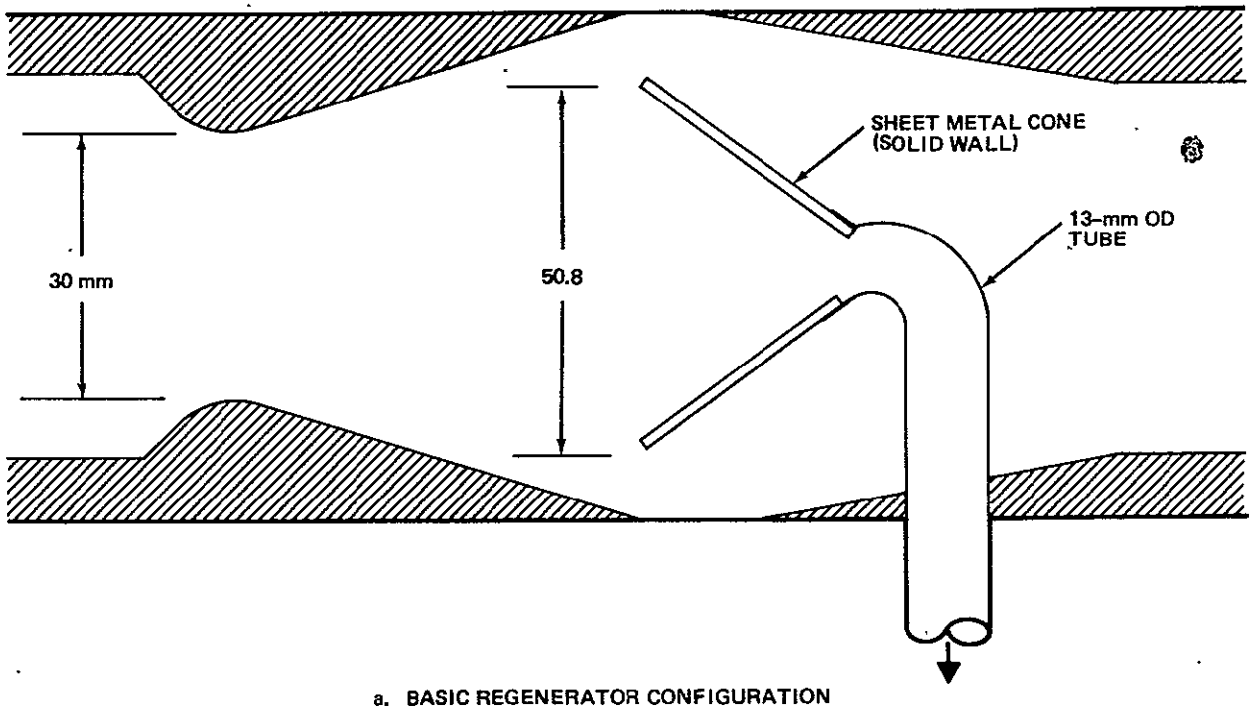

a. BASIC REGENERATOR CONFIGURATION

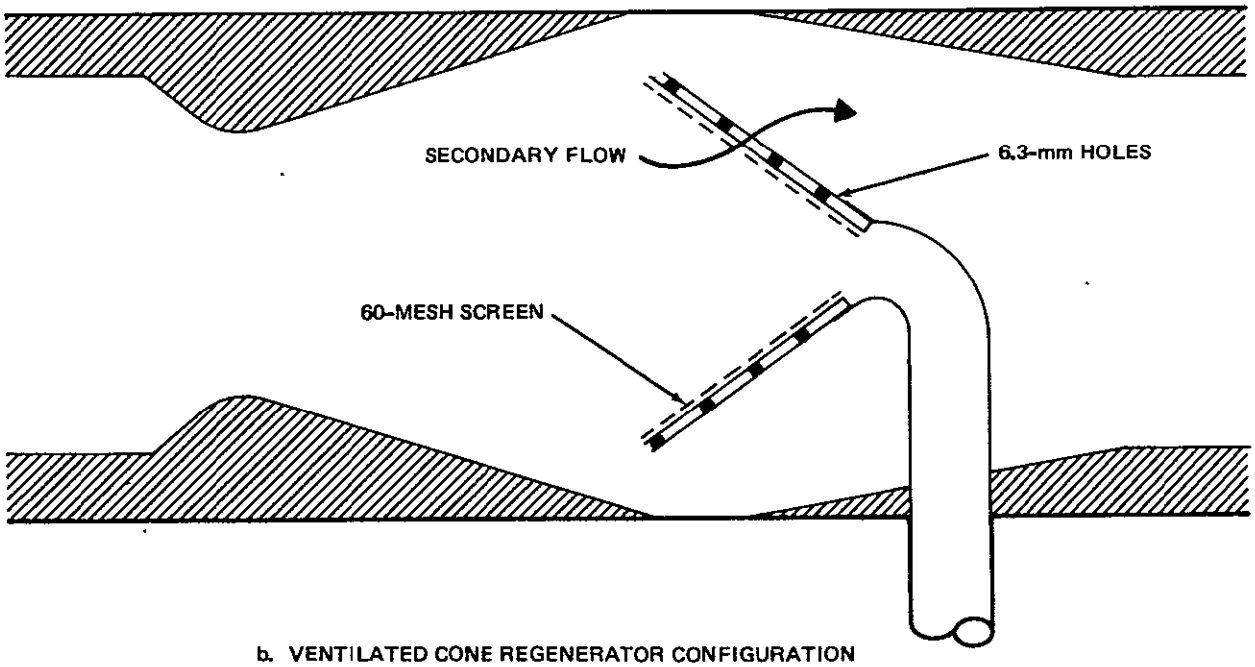

b. VENTILATED CONE REGENERATOR CONFIGURATION

Figure 3-27. Regenerative Trap Arrangement

Since the flow restrictions through the entire regenerative bypass system affect the stagnation pressure buildup at the trap assembly inlet, the selection of the sizing of this bypass system is not straightforward. Further, the required secondary flow may consist of the regenerative carrier fluid, a direct secondary bleed flow through a screen assembly, or a combination of both. To obtain a preliminary indication of the probable requirements for the secondary flow quantity and the corresponding separator efficiency a baseline regenerative test model was designed. This regenerative system was designed to fit into the existing set of test adapters and therefore was geometrically similar to the nonregenerative multiple screen trap arrangement. The first regenerative configuration was made by adding a single solid wall sheet metal cone in the position formerly occupied by the four-screen trap cones and then connecting a 13-mm O. D. tube to the apex of the cone. This tube was selected to provide a secondary flow bleed system and as a duct to carry the particulate through an externally mounted filter system and then to return the filtered bypass fluid back into the main flow duct. This arrangement is shown on Figure 3-28. This version of a regenerative system incorporates equal areas of the trap cone inlet and the surrounding annulus bypass area. The theorical bleed flowrate was approximately 2 percent of the total flow (neglecting flow resistance in the external filter and flow line). A single test run was made with this arrangement in the LN_2 flow loop. A total of 2 grams of Al_2O_3 particles was injected during this test run. The test particulate consisted of 0.5 gram each of the A_1, A_2, A_3, and A_4 sizes. The separation efficiency measured was approximately 10 percent and this value indicates an almost complete loss of secondary flow (and hence almost all of the fluid/particles were diverted around the trap assembly). Since the basic design concept of the separator has a wide latitude in responding to changes in design variables,

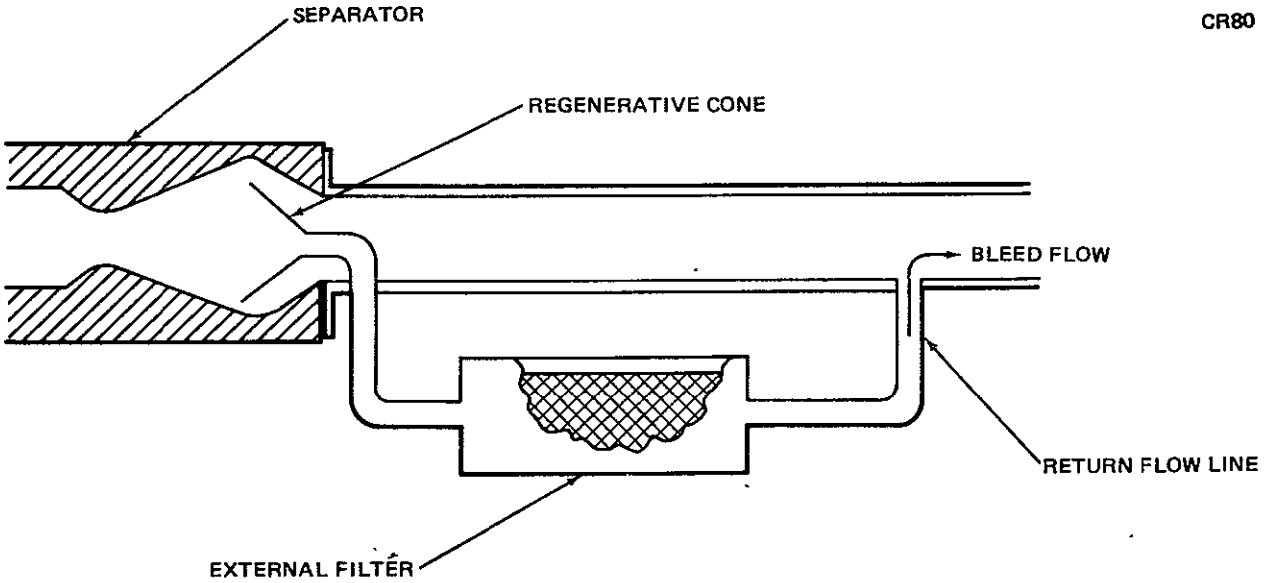

Figure 3-28. Regenerative Separator Installation

a number of methods were available which could produce a normal separator operation in a cryogenic fluid system. However, the relative improvement of each design change will require evaluation before an optimum system can be designed. The basic separator design criteria indicates that the overall separation efficiency should vary as a function of the density of the contamination particles.

A modification was then made to the regenerative trap to improve the performance of this arrangement. The solid cone wall of the trap cone was drilled in a number of places with a 6.3 mm drill and then an existing screen assembly was installed in the cone as shown in Figure 3-29. This arrangement increases the secondary flow through the trap and reduces the stagnation pressure buildup in the trap assembly. This modification was tested in the LN_2 system and some improvement in performance was noted. However, the performance was still very low and external flow restriction in the regenerative bleed tube was still indicated. Since this high flow restriction was most likely due to LN_2 boiloff in the regenerative bleed tube, the regenerative system was moved to the GN_2 test system. A series of test runs were made with the regenerative system. The results of these GN_2 regenerative runs were much better than those obtained in the LN_2 runs and this tends to confirm the LN_2 boiloff problem with the cryogenic liquid. The overall separator efficiencies measured with the GN_2 regenerative system was in the 65 to 88 percent range as shown on Table 3-12.

CR80

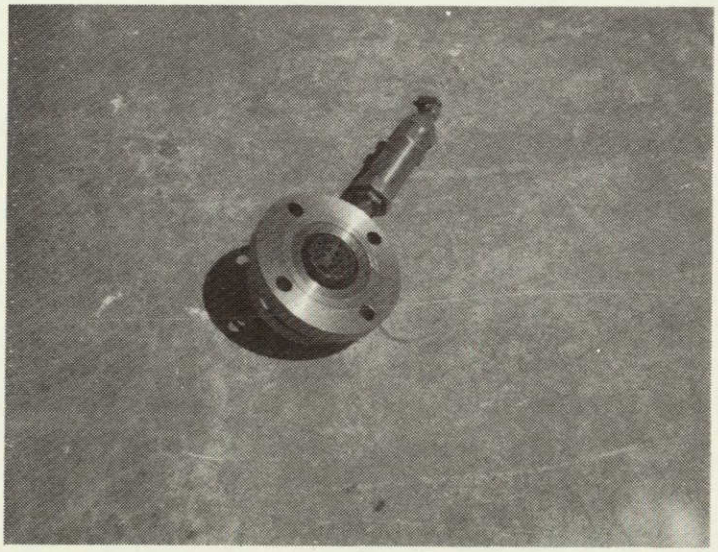

Figure 3-29. Regenerative Cone Installed in Separator Adapter

Table 3-12

SEPARATOR PERFORMANCE IN GN_2 WITH REGENERATION TRAP

Run No.	Venturi Diameter (mm)	Powder	Weight No. 1	Weight No. 2	Filter	η Efficiency (%)
R1	29	0.5 A_2/A_3		0.61	0.24	72
R2	29	1 CX_2		0.555	0.297	65
R3	19	0.5 A_2/A_3		0.764	0.206	78
R4	19	1 CX_2		0.631	0.290	68
R5	19	0.5 B_2/B_3		0.736	0.244	75
R6	35	0.5 A_2/A_3		0.807	0.192	81
R7	35	0.5 B_2/B_3		0.740	0.273	74
R8	35	1 CX_2		0.655	0.295	69
R9	43	0.5 A_2/A_3		0.885	0.137	88
R10	43	0.5 B_2/B_3		0.883	0.120	88
R11	43	1 CX_2		0.755	0.210	78

The difficulties encountered on the regenerative system on a cryogenic setup appear to be due primarily to the thermal conditioning difficulties of the external bleed system of the regenerator. Since the total run time possible with the existing open-loop system was limited to less than a minute of total flow, it was not possible to obtain thermal equilibrium for the external bleed system used on these tests. The amount of time required to reach stable thermal conditions could have been reduced significantly by providing a completely jacketed regenerative bleed system. However, the fabrication of such a system would have been out of the scope of the program and was not attempted on this effort. The encouraging results obtained with the regenerator in the GN_2 system indicates that this approach deserves further considerations and a detailed study of the regenerative system for cryogenic service should be considered on future investigations.

3.1.9 Analysis and Interpretation of Results

The analysis and testing completed on this effort were undertaken to verify or modify the original assumption used in the generation of a generalized performance map for dynamic particulate separators (Figure 3-3) and to demonstrate that the predicted performance can be obtained in actual operation.

The results obtained on this program indicate that the general principles utilized in the design of the particulate separator are valid and the use of these principles will lead to a successful separator design; however, the number of test variables encountered prevented the accurate assessment of the original assumptions. Hence, the original performance map establishes a set of useful guidelines for separator design which is configured to meet a fixed set of requirements. With a real separator design it is difficult to select a single fixed point which represents the apex of the triangle that reflects the turning angle of a given particle. The original assumption was that the particles left the venturi throat in an axial direction and with the particle traveling the same velocity as the fluid in the venturi throat area. The testing completed to date indicates that the inlet cone angle establishes the direction that a particle is traveling at the venturi throat exit and that small changes in this angle can produce significant changes in the particle trajectory at the venturi throat exit. To establish an optimum inlet cone angle for a given set of conditions it is necessary that the throat exit velocity of the particle is known. However, since the rate of change in the inlet cross-sectional area will have a significant effect on the degree of acceleration experienced by the particles as they pass through the inlet section a difficult analytical problem is encountered. This can be seen from the fact that the optimum inlet angle cannot be selected without knowing the particle velocity and the particle velocity cannot be determined without knowing the inlet cone angle. To complicate the matter further the particle velocity (acceleration) will be influenced by the shape of the particles and in the real world the particles tend to have random shapes.

While it is easier to assume spherical shaped particles for analytical calculations (than to account for a number of different random shapes) and to obtain special spherical metallic particles for testing purposes, neither of these considerations reflect the most probable condition in a real vehicle system. The test powders used for the majority of these tests (Al_2O_3) are difficult to size grade, tend to splinter on impact, and probably have a wide variation in drag coefficient. Notwithstanding these difficulties, a number of tests were completed with measured efficiencies at 90 percent or higher. Since some test powder may have splintered on impact (and therefore pass through the smallest screen mesh in the trap assembly) and since some loss of powder occurs in the collection and weighing procedures, it appears that a properly configured separator of the 180-deg venturi type can operate at high separation efficiencies at design velocity conditions. Since many aerospace fluid systems are designed to operate at (or near) a specific flowrate, the use of this particulate separator design could greatly minimize the potential problem of component damage and failure for particulate contamination damage.

It appears that the inlet cone section operates as a particle accelerating device and as a mechanical director. While the degree of acceleration required for a specific separator should account for the drag coefficient of the particles and this function can best be handled by a computer program, the inlet cone angle can be specified on the basis of a mechanical director. Based on the work completed on this program, the following guidelines can be established for separator design.

A. The inlet cone angle should be selected such that a line extending from the surface of the inlet cone will intersect the inlet to the particulate trap assembly within the middle half of the trap inlet area.

B. The venturi throat ratio should be kept to the minimum which can be used for the particular combination of fluid density/particle density. Relatively mild area ratios are satisfactory for large density differences (metal particles in gaseous or light liquid flow), while more severe area ratios will be needed for satisfactory performance with small density ratio conditions (light particles in liquid flow).

C. The projected area of the trap inlet can be made somewhat larger than the inlet area without undue pressure losses as long as an adequate secondary flow is maintained. The oversized trap (undersized bypass) will work better in gaseous flow system than in liquid flow conditions.

D. The venturi area ratio should be selected in such a manner that throat cavitation in the venturi is minimized. While fluid cavitation in the throat may not have a significant effect on the separation efficiency, it may produce a serious pressure loss and can limit the fluid flow through the system.

The specific results observed in this task include:

A. The two-dimensional flow models will not duplicate a three-dimensional model accurately; however, qualitative data can be obtained with the 2D optical testing.

B. The trajectories of shiny particles can be recorded optically with photographic equipment, and these data could be used to measure the actual acceleration (and peak particle velocity) of random shaped particles passing through a venturi section.

C. The 180-deg venturi type of particulate separator can be configured to work effectively in both liquid and gaseous flow systems; however, the optimum configurations will be different for each fluid.

D. The difference in density between the particle and the flowing fluid has a significant effect on the separator configuration which produces the highest performance. With a large difference in density (heavy particle-light fluid), the flow velocity through the separator can change over a rather broad range (50 to 300 percent) with little change in separation efficiency.

E. The capacity of the multiple conical screen trapping arrangement will vary to some extent depending on the momentum of the fluid in the system. A nonregenerative trap assembly which has enough openings in the mesh of the smallest screen to handle the total amount of particulate wedge into the screen mesh (area) will operate satisfactorily under all normal conditions with both liquid and gaseous flow media.

F. A regenerative trap assembly can be incorporated into the 180-deg venturi separator if the quantity of particulate to be separated is too

large for a practical size of fixed screen. The regenerative design will require a configuration which can maintain an adequate secondary flow through the trap assembly under all operating conditions. Further work will be required to establish the amount of secondary flow needed to meet a given set of particulate quantity requirements.

G. A refinement in the particulate injector design such that a controlled injection rate can be achieved without a flow disturbing effect on the main fluid flow would improve the accuracy of testing particulate separator in a full-size, open-loop test system.

3.2 TASK II – VALVE CONTAMINATION TOLERANCE TESTING

One method of improving the tolerance to contamination damage of propellant shutoff valves consists of applying a material on the critical sealing interfaces which is soft enough to embed contamination particles and hard enough to operate reliably for a specified number of operating cycles. This valve design concept requires that the sealing interfaces be located so that direct particle impingement is minimized and that provision is made to prevent particle retention at the critical sealing interface. The investigations of these design concepts were initiated on Contract NAS3-14375 and reported in Reference 1. The previous work covered the use of hard and soft gold plating on the sealing interfaces and the use of a conventional polyimide film (Teflon S) as a plastic coating material. The success obtained on the previous program indicated that further improvements could be obtained by incorporating additional modifications to the basic poppet and seat sealing interface design and with the utilization of thicker plastic films on these critical sealing surfaces. The thin films used on the previous work were found to be acceptable for service with particles of 75 microns or smaller and with marginal performance with particles in the 75 to 230 micron range. The thicker plastic films used on the present program were used to increase the tolerance of the valve to particles in the 125 to 420 micron range. The improvements made in this program have extended the particle size range which the valve will tolerate such that the present design appears to offer acceptable service with particles of 230 microns or less and marginal performance with particles in the 230 to 420 micron range. One coating material evaluated appears to be acceptable with particles in the 230 to 420 micron range; however, the cryogenic tolerance of this material has not been established for coating applications.

The present test work was conducted using GH_2 at ambient temperatures. The materials tested consisted of thin plastic coatings of:

A. Teflon S in multiple layers and with a chemical preclean surface treatment.

B. Xylon 1010 in multiple layers.

C. Kynar 207/202 in a single thick (0.254 mm-0.010 in) layer.

The contamination tolerance testing consisted of a series of 10 valve cyclic tests (valve fully opened and closed) at full-flow conditions. The contamination particles used for these tests consisted of size-graded Al_2O_3 particles

in the 125 to 230 micron size range and in the 230 to 420 micron range. The particles were injected at a continuous rate while the valve was cycled for at least five complete cycles at 1 Hz. The total number of cycles per test was determined by the actual rate of particulate injection and not less than 5 cycles of operation and 2 grams of particulate injection was accomplished for each test.

3.2.1 Component Design Evaluation

The design approach used to improve the tolerance of a typical propellant shutoff valve to damage from contamination particles consisted of minimizing the exposure of the critical sealing surfaces to particulate impacts and to provide a special coating on the sealing surfaces which could embed those particles which get trapped at the sealing surface interface.

To reduce the exposure of the sealing surfaces to contamination impact and entrapment a number of design modifications have been made to the 1T32095 valve. The original valve design utilized a flat-faced poppet and a raised seal sealing surface as shown in Figure 3-30a and discussed in Reference 2. The work on the original contract determined that this arrangement was susceptible to severe erosional damage from contamination particles and the sealing interface was modified as shown in Figure 3-30b. This modification cured the erosion problem but did not provide a contamination trap zone for catching the particles which were displaced from the sealing area during the self-cleaning portion of the valve closing cycle. These particulate trap grooves were incorporated into the valve design tested on this program. The final design configuration is shown in Figure 3-30c. The final design still retains the close-fitting alignment bumper which allows the seating surfaces to remain unloaded until a precise surface alignment is achieved and also limits the entry of large particles into the sealing surface cavity during the final portion of the closing operation. With the bumper limiting entry of new particles into this critical area, the high-velocity flow of fluid across the sealing surface at the time of closure provides some degree of self-cleaning to this design. The two new relief grooves in the seat sealing area provide a collection zone for the self-cleaned particles at a location adjacent to the primary sealing area.

To accomplish the addition of the two relief grooves in the existing valve seat assemblies it was necessary to widen the seat sealing recess area.

However this change required an increase in the seat groove width to accommodate the desired trap grooves and still have sufficient seat width to allow for proper seating alignment. The present design (-505) was such that the raised poppet surface indexes with the seat groove near the outer portion of the seat groove as shown in Figure 3-31a. To allow for this centerline offset, an increase in seat groove width was made as shown in Figure 3-31b. This change did not require extensive remachining and did allow for the addition of two 0.50-mm trap grooves in the existing hardware. This arrangement produced a significant improvement in contamination tolerance for both the small and large size particles.

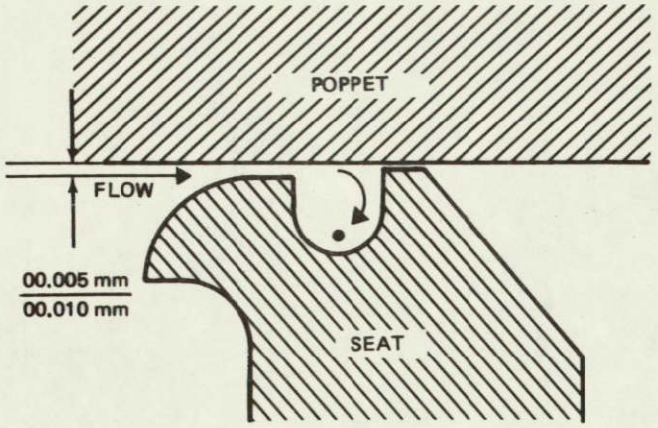

a. ORIGINAL -1 CONFIGURATION

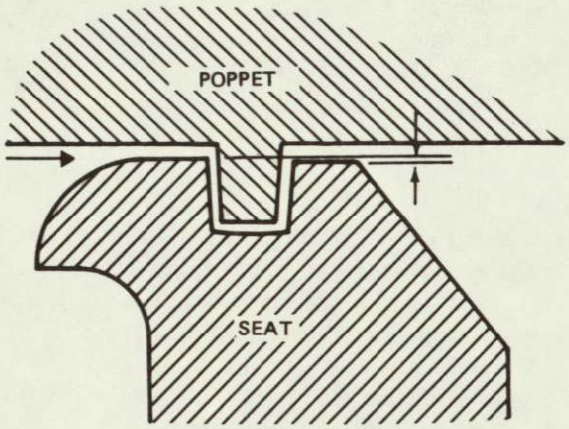

b. -505 CONFIGURATION (NAS3-14375)

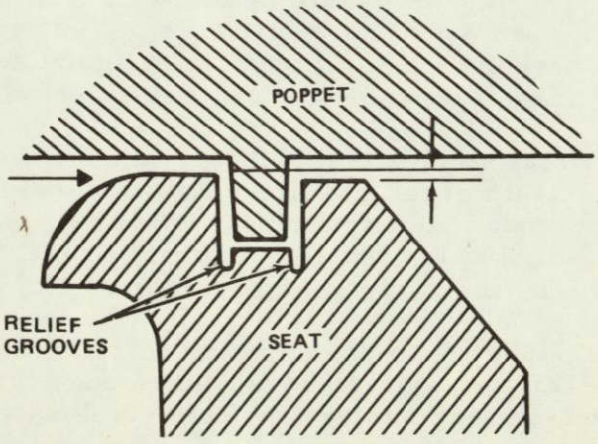

c. -507 CONFIGURATION (PRESENT)

Figure 3-30. Valve Seat Redesign

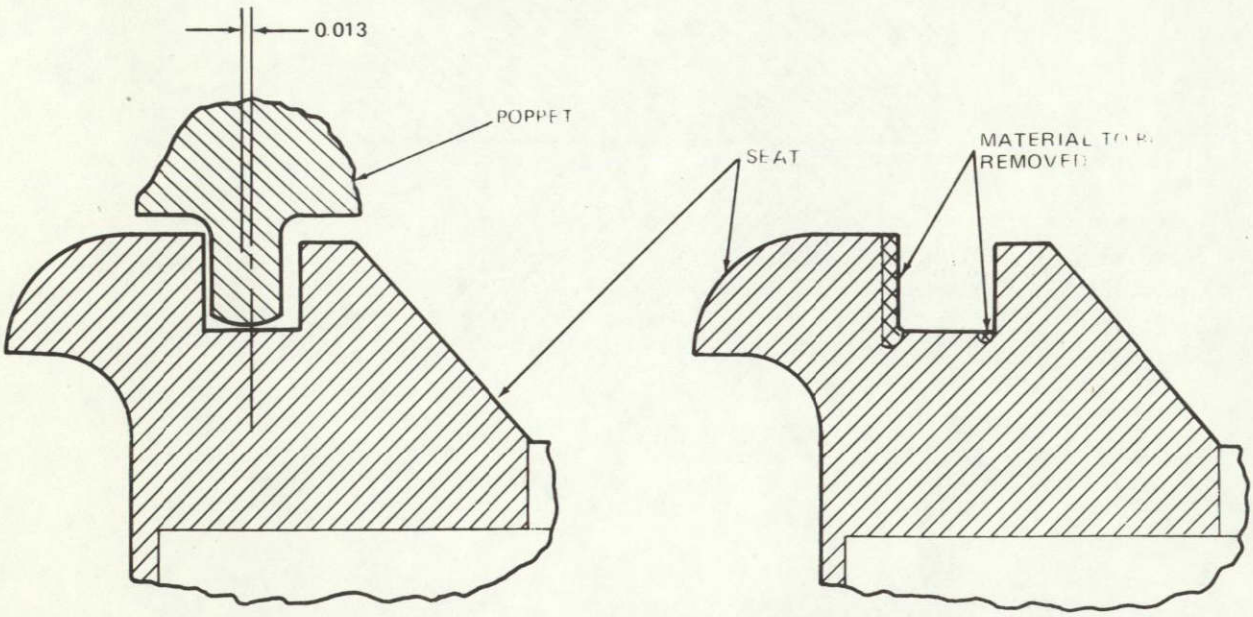

Figure 3-31. Seat Modification

The -505 configuration tested on the original contract had a single coat of Teflon S on the seat surface. A single coat of Teflon S has a nominal thickness of 0.025 mm (0.001 in) and something less in the test condition (after lapping the surface for smoothness and flatness).

This coating thickness was too thin for proper embedment of trapped particles. To handle particles in the 75 to 250 micron range a thicker coating was needed. A total film thickness of 0.305 mm would be capable of embedding a 300-micron particle completely; however, a single coated surface with a 0.305-mm-thick plastic is not easy to produce. The Teflon S material can be given multiple coatings (about 0.025 mm each) by using an intermediate heat cure (15 min at 422°K) after each coating. While it is not known how many coats can be applied without a serious loss of physical properties of the material, a reasonable limit of three coats (of 958-203) was selected as a starting point.

Results from the analytical studies completed on the first program (NAS3-14375) indicate that the relationship of fatigue life-coating thickness will apply in the operating regime of interest. A considerable cost saving was obtained on the complete program by establishing the embedability properties of a coating system before determining the cycle life characteristics.

A coating system which appears to offer improved contamination avoidance characteristics is the Teflon S material with three coatings per surface, on both the poppet and seat-sealing surfaces. This combination would provide a total coating thickness of approximately 0.152 mm and could embed a 150-micron particle. The Teflon S material combination selected consisted of single-coat and multi-coat (high build) plastic applied to the -507 configuration.

A chemical precleaning procedure was used instead of the sand blast cleaning technique. The chemical precleaning treatment was selected to minimize the substrate damage which had been experienced with the grit blast system. When the substrate damage has a greater depth than the coating thickness, it is not possible to lap the coating to the required smoothness and flatness without lapping completely through the plastic coating. This problem has been encountered on the original program and it was necessary to recoat some assemblies a number of times before a satisfactory coating was obtained. With the chemical precleaning process (chemical etching) the substrate damage is minimized; however, some loss in coating adhesion would be expected. To evaluate the adhesive and "high build" characteristics of a fluorocarbon-filled polyimide the Teflon S material was selected for testing. A second system selected was a polyimide fluorocarbon film identified as Xylon 1010.

The Xylon film is similar to the Teflon S film in that both use a similar polyimide matrix. However, the Xylon uses an uncured Teflon TFE nonstick additive in the form which has very small particle sizes (wax) while the Teflon S uses a cured Teflon as an antistick agent. Depending on the type of Teflon S, the cured antistick agent will be either FEP or TFE Teflon. Since the Teflon S uses antistick material in a larger physical size than is used in the Xylon, the Teflon coatings are more sensitive to precoating surface preparation. The Xylon material requires only a relatively simple cleaning procedure for good adhesion between the polyimide matrix and the substrate. The Teflon material requires a more complicated cleaning because of the need for adhesion between the polyimide matrix and the antistick additive. Both of these materials can provide coating systems with excellent physical properties. The Xylon material has a different advantage in having a less destructive precoating cleaning procedure and, hence, the least effect on the precision surface finishes needed for low leakage valves. Xylon 1010 is available from the Whitford Corporation, West Chester, Pa., in bulk quantities and is applied locally by the same supplier as the Teflon S coatings. The Xylon 1010 coating has a single-coat thickness of 0.05 to 0.07 mm and can be applied in multiple layers (as can Teflon S). However, the greater thickness of the single Xylon coat will result in a thicker final coating with the same number of operations used for the Teflon S.

In addition to the two types of fluorocarbon-filled polyimide coatings, a third material was evaluated on this program. This material was a polyvinylidene fluoride (PVF_2) available under the trade name of Kynar from the Pennwalt Corporation. The Kynar material is known to have good high build characteristics with acceptable hardness and abrasive resistances. Kynar in bulk form was tested earlier at the NASA-LeRC on a liquid fluorine program and was reported in Reference 3. The bulk Kynar was found to have a somewhat higher reactivity rate in cryogenic liquid fluorine than did the Teflon TFE; however, no difficulties due to exposures to cryogenic temperatures was indicated. The cryogenic characteristics of thin Kynar coatings have not been established; however, the other characteristics of this material were good enough to select the Kynar coatings as a third candidate material for valve tolerance testing. The plastic material properties are discussed in Reference 4, 5, and 6.

3.2.2 Contamination Tolerance Testing

The test setup for the Task II tests was similar to the setup used previously on Contract NAS3-14375 except that GH_2 was used as a test fluid in place of the GN_2 fluid. This setup is shown schematically in Figure 3-32.

The test setup was completed using commercially available bottles of GH_2 as a pressurant source. The system was installed with four banks of six bottles manifolded together in a common manifold as shown in Figure 3-33. The GH_2 flowrates obtainable with this system were controlled by the size of the six-pack outlet fittings and hence the flowrate varied as the pressure in the bottles varied. A flowrate of 0.20 kg/sec of GH_2 was measured at 1.6×10^7 N/m^2 (2,400 psi) supply pressure. This value dropped to less than one half of that value for the last test made with a given set of bottles.

The test powders used for these tests were two sizes of Al_2O_3 graded at MDAC (Appendix B and Reference 7).

The overall flow system and test valve installation is shown in Figure 3-34. The SS white abrasive unit used for particle injection operated satisfactory with the small D-1 powder (125 to 250 microns); however, some difficulty was experienced with the larger D-2 powder (250 to 420 microns). All existing passages in the SS white unit were enlarged for the D-2 powder and improved performance was obtained. Since the injection system was subjected to random hose plugging with the large particles, a measured portion

CR80

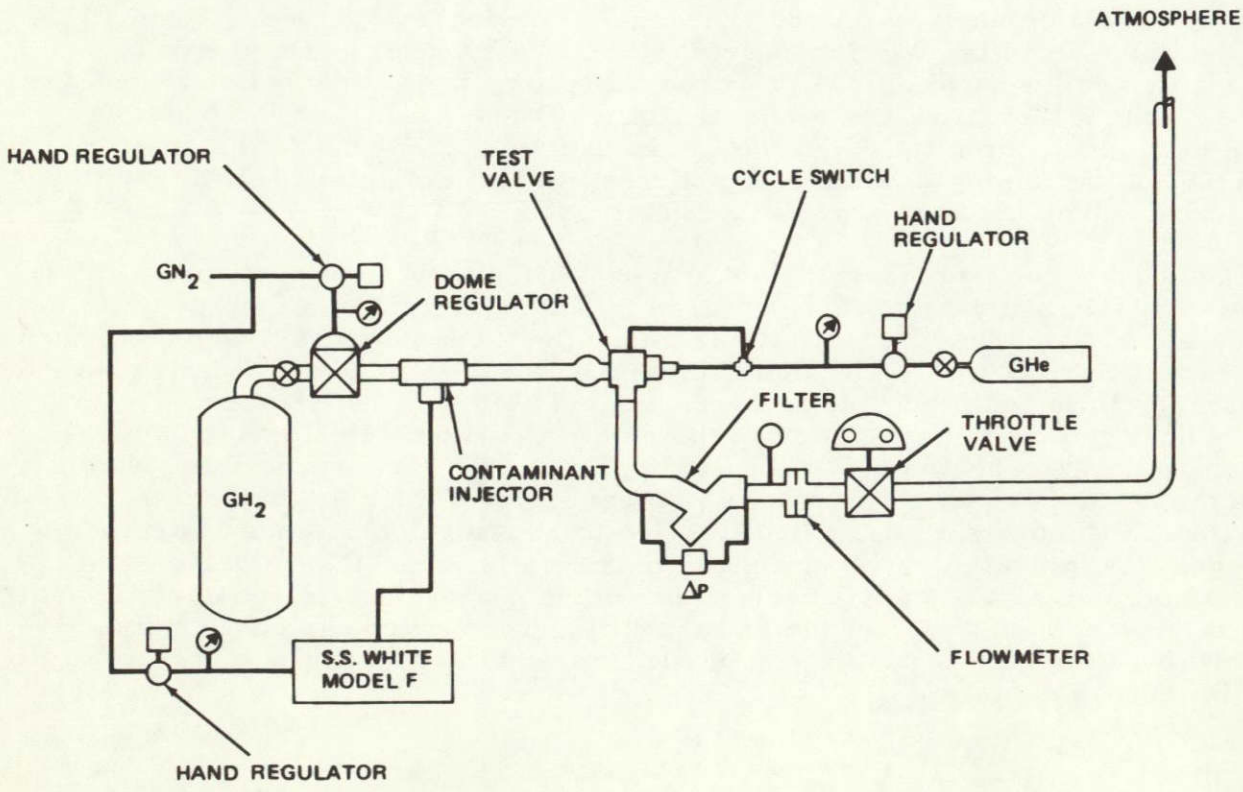

Figure 3-32. Full-Flow Test Setup

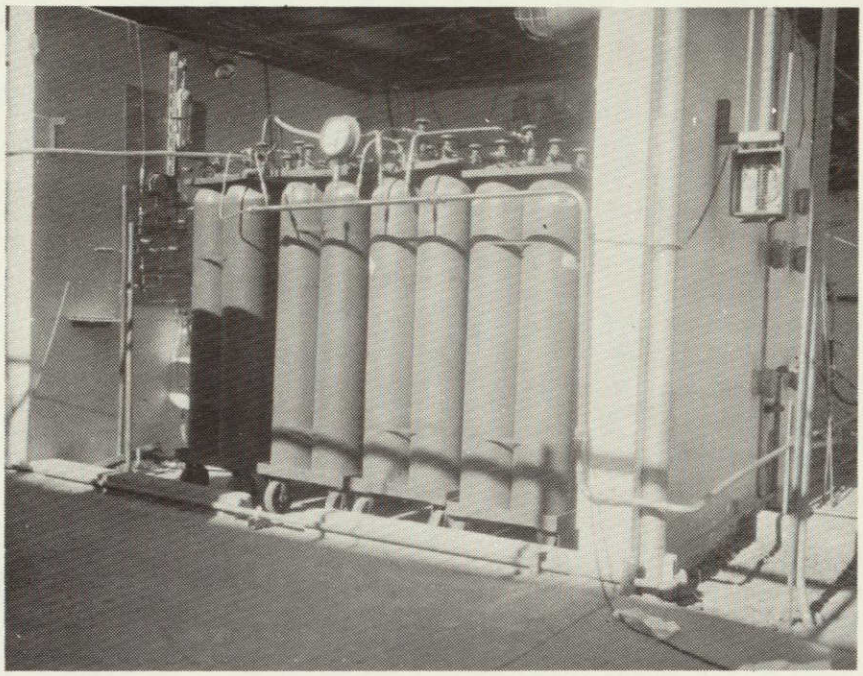

Figure 3-33. Gaseous Hydrogen Supply System – Task II

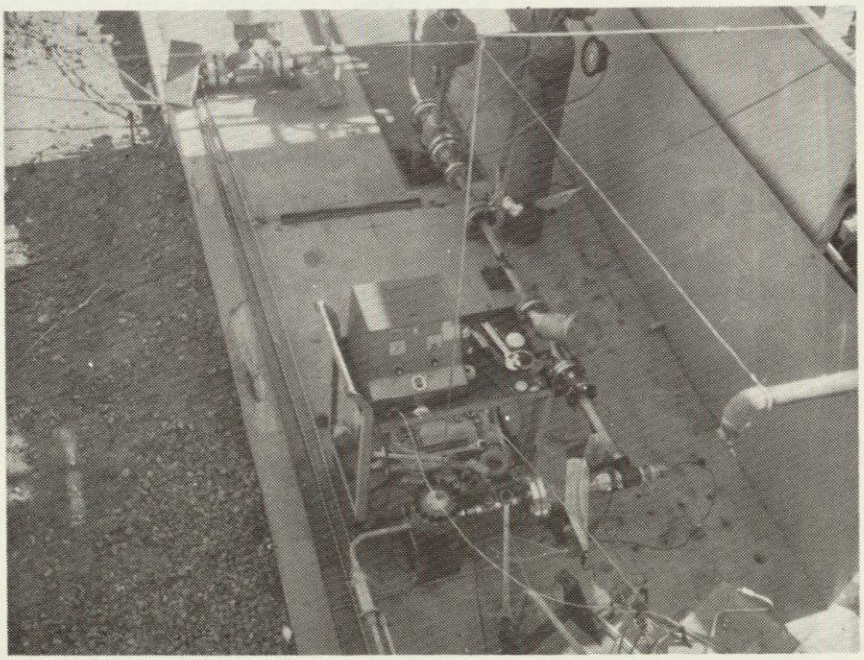

Figure 3-34. GH_2 Flow Test Installation – Task II

of the desired quantity of injection powder was placed directly in the flow duct at the point of the injector nozzle installation. This measured portion of test powder was picked up by the flow stream on the first cycle of operation and hence passed through the valve at a very dense rate. The SS white injector was operated throughout the cyclic operation and the majority of the D-2 test powder was injected at a normal steady rate. This combined method of injection proved to be satisfactory for the testing completed with test powders of up to 420 micron size even though the original S.S. White unit was designed to handle powders that were smaller than 25 microns in size.

The testing was completed and the results of the Task II tests are shown on Table 3-13. The column showing the number of valve cycles represents the actual number of valve cycles needed to get the required amount of test powder injected. The basic test pattern used consisted of a test run of five valve cycles. After the basic run was completed the amount of powder injected by the injection system was determined. When the amount of powder injected was not sufficient, additional runs were made until the desired amount of particulate was injected. On four runs the desired amount was obtained on the basic five cycles of operation. On the other six runs, additional cycles were needed to reach the desired level. The values shown for the amount of powder injected were determined by the weight loss of powder in the injection supply system.

The values shown for the amount of powder recovered represent the actual amount recovered from the downstream filter and the weight determined after the tests. Since some loss of powder occurs in the disassembly of the test system, in recovering the powder from the filter element and in the weighing process, the amount of powder which passed through the valve will always be something higher than the amount recovered and something less than the amount injected. While both values are shown on Table 3-13, the amount of powder passes through the valve on each test is probably close to the average value between the two figures shown.

The internal leakage rates measurements were made before and after each test using GHe at 6.9×10^5 N/m^2 (100 psig) and ambient temperature. The readings shown consisted of the average of three separate readings taken for a time period of at least 5 minutes each using a water displacement measuring system. The test powders used for these tests are described more fully in Appendix B.

A summary of the characteristics and performance of each of the material combinations is given below. All of these material combinations were tested with the -507 design configuration valve with the two contamination trap grooves added to the submerged seat design.

A. Teflon S/Inconel 718. This combination was tested with a thin coat of Teflon S applied to the seat surface. The poppet was uncoated. The Teflon S used was the 958-203 material applied on the A286 surface after the surface was prepared with a very mild chemical etch process using a chemical cleaner (National Chemsearch-Etch Klenz). The surface was sprayed with a very thin coating of Teflon S, air dried, sprayed with a final coating, and then oven cured. This material had good mechanical properties and very

Table 3-13

VALVE CONTAMINATION TOLERANCE TESTS (GH_2)

Test No.	Configuration	Leakage		Cycles	Type	Amount Injected (g)	Amount Recovered (g)
	1T32095-507 – Configuration	Pretest	Post-test				
1	Inconel 718 poppet/Teflon S seat (0.025 mm)	2 cc/M	0	5	D-1	3	1.2
2	Inconel 718 poppet/Xylon seat (0.025)	0	0	7	D-1	2.5	1.5
3	Xylon 1010 (3 coats) poppet and seat	0	0	7	D-1	2.5	1.7
4	Teflon S (3 coats) poppet and seat	0	0	5	D-1	3.5	1.25
5	Teflon S (3 coats) poppet and seat	0	0	10	D-2	3.5	1.4
6	Xylon 1010/Xylon 1010 HB 4 coats	0	(+)	16	D-2	3.7	2.0
7	Teflon S (2 coats) poppet and seat (GN_2)	0	0	9	D-2	2.2	1.3
8	Inconel 718 poppet/Teflon S seat (0.05)	0.24 SCCM	0.16 CCM	7	D-2	4.7	1.95
9	Kynar 207/202 poppet and seat (0.25 min each)	0	0	5	D-2	5.2	4.3
10	Inconel 718/Kynar 207/202	0	0	5	D-2	2.9	1.7

(+) Too high to measure *D-1 125 to 250μ Al_2O_3 powder *D-2 250 to 420μ Al_2O_3 powder

good adhesion between layers. The final coating thickness was approximately 0.025 mm (0.001 in) and would therefore be suitable for exposure to the smaller sizes of particulate. This combination was used on Test No. 1 and No. 8 and was completely acceptable under the conditions tested. No visible damage or change in leakage rate was observed with this material and the performance of the valve was completely satisfactory.

B. Xylon 1010/Inconel 718. This material combination was applied in the same manner as the Teflon S in No. 1 except that a Xylon cleaner was used for the precleaning. The Xylon coating is somewhat thicker than the Teflon S coating and was approximately 0.05 mm (0.002 in) thick. This two-coat Xylon system (thin undercoat and one finish coat) had good adhesion with the A286 seat; however, the coating does have a tendency to break up physically and to scratch more easily than the corresponding Teflon S coating. The Xylon coating is thicker (per coat) and could be used with large particulate sizes. An aerosol version of Xylon 1010 (i.e., Xylon 330) was used on Test No. 2. While this particular plastic coating came out somewhat poorer than the normal Xylon coating, it was still satisfactory for the conditions imposed on the test. No visual damage was detected after the test from particulate entrapment; however, some permanent compressive yielding had occurred due to the valve closing forces.

C. Xylon 1010/Xylon 1010. This combination used a three-coat Xylon 1010 system on both the poppet and the seat. This arrangement gave approximately 0.25 mm (0.010 in) total plastic thickness for embedding contaminant particles. This set of coatings used the regular spray type of Xylon, with the same procedure used for Test No. 2. This coating had good adhesion to both metal surfaces; however, the mechanical properties and physical appearance of this "high-build" material appears to be poorer than the Teflon S coatings due to entrapped air bubbles and pin holes in the surface. This material can be finished to a smooth finish using the Al_2O_3 lapping tool without difficulty; however, the rapid rate that material is removed during this lapping process indicates that the high-build Xylon is softer than some of the other coating systems tested. This coating system was used for Test No. 3 and was satisfactory for the conditions tested. No visual damage was detected after the completion of the test.

D. Teflon S/Teflon S. This combination consisted of three coats of Teflon S applied to both the poppet and seat using the procedures described in combination A. This combination produced two surfaces which appear to have excellent qualities of adhesive, hardness, and abrasive resistance. The only drawback to this material is that the thin Teflon S coats do not produce a thick plastic coating. The estimated thickness of both the poppet and seat materials is 0.10 to 0.12 mm.

This material can be lapped to a smooth surface finish without difficulty and the three-coat system has enough total thickness to permit a reasonable amount of lapping to be completed before the

coating becomes too thin to embed particulate. This coating combination was tested successfully in Test No. 4 using the smaller D-1 powder and in Test No. 5 using the larger D-2 powder. The visual inspection of the valve made after Test No. 5 revealed several points of minor contamination damage had occurred to the plastic coating and one point of moderate damage. The impact damage to the seat sealing surface is shown in Figure 3-35 and the poppet surface in Figure 3-36. While a large portion of the crushed Al_2O_3 particle is still embedded in the poppet sealing finish, this condition did not affect the sealing performance of the valve and does not appear to have started any type of coating separation (which could lead to a later failure). The largest dimension of the coating damage measures approximately 150μ in size.

The good characteristics of the Teflon S/Teflon S three-coat material led to the selection of this material combination for the Task III cycle testing.

E. Xylon 1010/Xylon 1010 High Build. This material combination is similar to combination C except that the coating thickness was increased by using four coats of material on each surface. This high-build coating had a poor visual appearance and had more air bubbles and pin holes than was obtained in combination C. This material was tested on Test No. 6 and was the only material combination that failed during this test program. The outer layer of material on the poppet sealing surface separated from the lower (primer) coating for about 180 deg of poppet circumference and a complete loss of leakage control occurred. It appears that the coating separation started at a location which had been damaged from a particulate impact and then "peeled" around the sealing surface for a considerable distance. This type of failure is probably due to the poor physical characteristics of this material (in thick layers) and no further attempts to high build the Xylon material was made.

F. Kynar 207/202. Since the high-build Xylon material was not found to have acceptable tolerance to contamination damage, a third material was investigated. The alternate material selected was Kynar 207/202. This material can be applied in very thick coatings (0.25 to 0.50 mm) and can retain good mechanical properties. The Kynar system tested included:

1. A very light "grit blast" cleaning procedure

2. A Kynar 207 primer coat (black)

3. Kynar 202 finish coat (clear) with a 0.25 mm (0.010 in) thickness

In the as-sprayed condition this material appears to be rough and irregular; however, the Kynar finish can be sanded and lapped without difficulty. The abrasion resistance of this material is so high that removal of this material by sanding is a relatively slow process (however, it is not a difficult process).

CR80

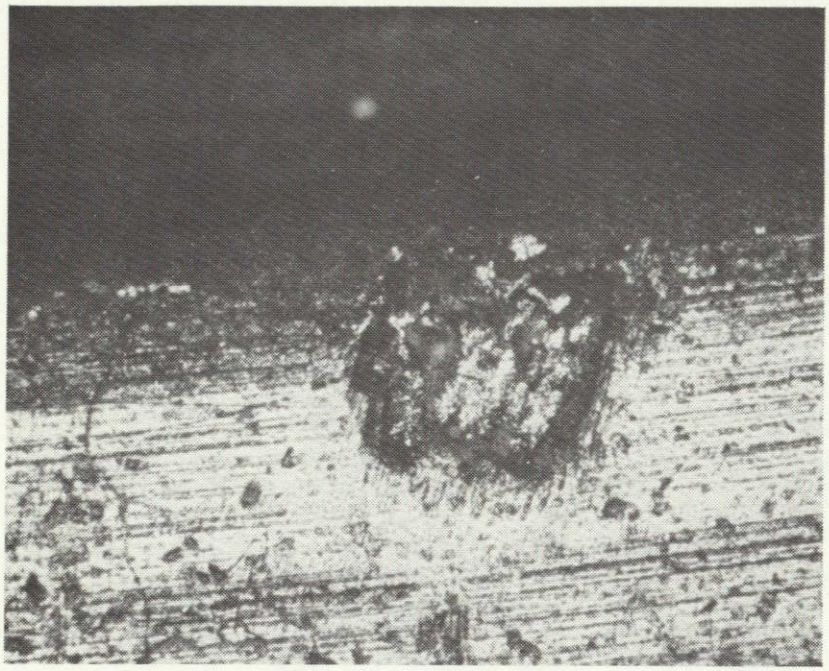

Figure 3-35. Damage on Seat Sealing Surface Coated with Teflon S (60X)

CR80

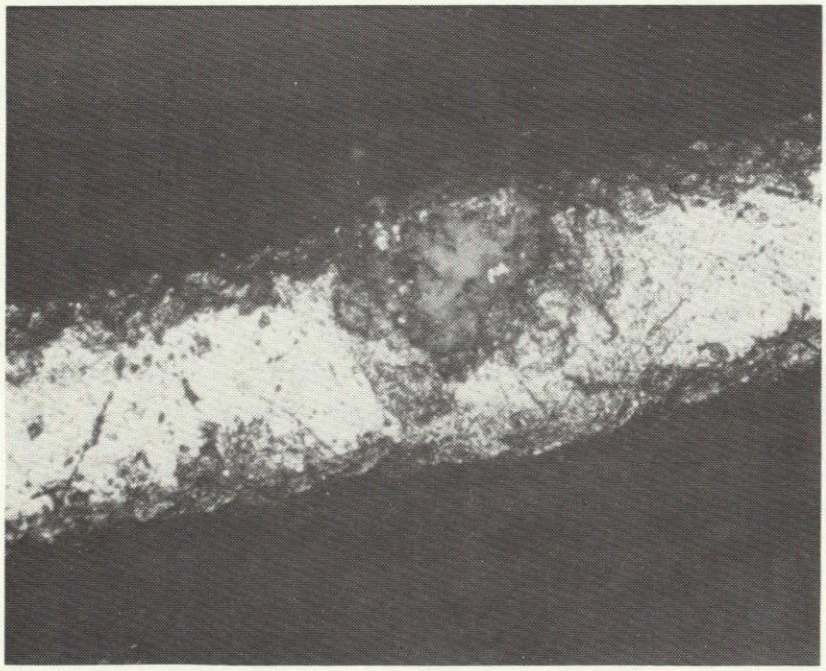

Figure 3-36. Damage on Poppet Sealing Surface Coated with Teflon S (60X)

The lapping operation on this material is also a slow process when using the same Al_2O_3 lapping tools which were used for lapping metal and Teflon S surfaces on this program. For extensive work with the Kynar material a new set of lapping tools would be desirable. These tools would have a surface finish rougher than the present tools. The preliminary work completed on this program indicates that a lapping tool finish with the roughness of 500 grit sand paper would produce an acceptable surface finish in a minimum of time.

The Kynar finish was tested on Test No. 9 and No. 10. On Test No. 9, the Kynar coating was on both the poppet and the seat sealing surfaces. No visible damage or change in leakage rate was observed on Test No. 9 even though the particulate injection rate was very high. As shown in Table 3-13 a total of over 4.3 grams of D-2 powder was passed through the valve without difficulty.

Test No. 10 was made with the same Kynar coating on the seat sealing surface, but with the plastic coating removed from the poppet sealing surface. No change in leakage rate was found with this Kynar/Inconel 718 combination although direct particle impact occurred on the test. The impact damage of a large particle on the seat sealing surface is shown in Figure 3-37. The mating surface of the poppet face is shown in Figure 3-38. It should be noted that the damage on the poppet interface occurred to the remaining Kynar film which was still attached to the side of the raised poppet surface and not to the primary sealing interface. If this side coating of material was removed from the poppet surface, no damage would have occurred. This side coating (on both sides) increased the poppet seat sealing surface width from 0.25 to 0.75 mm and therefore, caused some interference with the operation of the contamination trap grooves located on the mating seat sealing surface. Since these side coatings would not normally exist on a Kynar/Inconel 718 combination, the condition tested represents a case which is more severe than normal. Since the performance of this combination was still acceptable in this severe condition, this material combination appears to be very attractive for further investigation. The Kynar/Inconel 718 combination was selected for cycle life testing in the Task III effort.

G. Teflon S/Teflon S. This combination is similar to combination D except that two coats of material was used on each surface instead of the three coats used previously. This combination was tested on Test No. 7 using the D-2 powder and GN_2 as a test fluid. This test permitted a comparison of the effects of the test fluid density (GN_2 instead of GH_2) on a Teflon S material with an intermediate thickness. No damage to the coatings or changes in valve leakage rates were observed. It can be concluded that the fluid density differences between the two gases tested was not significant for this type of testing and that the two-coat Teflon S material can be used successfully with the larger D-2 powder. Unfortunately, there was no indication that any of the larger particles had impacted the sealing surface on this test so that no direct comparison can be made

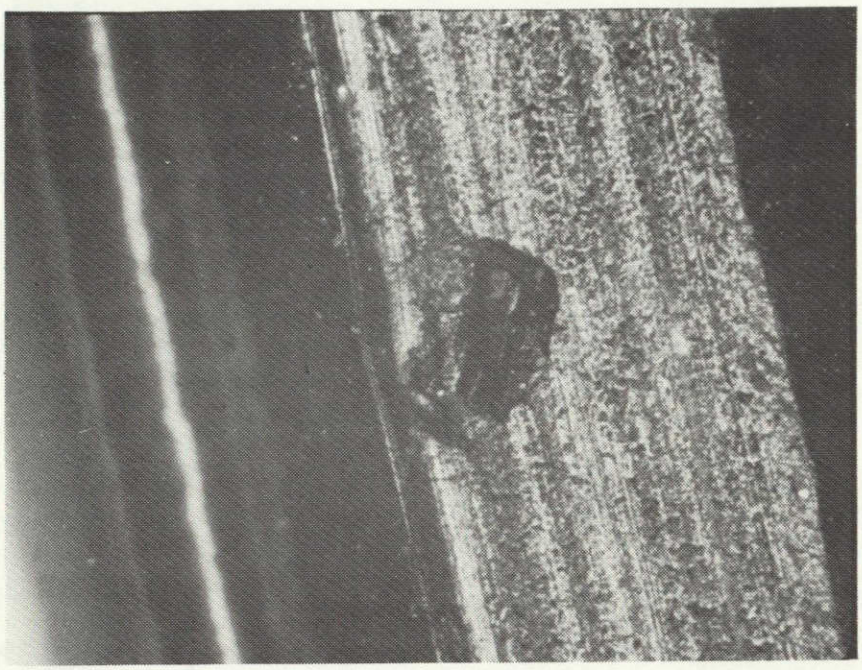

Figure 3-37. Damage on Seat Sealing Surface Coated with Kynar 207/202 (60X)

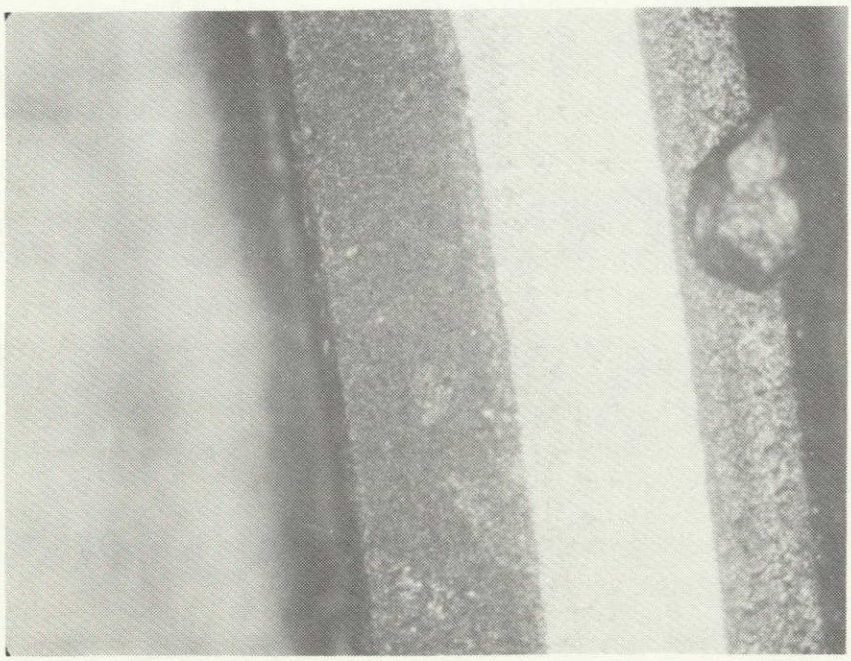

Figure 3-38. Damage on Poppet Sealing Surface – Inconel 718 with Side Coating of Kynar 207/202 (60X)

between the thinner Teflon S two-coat system and other potential high-build material. Since a greater margin of safety will exist with a high-build material that has good mechanical properties, it would appear that coats of more than two coats of Teflon S would be preferable to the two-coat configuration.

3.2.3 Summary of Results and Conclusions

The results of the Task II effort indicate that the technique of using thin coatings of relatively hard plastic materials on the seat sealing surfaces of fluid control valves can be utilized successfully to minimize the physical damage which could result from system contamination. This technique offers greater particulate embedding characteristics than is possible with hard metallic surfaces and can provide better mechanical properties than those normally obtained with bulk encapsulated plastics.

The total thickness of plastic needed to embed different sizes of particles depends somewhat on the type and hardness of the specific particle. Since some particle deformation occurs on most embedment operations, it is possible to maintain satisfactory leakage control (in some cases) when the total plastic thickness is less than the diameter of the contaminant particle. However, it is desirable to maintain some substrate plastic material between the embedded contamination particle and the metal substrate. Therefore, a total plastic thickness of 20 to 30 percent more than the largest anticipated particle diameter would be recommended. The results obtained on this program with particles of up to 420μ and with plastic thickness of 500μ would appear to verify this conclusion. Since the present work was conducted under dynamic operating conditions, it is not known if any 420μ particles were actually embedded into the sealing surface interface materials. These materials were exposed to particles of that size; however, the self-cleaning features of this valve design may have prevented the actual embedment of such large particles. A nondynamic test program could be conducted to further verify the conclusions reached on the present program. For a nondynamic test a known particle could be placed on the sealing interface before valve seat closure and the internal leakage of the valve measured after closure. A test of this type could be conducted with the existing equipment with little difficulty and should be considered as an extension to the present work.

While none of the materials tested were optimum in physical properties, antistick characteristics and "high-build" capabilities, the results obtained in this test series were very encouraging and further work in this area should produce even greater contamination damage tolerances in fluid control valves.

The conclusions that can be made from the complete Task II testing effort include:

A. The seat sealing surface design utilizing a submerged sealing interface, self-cleaning characteristics, contamination relief grooves, and hard plastic coatings (1T32095-507 configuration) can operate successfully during a cyclic operating mode with relatively large contamination particles entrained in the flow stream. The absolute size of the particles which can be tolerated varies as a function of the total thickness of the hard plastic coatings on the mating surfaces of the sealing interface. A total plastic thickness of 0.12 to 0.15 mm appears to be adequate for particles

of 250μ size or less. Thickness of 0.25 to 0.30 mm total appear capable of tolerating particles of up to 420μ in size.

B. The fluorocarbon-filled polyimide material Teflon S has the best all around properties for coating valve sealing interfaces; however, this material cannot be applied in layers thicker than approximately 0.05 mm using normal coating techniques.

C. The chemical precleaning method used for the Teflon S coatings provided adequate coating adhesion under the conditions tested.

D. The Xylon 1010 material does not retain acceptable mechanical properties in thick coatings and does not offer a measurable advantage over the Teflon S in thin coatings.

E. The Kynar 207/202 material has good mechanical properties in thick coating layers and can be coated in thick layers using normal coating techniques. The cryogenic characteristics of this material with the various primers available should be evaluated.

3.3 TASK III - VALVE CYCLE LIFE TESTING

A shutoff valve suitable for long-life reusable service with potential particulate contamination must have improved methods of minimizing potential damage due to contamination while still retaining an acceptable service life. The number of cycles over which a propellant feed system valve must provide an acceptable control of propellant leakage is a function of many system variables. Typical requirements for nonreusable vehicles are in the order of 100 to 1000 cycles. To allow for the unknown values of the system variables on future reusable vehicles, a value of 100,000 cycles was selected as a representative number for research and development evaluation. This value (10^5 cycles) represents a compromise between the normally assumed infinite life number of 10^6 cycles (for fatigue type failures) and the 10^3 to 10^4 cycle value representative of present valves. The 10^5 number should produce the greatest amount of information for the least amount of testing.

The use of thin plastic films as a coating for valve seating interfaces has shown promise of making a significant improvement in the contamination damage avoidance characteristics of poppet type shutoff valves. This improvement was verified in the Task II effort on this program and on the work completed on Contract NAS3-14375. The improved contamination damage tolerance is accomplished by increasing the embedability characteristics of the sealing surfaces by providing a relatively soft surface coating (for particle embedment) on a hard metal substrate. Since the relatively soft surface provides good physical compliance for leakage control and also accepts (and embeds) the contamination particles an ideal condition is obtained. However, as the thickness of the softer coating increases the effects of the hard metal substrate decreases and hence a potential loss in cycle life capabilities may be encountered. This potential loss in cycle life will be controlled by the mechanical properties of the coatings, the operating stress levels of the mating interface and the adhesive (nonstick) characteristics of the plastic coatings. The coatings selected for evaluation on this

program were selected to provide the maximum contamination damage avoidance characteristics while maintaining an acceptable leakage control for a cycle life of 100,000 cycles. The Task III Valve Cycle Life Testing effort covered the cycle life testing of the two most promising material combinations identified on the Task II effort. The material combinations tested were:

A. Teflon S on Teflon S

B. Kynar 207/202 on Inconel 718

Both material combinations operated successfully in a nonflow GH_2 environment for 100,000 cycles.

3.3.1 Design Analysis

The cycle life characteristics of the thin plastic coatings is controlled primarily by the:

A. Mechanical properties

B. Adhesive characteristics (nonstick)

For thin coatings of plastic materials, the measurement of mechanical properties is very difficult and very little data exists in this area. As the coating thickness increases the indicated mechanical properties tend to approach the bulk material properties; however, in thin coatings the indicated properties is influenced to a great extent by the substrate characteristics. The plastic coatings evaluated on this program have been in the 0.025 to 0.25 mm (0.001 to 0.010 in) thickness range and are in the range of greatest uncertainty of mechanical properties. To establish the most valid baseline for these materials, the closest known data have been utilized. These data are shown in Table 3-14 and are covered in References 4, 5, and 6.

Table 3-14

PROPERTIES OF PLASTIC COATINGS

	Teflon S	Xylon 1010	Kynar 207/202
Tensile strength (N/m^2)	2.1×10^7 to 3.5×10^7	1.4×10^7 to 2.8×10^7	3.6×10^7 to 5.1×10^7
Compressive strength (N/m^2)			5.5×10^7 to 6.9×10^7
Coefficient of friction	0.08 to 0.11	0.02 to 0.10	0.14 to 0.17
Coating thickness (mm)	0.025	0.025 to 0.063	0.12 to 0.25

In addition to the three coatings evaluated, a number of other materials were considered for this program. The materials were selected as being representative of the type which would be most likely to meet the requirements of this program. In most cases similar material is available from a number of different suppliers, under different trade names. The three materials tested were representative of their general types; however, equal performance would be expected from similar coatings supplied by other suppliers.

The effects of seat stress on cycle life were investigated originally on Contract NAS3-14375 and a cycle life of 100,000 cycles was obtained with a relative stress factor (RSF = actual seat stress/compressive yield strength) of up to 90 percent with the nonstick plastic coatings. Since the range of acceptable seat loadings (RSF) appear to be very broad, the valves were built to nominal dimensions and the RSF accepted for these conditions. The tapering section of the raised poppet sealing surface results in a change in seat width with the amount of surface lapping. The sealing surfaces of the two test valves were lapped until the internal leakage rate was acceptable and then the seat width was measured. By using this method it was determined that the Teflon S system was loaded to a seat stress of 1.7×10^7 N/m^2 (2500 psi) while the Kynar 207/202 was loaded at 1.3×10^7 N/m^2 (1900 psi). These values give an approximate RSF of 50 percent for the Teflon S and 20 percent for the Kynar 207/202. Both of these values were within the acceptable range for a 100,000-cycle life test in GH_2.

3.3.2 Cycle Life Tests

The test setup used for the Task III testing was the same system used for the cycle life tests on the previous contract and described in detail in Reference 1. The basic difference in the present setup resulted from the fact that both cycle life tests on this program were run with a single test valve (the cycle life tests on the original program were conducted with both a single valve setup and a double valve setup) and no further acoustical monitoring was attempted on the present program. The cycle life test setup used on this program is shown schematically in Figure 3-39 and the actual setup in Figure 3-40. The details of the two cycle life tests are as follows:

A. Cycle Life Test No. 1. The 1T32095-509 valve was cleaned and reassembled in the double acting operating mode required for the Task III tests. This configuration includes a seat assembly coated with a 0.25 mm (0.010 in) thick coating of Kynar 207/202 and an uncoated Inconel 718 poppet. The pretest leakage tests were conducted in the A12 clean room with GHe at 6.9×10^5 N/m^2 (100 psig). No leakage was measured in three 5-minute leakage tests. The valve was then installed on the cycle test fixture located on Unit 1 and the ambient leakage tests repeated. No leakage was measured on these three 5-minute leakage tests. The valve was then submerged in LN_2 for the cryogenic leakage test. No leakage was measured on the first leakage cycle but after cycling the valve opened and closed one time, the leakage rate was too high to measure. The valve was disassembled in the clean room and inspected. It was determined that a large portion of Kynar plastic overspray had come loose from the seat surface (Figure 3-41) and was trapped between the poppet and the seat. None of this loose coating was from the basic sealing

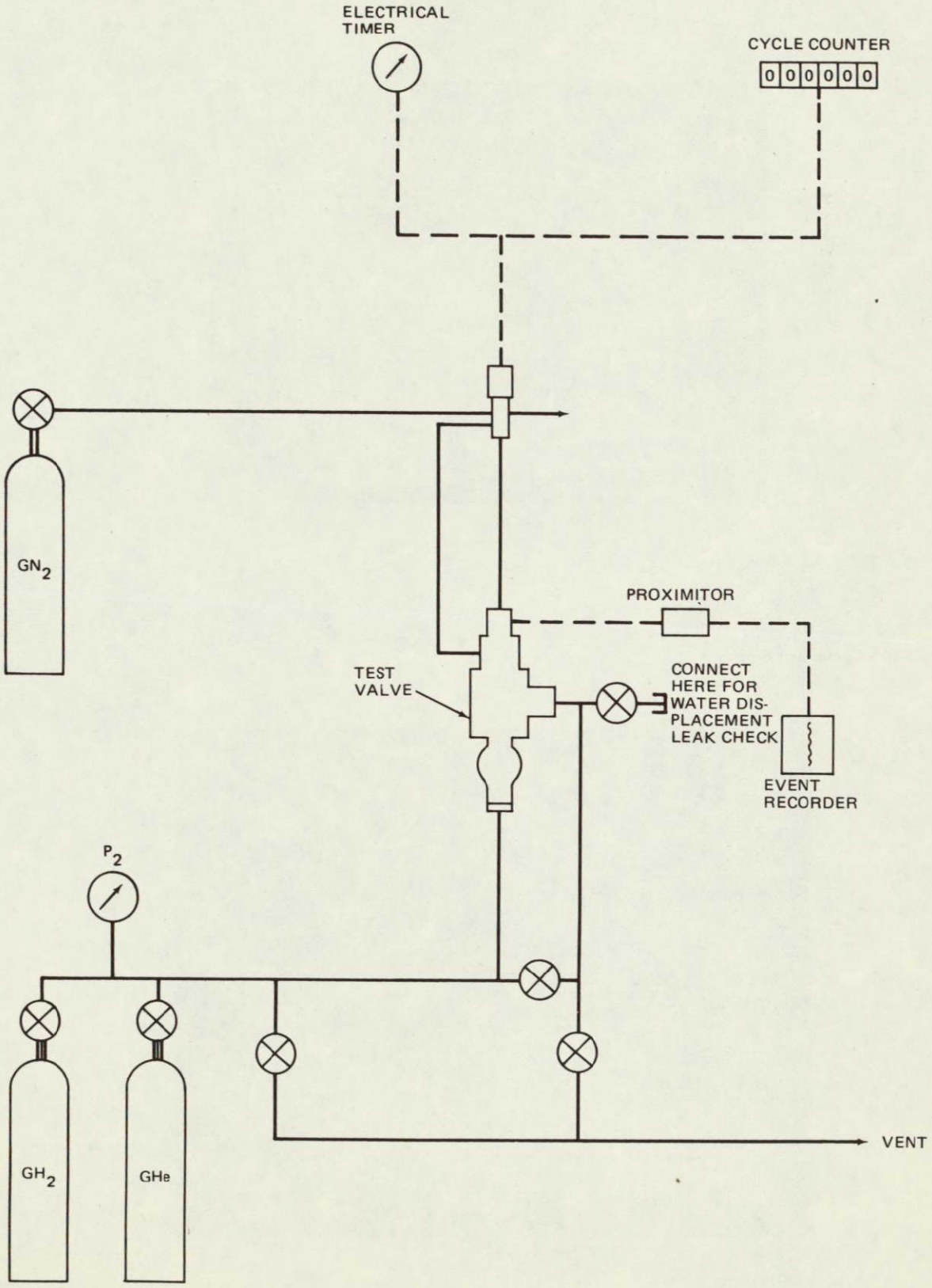

Figure 3-39. Cycle Life Test Setup

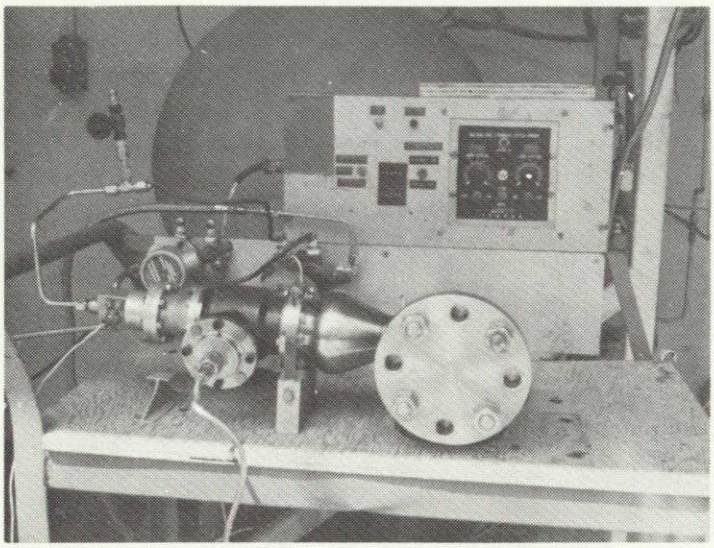

Figure 3-40. Cycle Test Setup

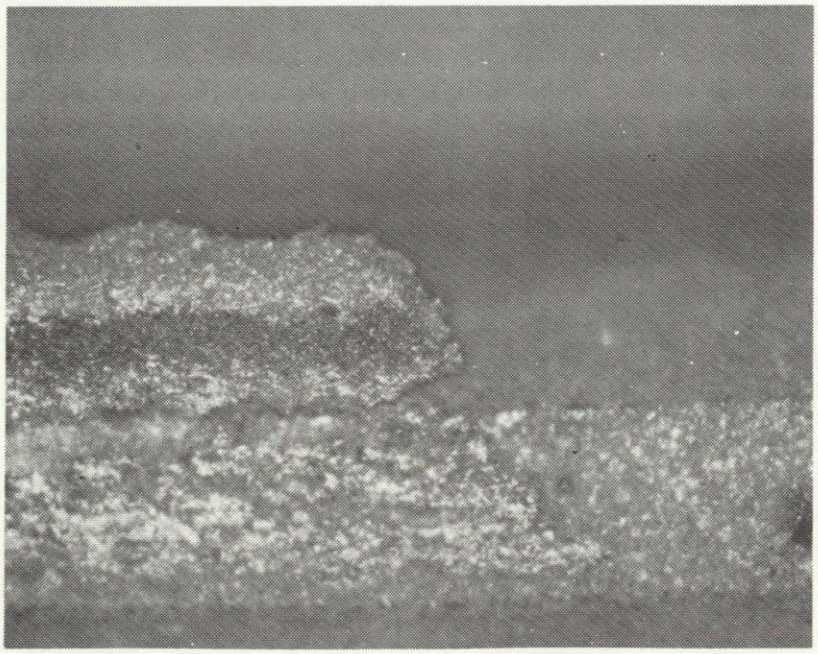

Figure 3-41. Kynar Film Strip

surface and, therefore, the test was continued after the loose material was removed. The valve was reassembled and returned to the life cycle test fixture. The cycle life tests in GH_2 was started and no leakage was measured after 1, 10, and 100 cycles of operation. At the 500 cycle point the leakage rate was too high to measure. The valve was returned to the clean room and disassembled. It was determined that a considerable number of large contaminant particles had gotten into the poppet and seat sealing interface and moderate damage resulted in the sealing surface. These particles were embedded into the plastic coating but due to the large diameters of some of the particles, the 0.25 mm (0.010 in) thick plastic coating was insufficient to accept the particles, and damage had occurred to the uncoated Inconel 718 sealing surface. The particles were removed from the plastic coating and the coating smoothed out with the Al_2O_3 lapping tool. A leak test was made on the valve without removing the damage to the Inconel 718 poppet surface. A value of 60 SCCM was measured under these conditions. Since this surface damage does not appear to have been caused by exposure to the GH_2, the valve sealing surfaces were refinished and this test was rerun. It should be noted that this type of contamination damage occurred when the valve was cycling in a nonflow condition (hence the self-cleaning features were not functioning) and had not been encountered on the Task II effort under normal flow conditions.

The test valve was refurbished and the number 1 test restarted. The Inconel 718 poppet surface was refinished using the MDAC Al_2O_3 lapping block. The plastic-coated seat assembly was returned to the commercial coating vendor and a new coating of Kynar 207/202 was installed. After refurbishment, the valve parts were cleaned in a sonic cleaner using special precautions to clean the restricted area between the shaft seal bellows and the adjacent protective shield. The valve was reassembled, leak tested and the number 1 test restarted. After 7500 cycles the internal leakage was excessive and the test was stopped. Inspection of the valve revealed a condition similar to that found on the first test attempt. A number of uncontrolled contamination particles were found embedded in the lower portion of the poppet and seat sealing interface. While the exact source of this sandy looking material is unknown, it appears that this contamination is a residual from the plastic precoating sand blasting operation used by the coating vendor and that these particles were wedged between adjacent convolutions of the machined bellows portion of the seat assembly. If particles were wedged into this area in the coating process, they would not work free until the bellows is compressed and expanded a number of times in the cycle test operation. This situation can be prevented in the future by using a special masking operation in the commercial coating process.

Since the surface damage was not extensive on the second test attempt, the poppet and seat sealing surfaces were refinished by MDAC and the test restarted at cycle one. The seat surface was refinished by removing the embedded particles with an Exacto knife

and then smoothing out the sealing surface with the MDAC lapping tool. The poppet was refinished using the MDAC Al_2O_3 lapping block.

The number one test was then restarted and no significant change in internal leakage was measured over 48,000 cycles of operation.

However, at this point it was determined that the loss of GH_2 pressurant was higher than normal and an investigation into the source of the GH_2 leakage was completed. It was found that a small crack had developed in the shaft seal bellows of the test valve. This crack would permit a relatively large leak to occur when the bellows was extended but was almost undetectable with the bellows compressed. This shaft assembly was returned to the original supplier for replacement of the cracked bellows. Further, the spare shaft assembly was modified to add the removable poppet thread provisions to the original unmodified shaft assembly.

An inspection was made of the seat sealing surface interface of the test valve after the 48,000 cycles were completed. No detectable damage was identified.

The shaft assembly with the new replacement shaft seal bellows was received (from Parker-Hannifin) and reinstalled in the test valve. An internal leakage test was conducted and the leakage value was unchanged from the value measured at the time of the bellows' failure (48,000 cycles). The valve cycling was then restarted at the 48,000-cycle point and continued to the final 100,000-cycle point. The internal leakage rates from cycle 1 to cycle 86,000 was 0 SCCM. At 94,000 cycles the measured value was approximately 0.5 SCCM and at 100,000 cycles the value was an unacceptable 6 SCCM. The valve was disassembled and a post-test inspection completed. It was found that no additional wear damage had occurred to the poppet or seat sealing interface (other than the damage previously caused by contamination particles). The particulate damage had occurred during the first 10,000 cycles and no further physical damage was encountered on the last 90,000 cycles. However, the Kynar 207/202 coating had lost its bonding with the metal substrate in one area and a small leakage path was established underneath the plastic coating. The entire Kynar film was peeled from the metal substrate (during post-test inspection) without difficulty and the entire coating from the submerged sealing groove was removed in one piece. The exact cause of this bond failure is not known; however, the supplier of this material has indicated two possibilities.

The 207 primer coating does not have the bonding strength of the 204 primer and for severe applications, the 204 material should be selected. Further, since the Kynar overspray on the poppet (not the seat) had lost its bond during the pretest cryogenic leakage test it is probable that some loss of adhesion occurred to the coating on the seat sealing surface at the same time.

A check was conducted to determine the relative merits of the 207 or 204 primer for cryogenic application. Kynar is a polyvinyldene-fluoride (PFV_2) fluoroplastic that has not been evaluated extensively for cryogenic service. This material (in bulk form) was evaluated by NASA-LeRC on a fluorine/flox compatibility program and no difficulties from exposure to cryogenic conditions were reported, although the PVF_2 did show a higher reactivity rate in LF_2 than did Teflon TFE. Since the high-build characteristics of the Kynar are much better than the Teflon TFE materials, it would appear that the Kynar is a superior coating for control of the contamination damage to shutoff valves and further work with this material is indicated.

B. Valve Cycle Life Test No. 2. The poppet and seat assemblies of the disassembled test valve were processed by the plastic coating vendor to remove the residuals of the Kynar coatings and install the Teflon S coatings. A three-coat system of Teflon S was placed on both the poppet and seat sealing surfaces. The valve was reassembled with the recoated parts and a leakage test performed. The internal leakage was found to be excessive. The valve was disassembled and the seat sealing surfaces lapped with the MDAC lapping tools. It was found that the irregularity of the metal substrate surface on both the poppet and the seat was greater than the thickness of the Teflon S coatings and therefore the Teflon S coating was removed completely in some areas without obtaining an acceptably flat surface. This condition was the result of the grit blast precleaning procedure used for the Kynar coating and not the chemical preclean treatment used for the Teflon S coating. Since the Kynar coating was considerably thicker than the Teflon S coating these substrate irregularities were not critical with the Kynar material but with the thinner Teflon S coating the same degree of surface variation could not be tolerated.

It was necessary to lap through the Teflon S coating to the degree required to smooth out the high spots in the metal substrate and then reapply the Teflon S coatings on both parts. This was completed and new coatings applied. The new coatings were four coats thick. The valve was reassembled with the four-coat plastic system and leak checked in the as-coated conditions. The internal leakage measured in the as-coated conditions was too high to start a cycle life test but was not excessive on an absolute basis. The poppet and seat sealing surfaces were given a light lapping operation to smooth out the new plastic coatings. The internal leakage was then found to be acceptable for cycle life testing.

The indicated leakage rate measured in the pretest conditions varies somewhat due to the increased friction in the actuator of the double acting valve configuration and readings of 0 to 0.3 SCCM of GHe at 6.9×10^5 N/m^2 (100 psig) were obtained. A pretest cryogenic leakage test was attempted; however, the actuator friction problem results in a wide scatter in leakage measurements (both plus and minus readings). The valve was then installed on the cycle life test fixture and the cycle life testing started.

At approximately 30,000 cycles of operation, it was determined that the consumption of GH_2 was occurring at a higher rate than normal. A preliminary check indicated a leak had developed in the shaft seal bellows of the test valve and some of the GH_2 pressurant was leaking out of the actuator outlet port. The valve was removed from the test stand and taken to the A12 clean room for disassembly. A visual inspection was made of the shaft bellows and no leak area was identified.

Since the second valve shaft assembly had been modified to incorporate the removable poppet feature, the second shaft assembly was installed in the test valve and the cycle testing restarted. The GH_2 leakage was much higher with the second shaft assembly than with the first shaft assembly so the valve was disassembled a second time. A special pressurizing fixture was made so that a pressure test could be made on the shaft bellows with the valve disassembled. This test was completed and it showed that the spare shaft assembly had developed a crack in one of the middle convolutions. This crack had progressed nearly half way around the bellows circumference and this assembly was not usable for further testing (without replacing the bellows). The pressure system was then used to test the original shaft assembly. No crack was found in the original bellows assembly using this method of test; however, a small zone of leakage was observed in the middle portion of the bellows. The test indicated that the source of the GHe leakage was probably a pinhole leak in the bellows weld seam and not the starting of a crack. Based on these findings the original shaft assembly was reinstalled in the test valve and the cycle testing resumed. To insure that this shaft bellows leakage could not affect the valve internal leakage reading, the leakage measurement procedures were changed slightly. With the new procedures, the actuator return line is removed and the outlet port capped before each leakage measurement. This method insures that even with a small leak in the bellows assembly the leakage measurements will represent the actual internal leakage of the main poppet and seat sealing surfaces.

No changes in the internal leakage measurements were noted throughout the 100,000 cycles of operation with the Teflon S/Teflon S valve configuration. The post-test leakage rate was still less than 0.2 SCCM of GHe at 6.9×10^5 N/m^2 (100 psi) and well within the 1 SCCM leakage limit. The post-test inspection showed the coating wear to have been insignificant after the 100,000 cycles of operation at a seat loading of 1.7×10^7 N/m^2 (2,500 psi) in the GH_2 environment.

3.3.3 Summary of Results and Conclusions

The results of the Task III testing confirm the suitability of using thin coatings of hard plastics to provide an acceptable cycle life capability to sealing surfaces which have improved embedability characteristics and hence improved contamination damage avoidance characteristics. The selection of a specific nonstick plastic coating should be made on the basis of anticipated contaminant particulate size, desired leakage rate, design operating stress, desired

cycle life, fluid, type, and system pressure. Specific conclusions made from these tests include:

A. A thin coating of polyvinylidene-fluoride (PVF_2) such as Kynar 207/202 is capable of operating for 100,000 cycles in GH_2 at a seat stress loading of 1.3×10^7 N/m^2 (1,900 psi).

B. A grit blast precleaning treatment can be used with the PVF_2 coating when the coating thickness is in the 0.20 to 0.25 mm (0.008 to 0.010 in) thickness range. This thickness permits the removal of enough material to obtain a smooth, flat surface when the substrate contains minor irregularities from a mild grit blast treatment.

C. The PVF_2 film can be lapped successfully with lapping tools having a surface similar to the surface of 500 grit sandpaper.

D. The use of Kynar 207 as a primer coating appears to be satisfactory for components operating at or near ambient temperature. The Kynar 207 primer does not appear to be acceptable for use on components of cryogenic systems. The evaluation of alternate PVF_2 primers (204 or 205) for cryogenic systems is recommended.

E. The fluorocarbon-filled polyimide coatings such as Teflon S (958-203) are capable of operating satisfactorily for 100,000 cycles in GH_2 at a seat loading of 1.7×10^7 N/m^2 (2,500 psi).

F. A mild chemical etch precleaning treatment can be used successfully with the Teflon S type of material.

G. The Teflon S material can be lapped successfully using the same type of lapping tools used for precision metal surfaces. Good results were obtained on this program using conventional Al2O3 lapping tools, either dry or with a water lubricant film. No loose lapping compound should be used with any of these plastic coatings.

3.4 SIGNIFICANCE OF PROGRAM RESULTS

The results obtained on the evaluation of a dynamic particle separator verify the feasibility of using such a device for the separation of particulate contamination from a flowing fluid stream. However, sufficient technology has not been developed to permit the translation of the baseline evaluation data to a workable service design. Additional analytical studies covering (1) the acceleration characteristics of contamination particles through the venturi director and (2) development testing of units with optimized inlet cone angles and trap-to-bypass area ratios will be needed to configure a practical separator for field service. These additional studies are discussed in greater detail in Sections 3.1.9 and 3.5.

Since this basic design is capable of removing a significant portion of particulate contamination while utilizing a very small and constant pressure drop, it offers some real advantages on a number of different types of flow

systems. Included in the types of systems which could use a device of this type are:

A. Long-term reusable space vehicles.

B. Coal gasification plants.

C. Geothermal power plants.

D. Pure gas generation systems (from solid propellants).

The work completed to date has established the technical feasibility of such a separator, but no universal design criteria have yet been established. Each separator installation will require a different design configuration for optimum service; however, two basic models (one for liquid and one for gases) can probably be generated for noncritical general service. The work covered on this program has subjected a basic separator design (constant velocity, nonregenerative) to a relatively large number of test conditions, and the results have provided the basic design verification needed to proceed with improved separator designs.

The results obtained in the valve contamination tolerance testing have verified the technical feasibility of utilizing thin plastic coatings on critical metal valve parts. This shows that excellent leakage control can be maintained when the valve is exposed to particulate contamination and that a relatively long cycle life capability in noncontaminated propellant flow conditions can also be maintained.

Both methods of providing contamination damage control for propulsion systems would appear to offer significant benefits on future long-term, reusable space vehicle designs. The utilization of both methods on a single vehicle should provide insurance against component failure due to contamination damage on all future space flights.

3.5 RECOMMENDATIONS

The encouraging results obtained on both types of contamination damage control indicate that further work in this area is justified. Specific recommendations for both systems include:

A. The venturi throat exit velocity characteristics of the contamination particles should be investigated. This investigation can be conducted using both an analytical and a test method of approach. The analytical study would consist of modifying an existing MDAC computer program to handle the contamination particle acceleration characteristics. The present computer program was designed to deteremine the trajectories and velocities of metallic particles in a rocket chamber and nozzle when an aluminized solid propellant is utilized. This program should require only minor modifications to handle the particle velocity/trajectory calculations needed to present the separator design criteria on a generalized basis. After the revision to the computer program is completed, the results can be checked by running a known trial case through the computer and then

duplicating the test conditions on an optical flow test (as described in Section 3.1.1). By combining the computer and optical test method results, a final determination of particle velocity can be established.

Further evaluations of the separator configuration are also recommended. These investigations should include the optimization of the inlet cone angle, the trap-bypass area ratio, and the amount of secondary bleed flow required for good separator performance. These factors should be established for both a gaseous and a liquid separator design. It is recommended that the liquid system version be evaluated in a water flow system such that the special effects of cryogenic liquids can be isolated from the basic flow separation process during the first steps of development. The final liquid version should be retested in an LN_2 system after acceptable performance is achieved with the regenerative separator in a water system.

B. Improved contamination damage tolerance of a poppet-type shutoff valve was demonstrated during the present program under ambient temperature operating conditions. To finalize these data for future space vehicle use, it is recommended that alternate primer systems be evaluated for the Kynar 202 coating material and that the final Kynar coatings be subjected to a series of cryogenic evaluation tests. If a suitable primer system can be found for the Kynar material (at cryogenic temperatures), a significant improvement in contamination damage tolerance will result.

Additional work on evaluation of the effects of specific amounts of damage on a plastic-coated seat is recommended. This work would include a test series which would determine the changes in internal leakage rate which could occur when specific sizes of contamination particles are placed on the seat sealing surface in a nonflow test condition. While the work on the present program has minimized the possibility of encountering a large particle in the critical sealing interface area, it is still possible that such an event could occur. Therefore, a greater level of design confidence is obtained by establishing the rate of deterioration in leakage control which could occur when different sizes of particles are embedded in plastic coatings of different thicknesses. This information would prove useful in establishing a realistic specification for filtration requirements on future reusable vehicles.

REFERENCES

1. D. L. Endicott. Contamination Avoidance Devices for Poppet Type Shutoff Valves. McDonnell Douglas Astronautics Company, NASA Report CR121125, January 1973.

2. D. L. Endicott. Space Storable Oxidizer Valve. McDonnell Douglas Astronautics Company, NASA Report CR 72690, November 1970.

3. H. W. Schmidt. Handling and Use of Fluorine and Fluorine-Oxygen Mixtures in Rocket System. National Aeronautics and Space Administration. NASA SP-3037, 1967.

4. Technical Information Bulletin A61844, August 1968. E. I. DuPont deNemours & Co., Fabrics and Finishes Dept., 308 E. Lancaster Ave. Wynnewood, PA.

5. Technical Information Bulletin 1018, Whitford Corp., Box 552, West Chester, PA.

6. Technical Information Bulletin K68A-10M, March, 1972. Pennwalt Corp., Pennwalt Building, Three Parkway, Philadelphia, PA.

7. FEPA Standard 30GB1971, Federation of European Producers of Abrasive Products, British Abrasive Federation, London, England, 1971.

Appendix A

VENTURI SEPARATOR ANALYSIS

A.1 INCOMPRESSIBLE FLOW MODEL

The venturi analysis described below treats only the fluid-dynamic, flow, and pressure loss processes through a venturi separator configured as shown in Figure A-1.

The purpose of the analysis is to determine the flowrate and overall separator pressure drop and define the pressure and velocity at various points in the device, as a function of fluid properties, venturi inlet conditions, venturi configuration, screen type, size, configuration and degree of blockage by contaminants. Details of the proper venturi configuration, analytical elements, and performance data were taken from the classic treatise on venturis (and other fluid meters), Reference 1.

First, the pressure loss from the inlet to the throat is found. This pressure loss is found in terms of the discharge coefficient (see nomenclature). The discharge coefficient is only a function of the contraction configuration and throat Reynolds number and is not affected by the following divergent section (Reference 1). The Bernoulli equation from inlet to throat is:

$$P_1 + \rho \frac{V_1^2}{2g} = P_2 + \rho \frac{V_2^2}{2g} + \Delta P_{f_1} \qquad (1)$$

For steady flow in the venturi

$$W_1 = \rho V_1 A_1 = \rho V_1 \frac{\pi D_1^2}{4} = W_2 = \rho V_2 \frac{\pi D_2^2}{4} \qquad (2)$$

Therefore

$$V_2 = V_1 \frac{D_1^2}{D_2^2} \qquad (3)$$

or in terms of the contraction ratio $B = D_2/D_1$,

$$V_2 = V_1/B^2 \qquad (4)$$

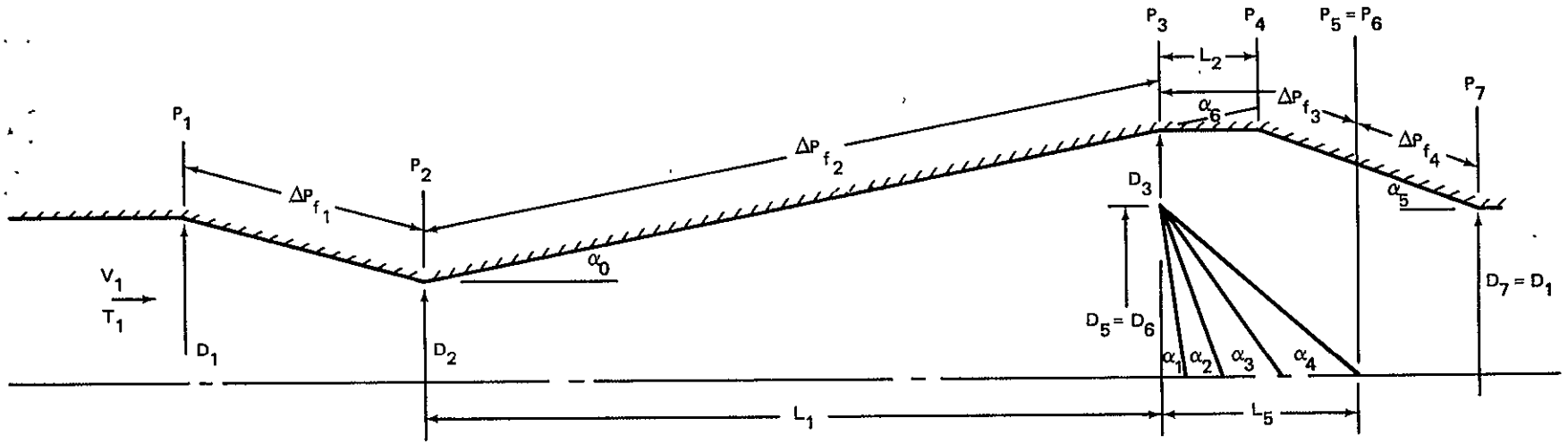
P1
P2
P3
P4
P5 = P6
P7
ΔPf1
ΔPf2
ΔPf3
ΔPf4
L2
α6
α0
α5
D3
V1
T1
D1
D2
D5 = D6
D7 = D1
α1
α2
α3
α4
L1
L5

From Equation (1),

$$\frac{V_1^2}{B^4} - V_1^2 = (P_1 - P_2 - \Delta P_{f_1}) \frac{2g}{\rho} \tag{5}$$

or

$$V_1 = \frac{B^2}{\sqrt{1 - B^4}} \sqrt{\frac{2g}{\rho} (P_1 - P_2 - \Delta P_{f_1})} \tag{6}$$

Thus, from Equation (2), the actual flowrate is

$$W_{act} = \rho \frac{\pi D_1^2}{4} \frac{B^2}{\sqrt{1 - B^4}} \sqrt{\frac{2g}{\rho} (P_1 - P_2 - \Delta P_{f_1})} \tag{7}$$

The theoretical flowrate is that which would occur if there were no losses,

$$W_{th} = \rho \frac{\pi D_1^2}{4} \frac{B^2}{\sqrt{1 - B^4}} \sqrt{\frac{2g}{\rho} (P_1 - P_2)} \tag{8}$$

Combining Equations (7) and (8)

$$W_{act}^2 = W_{th}^2 - \left(\rho \frac{\pi D_1^2}{4}\right)^2 \frac{B^4}{(1 - B^4)} \frac{2g}{\rho} \Delta P_{f_1} \tag{9}$$

or, in terms of the discharge coefficient,

$$C^2 = \frac{W_{act}^2}{W_{th}^2}$$

$$C^2 = 1 - \frac{\Delta P_{f_1}}{(P_1 - P_2)} \tag{10}$$

or

$$\Delta P_{f_1} = (1 - C^2) \left[\frac{\rho}{2g} (V_2^2 - V_1^2) + \Delta P_{f_1}\right] \tag{11}$$

or

$$\Delta P_{f_1} = \left(\frac{1 - C^2}{C^2}\right) \frac{\rho}{2g} \left(\frac{1 - B^4}{B^4}\right) V_1^2 \tag{12}$$

Discharge coefficients, C', have been plotted for B = 0.5 venturi in Reference 1. For other contraction ratios:

$$C^2 = \frac{1 - B^4}{1 - B^4 + \left(\frac{0.9375}{C'^2} - 0.9375\right)} \tag{13}$$

A curve fit from the plot in Reference 1, in terms of the throat Reynolds number,

$$R_2 = \frac{4 W_1}{\pi \mu D_2} \tag{14}$$

is

$$C' = 1 - \left[\frac{3.85}{R_2^{1/2}} + 0.0235 \left(0.3 + \frac{0.7}{1 + \left(\frac{253099}{R_2}\right)^{1.1367}}\right)\right] \tag{15}$$

The pressure at the throat is

$$P_2 = P_1 - \Delta P_{f_1} + \frac{\rho}{2g} (V_1^2 - V_2^2) \tag{16}$$

The pressure drop in the divergent section following the throat is found by integrating the pressure loss along the length from D_2 to D_3.

$$\int_{D_2}^{D_3} dP = \int_{D_2}^{D_3} \frac{f}{D} \rho \frac{V^2}{2g} \, dL \tag{17}$$

where f is the friction factor and

$$D = D_2 + 2L \tan \alpha_0 \tag{18}$$

C, 3

The velocity is

$$V = \frac{4W_1}{\rho\pi D^2} = \frac{4W_1}{\rho\pi(D_2 + 2L \tan \alpha_0)^2} \tag{19}$$

Therefore, substituting in Equation (17):

$$\Delta P_{f_2} = \int_{D_2}^{D_3} \frac{f\, 4^2\, W_1^{\,2}}{2g\ \rho\pi^2} \left(\frac{dL}{(D_2 + 2L \tan \alpha_0)^5}\right) \tag{20}$$

Integrating from D_2 to D_3 is equivalent to integrating from $L = 0$ to $L = L_1$ (see Figure A-1)

Therefore,

$$\Delta P_{f_2} = \frac{4^2\, W_1^{\,2}\, f}{2g\ \rho\pi^2\, 4\,(2 \tan \alpha_0)} \left(\frac{1}{D_2^{\,4}} - \frac{1}{D_3^{\,4}}\right) \tag{21}$$

The Moody friction factor, f, is found from a curve fit from the data in Reference 2, for a smooth venturi ($e/D \doteq 0.00003$) in terms of the Reynolds number at station 3 (which gives a maximum and conservative value),

$$f = \frac{0.47}{R_3^{\,0.33}} + 0.0075 \tag{22}$$

The pressure at station 3 is,

$$P_3 = P_2 - \Delta P_{f_2} + \frac{\rho}{2g} (V_2^{\,2} - V_3^{\,2}) \tag{23}$$

At this point, the flow in the venturi may encounter up to four screens in the separator section of the device. The flow will split and part of the flow will pass through the screens and the rest will bypass the screens, depending on the relative flow loss around and through the screens. The pressure loss for the portion of the total flow passing through the screens, from P_3 to P_5 (see Figure A-1) must equal the pressure loss for the balance of the flow around the screens, from P_3 to P_5, so that P_5 for the two flows is equal.

The pressure loss through the screens is additive and each screen loss is described by the Armour and Cannon form of dimensionless loss equation (see Reference 3):

$$f = \frac{\alpha}{R} + \beta$$

where α and β are experimentally determined coefficients,

$$f = \frac{\Delta P\ \epsilon^2 D_p g}{\rho\ V_s^2\ Qb}, \qquad R = \frac{\rho\ V_s}{\mu\ a^2 D_p} \tag{25}$$

Expanding gives:

$$\Delta P_s = \alpha \left[\frac{Qba^2}{\epsilon^2 g}\right] \mu\ V_s + \beta \left[\frac{Qb}{\epsilon^2 D_p g}\right] \rho\ V_s^2 \tag{26}$$

For square weave screens, the screen approach velocity V_s, is a function of the flowrate through the screens, the blockage fraction G, and the area of the screen, which may be assumed as the projected area,

$$V_s = \frac{W_s^4}{\rho \pi D_6^2 (1 - G)} \tag{27}$$

or, may be assumed as the actual area, as is the case for dutch weave screens where the screen approach velocity, V_s, is a function of the screen flowrate, the blockage fraction, and the actual screen area, or, since the screens are formed into cones of angle, α_n (see Figure A-1),

$$V_s = \frac{W_s^4}{\rho \pi D_6^2} \frac{\sin^2 \alpha_n}{(1 - G)} \tag{28}$$

For the flow around the screens,

$$W_{BY} = W_1 - W_s \tag{29}$$

the flow loss is divided into three parts: (1) a sudden contraction from D_3 to the bypass area; (2) a sudden expansion from the bypass area to the diameter, D_s, where the screens end; and (3) a friction loss from D_3 to D_s. The contraction and expansion loss are characterized by a loss coefficient, K, plotted in Reference 4, where

$$\Delta P = K \rho \frac{V_{BY}^2}{2g} \tag{30}$$

For contraction, a curve fit for K_c in terms of equivalent diameter ratio d_1/d_2 (where d_1 is the smaller equivalent diameter) is:

$$K_c = 0.5 - 0.15\ d_1/d_2 - 0.35\ (d_1/d_2)^2 \tag{31}$$

For our configuration,

$$d_1/d_2 = \left[\frac{\left(D_3^2 - D_6^2\right)}{\left(\frac{W_1 - W_s}{W_1}\right) D_3^2} \right]^{1/2} \tag{32}$$

and

$$V_{BY} = \frac{W_1 - W_s}{\rho\left(\frac{\pi D_3^2}{4} - \frac{\pi D_6^2}{4}\right)} \tag{33}$$

For expansion, from Reference 4,

$$K_e = \left[1 - \left(\frac{d_1}{d_2}\right)^2 \right]^2 \tag{34}$$

where

$$d_1/d_2 = \left[\frac{\left(D_3^2 - D_6^2\right)}{\left(\frac{W_1 - W_s}{W_1}\right) D_5^2} \right] \tag{35}$$

The friction loss is found from a friction factor based on the Reynolds number at station 4 (see Figure A-1) as in Equation (22):

$$F = \frac{0.47}{R_4^{0.33}} + 0.0075 \tag{36}$$

where

$$R_4 = \frac{4 (W_1 - W_s)}{\pi \mu D_4} \tag{37}$$

and

$$D_4 = D_3 + 2 L_2 \tan \alpha_6 \tag{38}$$

Similarly to Equation (21), the friction loss from station 3 to 4 is:

$$\Delta P_{f_{3'}} = \frac{4^2 (W_1 - W_s)^2 f}{2g \rho\pi^2 4 (2 \tan \alpha_6)} \left(\frac{1}{D_3^4} - \frac{1}{D_4^4}\right) \quad (39)$$

unless $\alpha_6 = 0$ in which case it is:

$$\Delta P_{f_{3'}} = \frac{4^2 (W_1 - W_s)^2 f}{2g \rho\pi^2} \left(\frac{L_2}{D_3^5}\right) \quad (40)$$

And from station 4 to 5 is:

$$\Delta P_{f_{3''}} = \frac{4^2 (W_1 - W_s)^2 f}{2g \rho\pi^2 4 (2 \tan \alpha_5)} \left(\frac{1}{D_5^4} - \frac{1}{D_4^4}\right) \quad (41)$$

The pressure at station 5 is

$$P_5 = P_3 - \Delta P_c - \Delta P_e - \Delta P_{f_3} + \frac{\rho}{2g} (V_3^2 - V_5^2) \quad (42)$$

and the pressure at station 6 is

$$P_6 = P_3 - \Delta P_s \text{ (1 through 4)} \quad (43)$$

The bypass and screen flowrates are adjusted until $P_5 = P_6$.

Finally, the friction loss from station 5 (6) to the device outlet is computed as in Equation (21):

$$\Delta P_{f_4} = \frac{4^2 W_1^2 f}{2g \rho\pi^2 4 (2 \tan \alpha_5)} \left(\frac{1}{D_1^4} - \frac{1}{D_5^4}\right) \quad (44)$$

where

$$f = \frac{0.47}{R_5^{0.33}} + 0.0075 \quad (45)$$

and the outlet pressure is:

$$P_7 = P_5 - \Delta P_{f_4} + \frac{\rho}{2g} (V_5^2 - V_1^2) \quad (46)$$

The overall pressure drop is

$$P_8 = P_1 - P_7 \tag{47}$$

The above equations were programmed in basic language for use on the MDAC Direct Access Computing system. A listing of this code, named LVENTURI, is shown in Table A-1.

A.2 COMPRESSIBLE FLOW MODEL

The analysis for compressible gas flow follows the same line of development as above except for including variation of the gas density due to pressure variations. The basic compressible flow assumption made is that friction effects are negligible, so that the isentropic relation is applicable.

$$\frac{P}{\rho^k} = \text{constant} \tag{48}$$

where, for a perfect gas

$$\rho_1 = P_1/RT_1 \tag{49}$$

From Equation (48),

$$\rho_2 = \rho_1 r_1^{1/k} \tag{50}$$

where $r_1 = P_2/P_1$ is the pressure ratio.

Following the development of Equations (1) to (12) above, gives:

$$\Delta P_{f_1} = \left(\frac{1-C^2}{C^2}\right)\left[\frac{\rho_1 V_1^2}{2g}\left(\frac{1-B^4 r_1^{2/k}}{B^4 r_1^{2/k}}\right)\left(\frac{k-1}{k}\right)\left(1+r_1^{1/k}\right) - P_1\left(r_1^{1/k} - r_1^{k-1/k}\right)\right] \tag{51}$$

and

$$P_2 = P_1 - \frac{\Delta P_{f_1}}{(1 - C^2)} \tag{52}$$

Table A-1

LVENTURI

```
100 PRINT 'FLUID PROPERTIES; DENSITY, VISCOSITY'
110 INPUT R, U
120 PRINT 'SCREEN 1,N,M,A,B,E,F,Q,X,Y,Z'
130 INPUT N1,M1,A1,B1,E1,F1,Q1,X1,Y1,Z1
140 PRINT 'SCREEN 2,DITTO'
150 INPUT N2,M2,A2,B2,E2,F2,Q2,X2,Y2,Z2
160 PRINT 'SCREEN 3,DITTO'
170 INPUT N3,M3,A3,B3,E3,F3,Q3,X3,Y3,Z3
180 PRINT 'SCREEN 4,DITTO'
190 INPUT N4,M4,A4,B4,E4,F4,Q4,X4,Y4,Z4
200 PRINT 'VENTURI P1,V1,D1,D2,X0,X5,X6'
210 INPUT P1,V1,D1,D2,X0,X5,X6
220 PRINT 'VENTURI L1,L2,D6'
230 INPUT L1,L2,D6
240 PRINT 'SCREEN BLOCKAGE 1,2,3,4,FLAG'
250 INPUT G1,G2,G3,G4,G5
260 B=D2/D1
270 V2=V1/B/B
280 W1=R*V1*3.1416*D1*D1/4/144
290 R2=48*W1/3.1416/U/D2
300 C0=1-(3.85/R2↑.5+.0235*(.3+.7/(1+(253099/R2)↑1.1367)))
310 C1=((1-B↑4)/(.0625-B↑4+(.9375/C0/C0)))↑.5
320 H1=(1-C1*C1)/C1/C1*R/2/32.2*(1-B↑4)/B↑4*V1*V1/144
330 P2=P1-H1+R/2/32.2/144*(V1*V1-V2*V2)
340 IF P2<15. GO TO 200
350 D3=D2+2*L1*TAN(X0*3.1416/180)
360 R3=R2*D2/D3
370 F5=.47/R3↑.33+.0075
380 V3=V2*D2*D2/D3/D3
390 H2=(1/D2↑4-1/D3↑4)/2/TAN(X0*3.1416/180)
400 H2=W1*W1*2*144/32.2/R/3.1416/3.1416*F5*H2
410 P3=P2-H2+R/2/32.2/144*(V2*V2-V3*V3)
420 B0=W1
430 S0=0.
440 G0=(B0+S0)/2
450 IF((B0-S0)/G0)<.0001 GO TO 1050
460 REM CONTRACTION LOSS
470 D0=((D3*D3-D6*D6)/D3/D3/(W1-G0)*W1)↑.5
480 K1=.5-.15*D0-.35*D0*D0
500 IF D0<1.0 GO TO 520
510 K1=0.
520 H3=K1*144/2/32.2/R*(W1-G0)↑2/3.1416/3.1416*4*4/(D3*D3-D6*D6)↑2
530 REM EXPANSION LOSS
540 L5=D6/TAN(X4*3.1416/180)/2
550 D5=D3+2*L2*TAN(X6*3.1416/180)-2*(L5-L2)*TAN(Y5*3.1416/180)
560 IF L5>L2 GO TO 580
570 D5=D3+2*L5*TAN(X6*3.1416/180)
580 D0=(D3*D3-D6*D6)/D5/D5/(W1-G0)*W1
590 K2=(1-D0)↑2
600 IF D0<1.0 GO TO 620
610 K2=0.
```

```
620 V5=V3*D3*D3/D5/D5
630 H5=K2*144/2/32.2/R*(W1-G0)↑2/3.1416/3.1416*4*4/(D3*D3-D6*D6)↑2
640 REM FRICTION LOSS
650 D4=D3+2*L2*TAN(X6*3.1416/180)
660 R4=R2*D2/D4*(W1-G0)/W1
670 F6=.47/R4↑.33+.0075
680 H4=L2/D3↑5
690 IF X6=0 GO TO 710
700 H4=(1/D3↑4-1/D4↑4)/2/TAN(X6*3.1416/180)/4
710 S1=(W1-G0)↑2*8*144/32.2/R/3.1416/3.1416*F6
720 H4=S1*(H4+(1/D5↑4-1/D4↑4)/2/TAN(X5*3.1416/180)/4)
730 REM SCREEN LOSS
740 U0=G0*4/R/3.1416/D6/D6/(1-G1)*144
750 J1=U0
760 IF N1=M1 GO TO 780
770 J1=U1*(SIN(X1*3.1416/180))↑2
780 H6=Y1*A1*A1*U*J1+Z1*R/F1*J1*J1
790 H6=H6*Q1*B1/144/E1/E1/32.2
800 J2=U0*(1-G1)/(1-G2)
810 IF N2=M2 GO TO 830
820 J2=U2*(SIN(X2*3.1416/180))↑2
830 H7=Y2*A2*A2*U*U2+Z2*R/F2*J2*U2
840 H7=H7*Q2*B2/144/E2/E2/32.2
850 U3=J0*(1-G1)/(1-G3)
860 IF N3=M3 GO TO 880
870 U3=U3*(SIN(X3*3.1416/180))↑2
880 H8=Y3*A3*A3*U*U3+Z3*R/F3*U3*U3
890 H8=H8*Q3*B3/144/E3/E3/32.2
900 U4=J0*(1-G1)/(1-G4)
910 IF N4=M4 GO TO 930
920 U4=U4*(SIN(X4*3.1416/180))↑2
930 H9=Y4*A4*A4*U*U4+Z4*R/F4*U4*U4
940 H9=H9*Q4*B4/144/E4/E4/32.2
950 P5=P3-H3-H4-H5+R/2/32.2/144*(V3*V3-V5*V5)
960 P6=P3-H6-H7-H8-H9
970 F0=P6-P5
980 IF F0<0 GO TO 1010
990 IF F0=0 GO TO 1050
1000 IF F0>0 GO TO 1030
1010 B0=G0
1020 GO TO 440
1030 S0=G0
1040 GO TO 440
1050 R5=R2*D2/D5
1060 F7=.47/R5↑.33+.0075
1070 H0=F7*W1*W1*8*144/32.2/R/3.1416/3.1416
1080 H0=H0*(1/D1↑4-1/D5↑4)/2/TAN(X5*3.1416/180)/4
1090 P7=P5-H0+R/2/32.2/144*(V5*V5-V1*V1)
1100 P8=P1-P7
1110 PRINT 'C0';C0;'C1';C1
1120 PRINT 'P2';P2;'P3';P3;'P5';P5;'P8';P8
1130 PRINT 'V2';V2;'V3';V3;'V5';V5
1140 PRINT 'H1';H1;'H2';H2;'H3';H3;'H4';H4;'H5';H5
1150 PRINT 'H6';H6;'H7';H7;'H8';H8;'H9';H9;'H0';H0
1160 PRINT 'TOTAL FLOW';W1;'SCREEN FLOW';G0
1170 IF G5=1 GO TO 240
1180 IF G5=2 GO TO 220
1190 IF G5=3 GO TO 200
1200 IF G5=4 GO TO 120
1210 IF G5=5 GO TO 1220
1220 END
```

An iteration technique is used to find P_2 and define r_1 in Equations (50) to (52). The value of C is again defined by Equations (13) through (15). A check is also made of r_1 to insure that it does not exceed the critical (sonic) pressure ratio r_C defined by

$$r_C^{(1-k/k)} + \left(\frac{k-1}{2}\right) B^4 r_C^{2/k} = \frac{k+1}{2} \tag{53}$$

The expansion loss follows the development of Equations (17) through (23) with

$$r_2 = P_3/P_2 \tag{54}$$

and

$$\rho_3 = \rho_2 r_2^{1/k} \tag{55}$$

The friction loss in the expanding section is:

$$\Delta P_{f_2} = \frac{4^2 W_1^2 f 2}{2g \pi^2 4 (2 \tan \alpha_0) \rho_2 (r_2^{1/k} + 1)} \left(\frac{1}{D_2^4} - \frac{1}{D_3^4}\right) \tag{56}$$

where f is found from Equation (22)

and

$$V_3 = V_2 \frac{D_2^2}{D_3^2} \frac{1}{r_2^{1/k}} \tag{57}$$

thus

$$P_3 = \frac{r_2^{1/k}}{1+r_2^{1/k}} \left[P_2 (r^{1/k}+1) - \Delta P_{f_2} + \frac{k-1}{k} \frac{\rho_2 (r_2^{1/k} + 1)}{2g} \left(V_2^2 - V_3^2\right) \right] \tag{58}$$

Again, an iteration technique is used to find P_3 and define r_2 in Equations (54) to (58).

The flow split and pressure loss through the screens is found from Equations (24) to (28) as before, with the density assumed at ρ_3 because there is only a small variation in static pressure through the screens.

For the flow around the screens, the contraction, friction, and expansion losses are developed as above in Equations (30) to (38). The friction loss from station 3 to 4 is similar to Equation (56):

$$\Delta P_{f_{3'}} = \frac{4^2 (W_1 - W_s)^2 f 2}{2g \pi^2 4 (2 \tan \alpha_6) \rho_3 (r_3^{1/k} + 1)} \left(\frac{1}{D_3^4} - \frac{1}{D_4^4} \right) \tag{59}$$

or if $\alpha_6 = 0$

$$\Delta P_{f_{3''}} = \frac{4^2 (W_1 - W_s)^2 f}{2g \pi^2 \rho_3 r_3^{1/k}} \left(\frac{L_2}{D_3^5} \right) \tag{60}$$

where $r_3 = P_9/P_3$, f is found from Equation (36) (61)

and P_9 is the pressure following the contraction loss ΔP_C:

$$\Delta P_C = \frac{k_C}{2g} \frac{2 (W_1 - W_s)^2 4^2}{\rho_3 (r_3^{1/k} + 1) \pi^2 (D_3^2 - D_6^2)^2} \tag{62}$$

and

$$P_9 = \frac{r_3^{1/k}}{(1+r_3^{1/k})} \left[P_3 (r_3^{1/k}+1) - \Delta P_C + \frac{k-1}{k} \frac{\rho_3 (r_3^{1/k}+1)}{2g} \left(V_3^2 - V_9^2 \right) \right] \tag{63}$$

where

$$V_9 = \frac{4}{\pi} \frac{2 (W_1 - W_s)}{\rho_3 (r_3^{1/k}+1) (D_3^2 - D_6^2)} \tag{64}$$

Similarly, the expansion loss

$$\Delta P_e = \frac{k_e}{2g} \frac{2 (W_1 - W_s)^2 4^2}{\rho_9 (r_4^{1/k}+1) \pi^2 (D_2^2 - D_6^2)^2} \tag{65}$$

where

$$\rho_9 = \rho_3 \, r_3^{1/k} \quad \text{and} \quad r_4 = P_5/P_9 \tag{66}$$

and

$$P_5 = \frac{r_4^{1/k}}{(1+r_4^{1/k})} \left[P_9 \, (r_4^{1/k}+1) - \Delta P_e - \Delta P_{f_3}, \right. \\ \left. + \frac{k-1}{k} \, \frac{\rho_9 \, (r_4^{1/k}+1)}{2g} \left(V_9^2 - V_5^2 \right) \right] \tag{67}$$

Again Equation (43) holds:

$$P_6 = P_3 - \Delta P_5 \text{ (1 through 4)} \tag{68}$$

and the bypass and screen flowrates are adjusted until $P_5 = P_6$.

The final friction loss is similar to Equation (56):

$$\Delta P_{f_4} = \frac{4^2 \, W_1^2 \, f \, 2}{2g \, \pi^2 \, 4 \, (2 \tan \alpha_5) \, \rho_5 \, (r_5^{1/k}+1)} \left(\frac{1}{D_1^4} - \frac{1}{D_5^4} \right) \tag{69}$$

where f is found from Equation (45), $\rho_5 = \rho_9 \, r_4^{1/k}$

and

$$r_5 = P_7/P_5 \tag{70}$$

The final pressure is:

$$P_7 = \frac{r_5^{1/k}}{(1+r_5^{1/k})} \left[P_5 \, (r_5^{1/k}+1) - \Delta P_{f_4} + \frac{k-1}{k} \, \frac{\rho_5 \, (r_5^{1/k}+1)}{2g} \left(V_5^2 - V_1^2 \right) \right] \tag{71}$$

The overall pressure drop is

$$P_8 = P_1 - P_7 \tag{72}$$

The above equations were programmed in basic language for use on the MDAC Direct Access Computing system. A listing of this code, named GVENTURI, is shown in Table A-2.

Table A-2

```
GVENTURI

100 PRINT 'FLUID PROPERTIES; TEMPERATURE, VISCOSITY'
110 INPUT T, J
120 PRINT 'SCREEN 1,N,M,A,B,E,F,Q,X,Y,Z'
130 INPUT N1,M1,A1,B1,E1,F1,Q1,X1,Y1,Z1
140 PRINT 'SCREEN 2,DITTO'
150 INPUT N2,M2,A2,B2,E2,F2,Q2,X2,Y2,Z2
160 PRINT 'SCREEN 3,DITTO'
170 INPUT N3,M3,A3,B3,E3,F3,Q3,X3,Y3,Z3
180 PRINT 'SCREEN 4,DITTO'
190 INPUT N4,M4,A4,B4,E4,F4,Q4,X4,Y4,Z4
200 PRINT 'VENTURI P1,V1,D1,D2,X0,X5,X6'
210 INPUT P1,V1,D1,D2,X0,X5,X6
220 PRINT 'VENTURI L1,L2,D6'
230 INPUT L1,L2,D6
240 PRINT 'SCREEN BLOCKAGE 1,2,3,4,FLAG'
250 INPUT G1,G2,G3,G4,G5
260 B=D2/D1
270 V2=V1/B/B
280 R1=P1/55.1/T*144
290 P2=P1-R1/2/32.2/144*(1-B↑4)/B↑4*V1*V1
300 W1=R1*V1*3.1416*D1*D1/4/144
310 S2=48*W1/3.1416/J/D2
320 C0=1-(3.85/S2↑.5+.0235*(.3+.7/(1+(253099/S2)↑1.136)))
330 C1=((1-B↑4)/(.0625-B↑4+(.9375/C0/C0)))↑.5
340 J=1
350 T3=0
360 I=0
370 J=J-T3
380 I=I+1
390 T1=1/J↑.2857+.2*B↑4*J↑1.4286-1.2
400 T2=(-1/J↑1.2857+B↑4*J↑.4286)*.2857
410 T3=T1/T2
420 IF I>20 GO TO 450
430 IF ABS(T3/J)<.00001 GO TO 450
440 GO TO 370
450 J1=P2/P1
460 IF J1<J GO TO 200
470 H1=(1-C1*C1)/C1/C1*(R1/2/32.2*(1-B↑4*J1↑1.4286)/B↑4/J1↑1.4286*.4/1.4
*(1+J1↑.7143)*V1*V1/144-P1*(J1↑.7143-J1↑.2857))
480 P2=P1-H1/(1-C1*C1)
490 J0=P2/P1
500 IF ABS((J0-J1)/J1)<.0001 GO TO 530
510 J1=J0
520 GO TO 460
530 V2=V1/B/B/J1↑.7143
540 R2=R1*J1↑.7143
550 D3=D2+2*L1*TAN(X0*3.1416/180)
560 S3=S2*D2/D3
570 F5=.47/S3↑.33+.0075
580 V3=V2*D2*D2/D3/D3
590 P3=P2+R2/2/32.2/144*(V2*V2-V3*V3)
600 J2=P3/P2
```

```
610 H2=(1/D2↑4-1/D3↑4)/2/TAN(X0*3.1416/180)
620 H2=W1*W1*2*144/32.2*2/3.1416/3.1416*F5*H2/R2/(J2↑.7143+1)
630 V3=V2*D2*D2/D3/D3/J2↑.7143
640 P3=J2↑.7143/(1+J2↑.7143)*(P2*(J2↑.7143+1)-H2+.4/1.4*R2/2/32.2/144*(1
+J2↑.7143)*(V2*V2-V3*V3))
650 J0=P3/P2
660 IF ABS((J0-J2)/J2)<.0001 GO TO 690
670 J2=J0
680 GO TO 610
690 R3=R2*J2↑.7143
700 B0=W1
710 S0=0.
720 G0=(B0+S0)/2
730 IF((B0-S0)/G0)<.0001 GO TO 1500
740 REM CONTRACTION LOSS
750 D0=((D3*D3-D6*D6)/D3/D3/(w1-G0)*W1)↑.5
760 K1=.5-.15*D0-.35*D0*D0
770 IF D0<1.0 GO TO 790
780 K1=0.
790 V9=4/3.1416*144/R3*(W1-G0)/(D3*D3-D6*D6)
800 P9=P3-R3/2/32.2/144*(V9*V9-V3*V3)
810 J3=P9/P3
820 H3=K1*144/R3/32.2 *(W1-G0)↑2/3.1416/3.1416*4*4/(D3*D3-D6*D6)↑2/(J3↑.
7143+1)
830 V9=4/3.1416*144/R3/(J3↑.7143+1)*2*(W1-G0)/(D3*D3-D6*D6)↑2
840 P9=J3↑.7143/(1+J3↑.7143)*(P3*(J3↑.7143+1)-H3+.4/1.4*R3/2/32.2/144*(1
+J3↑.7143)*(V3*V3-V9*V9))
850 J0=P9/P3
860 IF ABS((J0-J3)/J3)<.0001 GO TO 890
870 J3=J0
880 GO TO 820
890 R9=R3*J3↑.7143
900 REM FRICTION LOSS
910 D4=D3+2*L2*TAN(X6*3.1416/180)
920 S4=S2*D2/D4*(W1-G0)/W1
930 F6=.47/S4↑.33+.0075
940 H4=L2/D3↑5
950 IF X6=0 GO TO 970
960 H4=(1/D3↑4-1/D4↑4)/2/TAN(X6*3.1416/180)/4
970 S1=(W1-G0)↑2*8*144/32.2  /3.1416/3.1416*F6/R9
980 L5=D6/TAN(X4*3.1416/180)/2
990 D5=D3+2*L2*TAN(X6*3.1416/180)-2*(L5-L2)*TAN(X5*3.1416/180)
1000 IF L5>L2 GO TO 1020
1010 D5=D3+2*L5*TAN(X6*3.1416/180)
1020 D0=(D3*D3-D6*D6)/D5/D5/(W1-G0)*W1
1030 K2=(1-D0)↑2
1040 IF D0<1.0 GO TO 1060
1050 K2=0.
1060 V5=V3*D3*D3/D5/D5
1070 H4=S1*(H4+(1/D5↑4-1/D4↑4)/2/TAN(X5*3.1416/180)/4)
1080 REM EXPANSION LOSS
1090 P5=P9-R9/2/32.2/144*(V5*V5-V9*V9)-H4
1100 J4=P5/P9
1110 H5=K2*144/R9/32.2*(W1-G0)↑2/3.1416/3.1416*4*4/(D3*D3-D6*D6)↑2/(J4↑.
7143+1)
1120 V5=V3*D3*D3/D5/D5/J4↑.7143
1130 P5=J4↑.7143/(1+J4↑.7143)*(P9*(J4↑.7143+1)-H5-H4+.4/1.4*R9/2/32.2/14
4*(1+J4↑.7143)*(V9*V9-V5*V5))
1140 J0=P5/P9
```

```
1150 IF ABS((J0-J4)/J4)<.0001 GO TO 1180
1160 J4=J0
1170 GO TO 1110
1180 R5=R9*J4↑.7143
1190 REM SCREEN LOSS
1200 U0=G0*4  /3.1416/D6/D6/(1-G1)*144/R3
1210 U1=U0
1220 IF N1=M1 GO TO 1240
1230 U1=U1*(SIN(X1*3.1416/180))↑2
1240 H6=Y1*A1*A1*U*U1+Z1  /F1*U1*U1*R3
1250 H6=H6*Q1*B1/144/E1/E1/32.2
1260 U2=U0*(1-G1)/(1-G2)
1270 IF N2=M2 GO TO 1290
1280 U2=U2*(SIN(X2*3.1416/180))↑2
1290 H7=Y2*A2*A2*U*U2+Z2  /F2*U2*U2*R3
1300 H7=H7*Q2*B2/144/E2/E2/32.2
1310 U3=U0*(1-G1)/(1-G3)
1320 IF N3=M3 GO TO 1340
1330 U3=U3*(SIN(X3*3.1416/180))↑2
1340 H8=Y3*A3*A3*U*U3+Z3  /F3*U3*U3*R3
1350 H8=H8*Q3*B3/144/E3/E3/32.2
1360 U4=U0*(1-G1)/(1-G4)
1370 IF N4=M4 GO TO 1390
1380 U4=U4*(SIN(X4*3.1416/180))↑2
1390 H9=Y4*A4*A4*U*U4+Z4  /F4*U4*U4*R3
1400 H9=H9*Q4*B4/144/E4/E4/32.2
1410 P6=P3-H6-H7-H8-H9
1420 F0=P6-P5
1430 IF F0<0 GO TO 1460
1440 IF F0=0 GO TO 1500
1450 IF F0>0 GO TO 1480
1460 B0=G0
1470 GO TO 720
1480 S0=G0
1490 GO TO 720
1500 S5=S2*D2/D5
1510 F7=.47/S5↑.33+.0075
1520 P7=P5 +R5 /2/32.2/144*(V5*V5-V1*V1)
1530 J5=P7/P5
1540 H0=F7*W1*W1*8*144/32.2*2/3.1416/3.1416/R5/(J5↑.7143+1)
1550 H0=H0*(1/D1↑4-1/D5↑4)/2/TAN(X5*3.1416/180)/4
1560 P7=J5↑.7143/(1+J5↑.7143)*(P5*(J5↑.7143+1)-H0+.4/1.4*R5/2/32.2/144*(
1+J5↑.7143)*(V5*V5-V1*V1))
1570 J0=P7/P5
1580 IF ABS((J0-J5)/J5)<.0001 GO TO 1610
1590 J5=J0
1600 GO TO 1540
1610 P8=P1-P7
1620 PRINT 'C0';C0;'C1';C1
1630 PRINT 'P2';P2;'P3';P3;'P5';P5;'P8';P8
1640 PRINT 'V2';V2;'V3';V3;'V5';V5
1650 PRINT 'H1';H1;'H2';H2;'H3';H3;'H4';H4;'H5';H5
1660 PRINT 'H6';H6;'H7';H7;'H8';H8;'H9';H9;'H0';H0
1670 PRINT 'TOTAL FLOW';W1;'SCREEN FLOW';G0
1680 IF G5=1 GO TO 240
1690 IF G5=2 GO TO 220
1700 IF G5=3 GO TO 200
1710 IF G5=4 GO TO 120
1720 IF G5=5 GO TO 1730
1730 END
```

A.3 NOMENCLATURE

a	Screen surface area to unit volume ratio (1/ft)
A	Area (ft^2)
b	Screen thickness (ft)
B	Contraction ratio
C	Discharge coefficient
C'	Discharge coefficient for B - 0.5 Venturi
D	Diameter (ft)
e	Roughness dimension (ft)
f	Friction factor, $\frac{\Delta P\ 2g}{\frac{L}{D_h}\rho V^2}$, $\frac{\Delta P\ \epsilon^2\ D\ g}{\rho\ V^2\ Qb}$
g	Gravitational constant (32.2 ft/sec^2)
G	Screen blockage fraction
K	Loss coefficient
k	Isentropic exponent (ratio of specific heats)
L	Length (ft)
P	Pressure (psia)
ΔP	Pressure loss (psi)
Q	Screen tortuosity factor (1.0 for square weave, 1.3 for Dutch weave)
R	Reynolds number $\frac{\rho VD}{\mu}$, $\frac{\rho V}{\mu a^2 D}$
R	Gas constant (ft/°R)
r	Pressure ratio
T	Temperature (°R)

V	Fluid velocity (ft/sec)
W	Weight flowrate (lb/sec)
α, β	Experimentally determined constants
ϵ	Screen void fraction
μ	Viscosity (lb/ft-sec)
ρ	Density (lb/ft^3)
α	Angle (°)

Subscripts

act	Actual
by	Bypass
c	Contraction
e	Expansion
f	Frictional
p	Pore
s	Through the screen
TH	Theoretical
1	Inlet station
2	Throat station
3	Screen station in venturi
4, 5	Bypass stations
6	Screen
7	Outlet station
8	Inlet minus outlet
9	Bypass station

A.4 REFERENCES

1. Fluid Meters, Their Theory and Application, Part 1, ASME, Fourth Edition, 1937.

2. L. F. Moody, Friction Factors for Pipe Flow ASME Transactions, Vol. 66, p.p. 671 - 678, November 1944.

3. J. C. Armour and J. N. Cannon, Fluid Flow Through Woven Screens, AICHE Journal, p.p. 415 - 420, May 1968.

4. Flow of Fluids Through Valves, Fittings, and Pipe, Crane Technical Paper No. 410, 1957.

Appendix B

TEST POWDER PREPARATION

The test powders used on this program consisted of the following types of material.

A. Aluminum oxide (Al_2O_3)

B. Aluminum-metallic (Al)

C. Stainless steel-metallic (CRES)

Each of these materials were obtained from different sources and the respective test powders were prepared in different ways. The AL_2O_3 powders were prepared from graded abrasive grit stock. Samples of graded material in 35, 40, 46, 60, 70, 90, 100, 120, 150, 180, and 220 grit was obtained from the F. D. Davis Company of Los Angeles, CA. The sample powders were then placed in a Tyler grading machine which utilized a 35, 60, 80, 150, and 250 mesh sieve. The material recovered from the 250 mesh sieve was designated A1, the 150 mesh A2, the 80 mesh A3 and the 60 mesh A4. The material retained on the 35 mesh sieve and that which passed through the 250 mesh sieve was discarded. Each of the recovered powder sizes was placed in separate glass jars, labeled and used for testing.

The metallic aluminum test powders were obtained by mixing pregraded spherical aluminum particles obtained from the Particle Information Services, San Jose, CA. The final mixes contained the following material combinations:

B1 27-2Q, 27-2P, 27-2R

B2 27-2O, 27-2N

B3 27-2N, 27-2M

B4 27-2L, 27-2K, 27-2J

The stainless steel (CRES) test powder was obtained by grading a can of TD-6 (+150 mesh) material with the same Tyler sieves used for the Al_2O_3 grading. This material was obtained from the Hoeganaes Corp., Riverton, NJ (Lot 94-5230). Since the CRES material contained a large percentage of particles with irregular shapes, the C1, C2, C3, C4 material was replaced with a single CRES powder obtained from the NASA-LeRC program office. This material was a graded spherical 304L material in the 125-150μ size range. This final CRES powder was designated CX2 for identification on this program.

The D1 and D2 powders used in the Task II effort were similar to the A series of powders and were Al_2O_3. The grading sieves used for the D powders were 40, 60, and 120 mesh. The D1 powder was recovered on the 120 mesh sieve and the D2 powder from the 60-mesh sieve. The final sizing was, therefore, D1 = 125 to 250μ and D2 - 250 to 420μ.

DISTRIBUTION LIST

National Aeronautics & Space Administration
Lewis Research Center
21000 Brookpark Road
Cleveland, Ohio 44135

Attn:	Contracting Officer, MS 500-313	1
	E. A. Bourke, MS 500-205	5
	Technical Utilization Office, MS 3-16	1
	Technical Report Control Office, MS 5-5	1
	AFSC Liaison Office, MS 501-3	2
	Library, MS 60-3	2
	Office of Reliability & Quality Assurance, MS 500-211	1
	J. J. Notardonato, Project Manager, MS 500-203	10

National Aeronautics & Space Administration
Headquarters
Washington, D. C. 20546

Attn:	Office of Aeronautics & Space Technology	1
	F. W. Stephenson/RPI	1
	Office of Manned Space Flight Director, Advanced Manned Mission/MT	1
	Office of Space Science Director, Launch Vehicles & Propulsion/SV	
	Office of Technology Utilization Division Director, Technology Utilization/KT	

National Aeronautics & Space Administration
Ames Research Center
Moffett Field, California 94035

Attn:	Library	1

National Aeronautics & Space Administration
Flight Research Center
P. O. Box 273
Edwards, California 93523 1

National Aeronautics & Space Administration
George C. Marshall Space Flight Center
Huntsville, Alabama 35912

Attn:	Library	
	E. H. Hyde	2

National Aeronautics & Space Administration
Goddard Space Flight Center
Greenbelt, Maryland 20771

Attn:	Library	1

National Aeronautics & Space Administration
John F. Kennedy Space Center
Cocoa Beach, Florida 32931
Attn: Library — 1

National Aeronautics & Space Administration
Lyndon B. Johnson Space Center
Houston, Texas 77001
Attn: Library — 1

National Aeronautics & Space Administration
Langley Research Center
Langley Station
Hampton, Virginia 23365
Attn: Library — 1

NASA Scientific & Technical Information Facility
P. O. Box 33
College Park, Maryland 20740
Attn: NASA Representative — 10

Office of the Director of Defense
Research & Engineering
Washington, D. C. 20301
Attn: Office of Ass't Director (Chemical Technology) — 1

Jet Propulsion Laboratory
4800 Oak Grove Drive
Pasadena, California 91103
Attn: Library — 1

Defense Documentation Center
Cameron Station
Building 5
5010 Duke Street
Alexandria, Virginia 22314
Attn: TISIA — 1

Advanced Research Projects Agency
Washington, D. C. 20525
Attn: Library — 1

Aeronautical Systems Division
Air Force Systems Command
Wright-Patterson Air Force Base
Dayton, Ohio
Attn: Library — 1

Air Force Missile Test Center
Patrick Air Force Base
Flordia
Attn: Library — 1

Air Force Systems Command
Andrews Air Force Base
Washington, D. C. 20332
Attn: Library 1

Air Force Rocket Propulsion Laboratory (RPR)
Edwards, California 93523
Attn: Library 1

Air Force Rocket Propulsion Laboratory (RPM)
Edwards, California 93523
Attn: Library 1

Air Force FTC (FTAT-2)
Edwards Air Force Base
California 93523
Attn: Library 1

Air Force Office of Scientific Research
Washington, D. C. 20333
Attn: Library
Dr. J. F. Masi

U. S. Air Force
Washington, D. C.
Attn: Library 1

Air Force Aero Propulsion Laboratory
Research & Technology Division
Air Force Systems Command
U. S. Air Force
Wright-Patterson AFB, Ohio 45433
Attn: Library (APRP) 1

Arnold Engineering Development Center
Air Force Systems Command
Tullahoma, Tennessee
Attn: Library 1

Space & Missile System Organization
Air Force Unit Post Office
Los Angeles, California 90045
Attn: Library (Technical Data Center)
Captain W. Moll, Jr., XRZE

Office of Research Analyses (OAR)
Holloman Air Force Base
New Mexico 88330
Attn: Library (RRRD) 1

RTD (RTNP)
Bolling Air Force Base
Washington, D. C. 20332 1

Bureau of Naval Weapons
Department of the Navy
Washington, D. C.
Attn: Library — 1

Naval Research Branch Office
1030 E. Green Street
Pasadena, California 91101
Attn: Library — 1

Picatinny Arsenal
Dover, New Jersey 97801
Attn: Library — 1

U. S. Naval Research Laboratory
Washington, D. C. 20390
Attn: Library — 1

U. S. Army Research Office (Durham)
Box CM, Duke Station
Durham, North Carolina 27706
Attn: Library — 1

U. S. Army Missile Command
Redstone Scientific Information Center
Redstone Arsenal, Alabama 35808
Attn: Document Section — 1

U. S. Naval Missile Center
Point Mugu, California 93041
Attn: Technical Library — 1

U. S. Naval Weapons Center
China Lake, California 93557
Attn: Library — 1

Aerojet-General Corporation
Electronics Division
P. O. Box 296
Azusa, California 91703
Attn: Library — 1

Aerojet-General Corporation
Space Division
9200 East Flair Drive
El Monte, California 91734
Attn: Library — 1

Aerojet-General Corporation
Aerojet Ordance & Manufacturing
11711 South Woodruff Avenue
Fullerton, California 90241
Attn: Library — 1

Aerojet Liquid Rocket Company
P. O. Box 15847
Sacramento, California 95813
Attn: Technical Library 2484-2015A 1

Aerospace Corporation
2400 E. El Segundo Blvd.
Los Angeles, California 90045
Attn: Library
V. H. Monteil 1

Garrett Corporation
Airesearch Mfg. Division
9851 Sepulveda Blvd
Los Angeles, California
Attn: Library 1

Garrett Corporation
Airesearch Mfg. Division
402 South 36th Street
Phoenix, Arizona 85034
Attn: Library 1

Aro Incorporated
Arnold Engineering Development Center
Arnold AF Station, Tennessee 37389
Attn: Library 1

Battelle Memorial Institute
505 King Avenue
Columbus, Ohio 43201
Attn: Library 1

Beech Aircraft Corporation
Boulder Facility
Box 631
Boulder, Colorado 1

Bell Aerosystems Inc.
Box 1
Buffalo, New York 14240
Attn: Library
J. M. Senneff
J. Flanagan 2

Bendix Corporation
Instruments & Life Support Division
P. O. Box 4508
Davenport, Iowa 52808
Attn: Library 1

Boeing Company
Space Division
P. O. Box 868
Seattle, Washington 98124
Attn: Library 1

Boeing Company
1625 K. Street N. W.
Washington, D. C. 1

Boeing Company
P. O. Box 1680
Huntsville, Alabama 35801 1

Chemical Propulsion Information Agency
Applied Physics Laboratory
8621 Georgia Avenue
Silver Spring, Maryland 20910 1

Chrysler Corporation
Missile Division
P. O. Box 2628
Detroit, Michigan
Attn: Library 1

Chrysler Corporation
Space Division
P. O. Box 29200
New Orleans, Louisiana 70129
Attn: Library 1

Curtiss-Wright Corporation
Wright Aeronautical Division
Woodridge, New Jersey
Attn: Library 1

Denver Research Institute
University of Denver
P. O. Box 10127
Denver, Colorado 80210
Attn: Security Office 1

Fairchild Stratos Corporation
Aircraft Missile Division
Hagerstown, Maryland
Attn: Library 1

Fairchild Hiller Corporation
Research Center
Germantown, Maryland
Attn: Library 1

Fairchild Hiller Corporation
Republic Aviation
Farmington, L. I. N. Y. 1

General Dynamics/Convair
P. O. Box 1128
San Diego, California 92112
Attn: Library 1
R. Tatro 1
R. Nau 1
C. F. Peters 1

General Electric Company
Missiles & Space Systems Center
Valley Forge Space Technology Center
P. O. Box 8555
Philadelphia, Pennsylvania 19101
Attn: Library 1

General Electric Company
Apollo Support Department
P. O. Box 2500
Daytona Beach, Florida 32015
Attn: C. Bay 1

Grumman Aircraft Engineering Corporation
Bethpage, L. I. N. Y.
Attn: Library 1

Hamilton Standard Corporation
Windsor Locks, Conn. 06096
Attn: Library 1

Hercules Powder Company
Allegheny Ballistics Lab
P. O. Box 210
Cumberland, Maryland 21501
Attn: Library 1

Honewell Inc.
Aerospace Division
2600 Ridgeway Road
Minneapolis, Minnesota
Attn: Library 1

IIT Research Institute
Technology Center
Chicago, Illinois 60616
Attn: Library 1

International Nickel Company
One New York, Plaza
New York, N. Y. 10004
Attn: C. B. Sanborn 1

Kidde Aerospace Division
Walter Kidde & Company
567 Main Street
Belleville, New Jersey 07109
Attn: Library 1

Linde, Division of Union Carbide
P. O. Box 44
Tonawanda, N. Y. 11450
Attn: G. Nies 1

Ling-Temco-Vought Corporation
P. O. Box 5907
Dallas, Texas 75222
Attn: Library 1

Lockheed Missiles & Space Company
P. O. Box 504
Sunnyvale, California 94087
Attn: Library 1
R. T. Parmley 1

Lockheed Propulsion Company
P. O. Box 111
Redlands, California 92374
Attn: Library 1

Marquardt Corporation
16555 Saticoy Street
Box 2013 South Annex
Van Nuys, California 91409
Attn: Library 1
L. R. Bell, Jr. 1

Minnesota Mining & Manufacturing Company
900 Bush Avenue
St. Paul, Minnesota 55106
Attn: Library 1

Martin-Marietta Corporation
P. O. Box 179
Denver, Colorado 80201
Attn: Library 1
G. G. Skartvedt 1

Martin-Marietta Corporation
Box 5827
Orlando, Flordia
Attn: Library 1

McDonnell Douglas Astronautics
5301 Bolsa Avenue
Huntington Beach, California 92647
Attn: Library 1

McDonnell Douglas Aircraft Corporation
P.O. Box 516
Lambert Field, Missouri 63166
Attn: Library 1
L. F. Kohrs 1

Northrop Space Laboratories
3401 West Broadway
Hawthorne, California
Attn: Library 1

Philco-Ford Corporation
Aeronutronic Division
Ford Road
Newport Beach, California 92663
Attn: Library 1

Purdue University
Lafayette, Indiana 47907
Attn: Library 1

Radio Corporation of America
Astro-Electronics Products
Princeton, New Jersey
Attn: Library 1

Rocketdyne
A Division of Rockwell International
6633 Canoga Avenue
Canoga Park, California 91304
Attn: Library 1

Rocketdyne
A Division of Rockwell International
12214 Lakewood Blvd
Downey, California
Attn: Library 1

Rocket Research Corporation
Willow Road at 116th Street
Redmond, Washington 98052
Attn: Library 1

Stanford Research Institute
333 Ravenswood Avenue
Menlo Park, California 94025
Attn: Library 1

Susquehanna Corporation
Atlantic Research Division
Shirley Highway & Edsall Road
Alexandria, Virginia 22314
Attn: Library 1

Thiokol Chemical Corporation
Redstone Division
Huntsville, Alabama
Attn: Library 1

TRW Systems Inc.
1 Space Park
Redondo Beach, California 90278
Attn: Library 1

TRW
TAPCO Division
23555 Euclid Avenue
Cleveland, Ohio 44117
Attn: Library 1

United Aircraft Corporation
Corporation Library
400 Main Street
East Hartford, Connecticut 06108 1

United Aircraft Corporation
United Technology Center
P.O. Box 358
Sunnyvale, California 94038
Attn: Library 1

United Aircraft Corporation
Pratt & Whitney Division
Flordia Research & Development Center
P.O. Box 2691
West Palm Beach, Florida 33402
Attn: Library 1

Vickers Incorporated
Box 302
Troy, Michigan
Attn: Library 1

Vought Astronautics
Box 5907
Dallas, Texas
Attn: Library 1

Naval Surface Weapons Center
White Oak Laboratory
White Oak, Maryland
Attn: Mr. Russel Bardos 1

TRW System & Energy
1 Space Park
Redondo Beach, California 90278
Attn: W. D. English 1

Fairchild Industires
1800 E. Rosecrans
Manhattan Beach, California
Attn: Mr. F. F. Stecker 1

Wintec Division
Brunswick Corporation
5223 W. Imperial Highway
Los Angeles, California
Attn: Mr. J. Winzen 1